AD-A064 921 IOWA INST OF HYDRAULIC RESEARCH IOWA CITY F/G 20/4
THICK AXISYMMETRIC TURBULENT BOUNDARY LAYER AND WAKE OF A LOW-D--ETC(U)
DEC 78 Y LEE N00014-75-C-0273
UNCLASSIFIED NL

1 OF 2
AD A064921

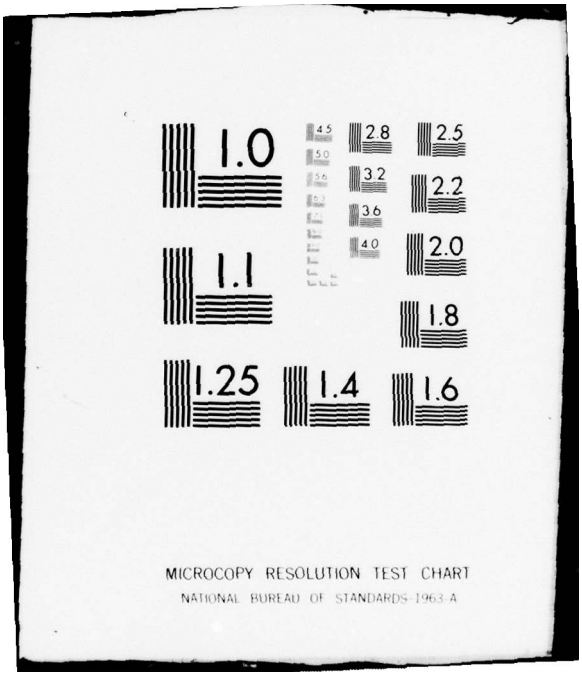
1.0
1.1
1.25
1.4
1.6
1.8
2.0
2.2
2.5
2.8
3.2
3.6
4.0
4.5
5.0
5.6
MICROCOPY RESOLUTION TEST CHART
NATIONAL BUREAU OF STANDARDS-1963-A

LEVEL II

THICK AXISYMMETRIC TURBULENT BOUNDARY LAYER AND WAKE OF A LOW-DRAG BODY

By Yu-Tai Lee Dec 1978

THESIS - U/IOWA SPONSORED BY:
Naval Sea Systems Command General Hydromechanics Research Program administered by David W. Taylor Naval Ship R&D Center under Contract N00014-75-C-0273

Thick Axisymmetric Turbulent Boundary Layer and Wake of a Low-Drag Body, by Yu-Tai Lee Dec 1978, THESIS University of Iowa. Sponsored by the Naval Sea Systems Command General Hydromechanics Research Program administered by David W. Taylor Naval Ship R&D Center under Contract N00014-75-C-0273

(1) LEVEL II

(15) ok

(6) THICK AXISYMMETRIC TURBULENT BOUNDARY LAYER AND WAKE OF A LOW-DRAG BODY.

(9) Final rept.,

by

(10) Yu-Tai Lee

(16) SR02301

(17) SR0230101

An Abstract

Of a thesis submitted in partial fulfillment of the requirements for the degree of Doctor of Philosophy in Mechanics and Hydraulics in the Graduate College of The University of Iowa

(11) December, 1978 (12) 139 p.

Thesis co-supervisor: Professor Virendra C. Patel
Thesis co-supervisor: Professor Louis Landweber

410 439

79 02 21 071 LB

ABSTRACT

Detailed measurements of pressure distributions, mean velocity profiles and Reynolds stresses were made in the thick, axisymmetric boundary layer and the near wake of a low-drag body of revolution. These measurements shed some light on the joint influence of transverse and longitudinal surface curvatures and pressure gradients on the boundary-layer development and on the manner in which an axisymmetric boundary layer becomes a fully-developed wake. The present data have been used to provide an independent check on the accuracy of the simple integral method proposed by Patel, and its extension to the calculation of the near wake made by Nakayama, Patel and Landweber. Calculations have also been performed using the differential equations of the thick axisymmetric turbulent boundary layer and a rate equation for the Reynolds stress derived from the turbulent kinetic-energy equation along the lines suggested by Bradshaw and others. It is shown that the boundary layer in the tail region of a body of revolution is dominated by the extra strain rates arising from longitudinal and transverse surface curvatures. A new differential method is incorporated into the iterative procedure developed by Nakayama, Patel and Landweber for the solution of the interaction between the boundary layer, the wake and the external inviscid flow. The results of the iterative method have been compared

with the experimental data obtained from the present low-drag body and those obtained earlier on a modified spheroid to demonstrate the agreement.

Abstract approved: Vernera C. Oehlf
Thesis co-supervisor

Professor Mechanics & Hydraulics
Title and department

Sept 22, 1978
Date

Louis Landweber
Thesis co-supervisor

Professor Mechanics & Hydra.
Title and department

Sept. 22, 1978
Date

THICK AXISYMMETRIC TURBULENT BOUNDARY LAYER AND WAKE OF A LOW-DRAG BODY

by

Yu-Tai Lee

A thesis submitted in partial fulfillment of the
requirements for the degree of Doctor of
Philosophy in Mechanics and Hydraulics
in the Graduate College of
The University of Iowa

December, 1978

Thesis co-supervisor: Professor Virendra C. Patel
Thesis co-supervisor: Professor Louis Landweber

Graduate College
The University of Iowa
Iowa City, Iowa

CERTIFICATE OF APPROVAL

PH.D. THESIS

This is to certify that the Ph.D. thesis of

Yu-Tai Lee

has been approved by the Examining Committee for the thesis requirement for the Doctor of Philosophy degree in Mechanics and Hydraulics at the December, 1978 graduation.

Thesis committee: Thomas C. Calvert
Thesis co-supervisor -

Louis Landweber
Thesis co-supervisor

Member

Member

Member

ACKNOWLEDGEMENTS

The author wishes to express his gratitude to Professor V.C. Patel for his guidance, discussion, and encouragement during the course of this study. The author is also indebted to Professor L. Landweber and Dr. B.R. Ramaprian for their fruitful suggestions and to Dr. A. Nakayama, who initiated the present experiment, and Dr. O. Güven, who assisted in the turbulence measurements.

This research was carried out under the sponsorship of the Naval Sea Systems Command, General Hydro-Mechanics Research Program, Subproject SR023 01 01, administered by the David W. Taylor Naval Ship Research and Development Center, Contract N00014-75-C-0273.

Finally, appreciation is due to his wife, Rosa, for her patience and continuous encouragement.

TABLE OF CONTENTS

LIST OF TABLES

LIST OF FIGURES

LIST OF SYMBOLS

a_1	structure parameter ($= -\overline{uv}/q^2$)
C_D	drag coefficient ($= D/\frac{1}{2}\rho U_o^2 S$)
C_E	entrainment coefficient
C_f	skin-friction coefficient ($= \tau_w/\frac{1}{2}\rho U_\delta^2$)
C_p	pressure coefficient
D	drag force
e	extra rate of strain
e_{eff}	effective rate of strain
e_ℓ	rate of strain due to longitudinal curvature
e_t	rate of strain due to transverse curvature
G	diffusion function
h_1	metric coefficient in the x-direction
H	axisymmetric shape factor ($= \Delta_1/\Delta_2$)
$\overline{H}$	planar shape factor ($= \overline{\delta}_1/\overline{\delta}_2$)
$\overline{H^*}$	entrainment shape parameter ($= \frac{\delta - \overline{\delta}_1}{\overline{\delta}_2}$)
I_k	integral defined by equation (11)
I_p	integral defined by equation (12)
k_1, k_2, k_3	constants
ℓ	mixing length or length scale
ℓ_o	length scale with no extra rate of strain
L	body length

p	static pressure
P_o	free-stream static pressure
q	$(\overline{u^2} + \overline{v^2} + \overline{w^2})^{\frac{1}{2}}$
Q	$(U^2 + V^2)^{\frac{1}{2}}$
r	radial distance
r_o	local radius of the body
r_m	maximum r_o
Re	Reynolds number ($= U_o L/\nu$)
S	a representative area (maximum cross-sectional area of the body)
u	fluctuating velocity in the x-direction
U	mean velocity in the x-direction
U_c	mean velocity in axial direction at wake center
$\overline{U}_c$	$1 - U_c/U_\delta$
U_d	defect velocity ($= U_o - U$)
$U_{d_{max}}$	maximum U_d
U_o	velocity of the approach stream
v	fluctuating velocity in the y-direction
V	mean velocity in the y-direction
w	fluctuating velocity in the azimuthal direction
x	coordinate parallel to the body surface and the centerline of the wake
X	axial coordinate
X_m	X where $r_o = r_m$
y	coordinate normal to the surface
$y_{\frac{1}{2}}$	y where $U_d = \frac{1}{2}U_{d_{max}}$

α	constant
δ	boundary-layer thickness or radius of the wake
δ_o	δ at the tail of the body
δ^*	radius of the displacement surface
$\overline{\delta_1}$	planar displacement thickness (equation 2)
$\overline{\delta_2}$	planar momentum thickness (equation 2)
Δ_1	mass-deficit area (equation 3)
Δ_2	momentum-deficit area (equation 3)
$\Delta_{2\infty}$	asymptotic value of Δ_2
ϵ	eddy viscosity
θ	angle between axis and tangent to the body surface
θ_o	θ at the tail of the body
κ	longitudinal curvature of the body surface
λ	constant
μ	dynamic viscosity
Λ	Pohlhausen parameter
ν	kinematic viscosity
ξ_1	X/X_m
ξ_2	$(L - X)/(L - X_m)$
ρ	density
τ	total shear stress $(= \mu\frac{\partial U}{\partial y} - \rho\overline{uv})$
τ_{max}	maximum τ
ψ_e	stream function at $y = \delta$

Subscripts

c	quantities evaluated at the wake centerline
M	quantities evaluated at the fixed matching boundary in iteration
w	quantities evaluated at the wall
δ	quantities evaluated at the edge of the boundary layer or wake

CHAPTER I

INTRODUCTION

The flow past a body of revolution with a pointed tail is considered. If the shape of the body is such that there is no separation, conservation of mass requires the boundary layer to grow in thickness up to the tail. For most shapes at large Reynolds numbers, this leads to a thick turbulent boundary layer over the rear of the body. In this region, which may constitute as much as the rear third or quarter of the body length, the usual thin boundary-layer assumptions fail. Specifically, it is observed that (a) the boundary-layer thickness becomes comparable with, and even larger than, the local transverse and longitudinal radii of surface curvature, (b) the component of velocity normal to the surface is not small compared with the longitudinal component, implying a substantial variation of the longitudinal curvature of the mean streamlines across the boundary layer, (c) the pressure gradient in the direction normal to the surface, associated with the surface and streamline curvature, cannot be neglected, and (d) the surface pressure distribution does not conform with that predicted by inviscid-flow theory. Taken together, these flow features indicate a strong interaction between the flow in the boundary layer and the external flow. Since the boundary layer results in a broad wake, the interaction involves the wake also.

These flow features have been documented in the measurements of Patel, Nakayama and Damian (1974) in the tail region of a modified spheroid. These measurements also led to the development of a simple integral entrainment method (Patel, 1974) and a similarity-law entrainment method (Granville, 1975) for the calculation of thick axisymmetric turbulent boundary layers. Since the experiments indicated that a proper theoretical treatment of the flow in the tail region should consider the interaction mentioned earlier, an iterative technique was proposed (Nakayama et al., 1976a,b) for the solution of the viscous and inviscid regions by successive approximations. This necessitated the incorporation of the body wake in the interaction process, and therefore a procedure was proposed for the continuation of the boundary-layer calculations into the wake. The lack of detailed data in the near wake of an unseparated body of revolution, however, precluded the assessment of the proposed extension of the boundary-layer calculation method into the wake, and provided the incentive to perform a new set of experiments.

The selection of the model shape for these experiments was based on a number of considerations, as well as on the experience gained from the previous experiments (Patel et al., 1974). First of all, it was desirable to select a practically important configuration rather than a simple geometric shape. Secondly, in order to highlight the influence of strong transverse surface curvature, it was necessary to maintain a thick boundary layer over an extended region of the body. Thirdly, it was essential to avoid separation in the tail region so

that the near wake could be explored in detail. Finally, in order to avoid the experimental (Patel et al., 1974) and theoretical (Nakayama et al., 1976b) difficulties encountered in the earlier work with a conical tail, it was thought convenient to consider a cusped-tail body so that the transition from the boundary layer to the wake would be smooth. The study of Parsons and Goodson (1972), published at the time these experiments were being planned, provided a family of low-drag forms, from which the so-called F-57 body was selected. The experimental investigation of the boundary layer and wake of this body is described in Chapter II.

Although the overall iteration scheme due to Nakayama, Patel and Landweber (1976a,b) proved quite successful when applied to the earlier spheroid measurements, the treatment of the boundary layer using the integral method, and particularly its extension to calculate the near wake, required many assumptions which remained untested. The performance of the integral approach is therefore reexamined in Chapter III in the light of the new data. It is shown that, although such methods give adequate information on the gross behavior of the boundary layer and wake, they are not altogether suitable for interactive calculations which require more detailed knowledge of the flow behavior in the tail region.

Chapter IV therefore describes the development of a more rational procedure in which the differential equations of the thick boundary layer and the near wake are solved by means of a numerical method. This procedure provides not only a more reliable vehicle for the

extension of the boundary-layer solution into the wake, but also yields the detailed information on the velocity profiles required for the interaction calculations.

The new differential method is incorporated in the iteration scheme of Nakayama, Patel and Landweber (1976a,b), but with a fixed matching boundary, as proposed by Mahgoub and Bradshaw (1977). Chapter V describes the various steps in the complete calculation in which the external inviscid flow is matched with the boundary layer and the wake by successive iterations at a predetermined boundary in the inviscid-flow region close to the edge of the boundary layer and wake. The success of the iterative procedure is demonstrated by comparison with the data obtained from the low-drag body as well as the modified spheroid.

Finally, the major conclusions drawn from the study are summarized in Chapter VI.

Interactions between viscous and inviscid flow regions occur in many situations and the associated literature is vast. The axisymmetric problem considered here is one of a large class of such problems. However, in most instances, the influence of the boundary layer on the external inviscid flow is represented by adding the displacement thickness to the body shape and either accounting for the near wake by somewhat arbitrary extrapolations (Huang et al., 1976) or, more commonly, ignoring it altogether. A detailed review of such procedures is not made here since the primary emphasis in the

present work is placed on the detailed exploration of the flow within the thick boundary layer and near wake.

CHAPTER II

EXPERIMENTAL STUDY ON THE LOW-DRAG BODY

II.1 Experimental Setup and Instrumentation

II.1.1 Wind Tunnel and Model. The experiments were performed in the large wind tunnel (Patel et al., 1974) of the Iowa Institute of Hydraulic Research. The coordinates of the F-57 low-drag body of Parsons and Goodson (1972) selected for the present study are given by

$$\frac{r_o}{r_m} = \begin{cases} [(-1.1723\xi_1^4 + 0.7088\xi_1^3 + 1.0993\xi_1^2 + 0.3642\xi_1)]^{\frac{1}{2}} \\ \qquad\qquad (0 \le X \le X_m) \\ [(-0.11996\xi_2^5 - 2.58278\xi_2^4 + 3.52544\xi_2^3 + 0.17730\xi_2^2)]^{\frac{1}{2}} \\ \qquad\qquad (X_m \le X \le L) \end{cases}$$

where $\xi_1 = X/X_m$, $\xi_2 = (L-X)/(L-X_m)$, X is the axial distance measured from the nose, r_o is the local radius, X_m is the axial location of the maximum radius r_m, and L is the total length of the body. The location of maximum radius is $X_m/L = 0.4446$ and the length-to-maximum-diameter ratio is $L/2r_m = 4.2735$.

A model was constructed with L = 1.219 m. It was made hollow and in two parts in order to accommodate a scanivalve which was

connected to forty-seven pressure taps on the surface. Thirty-two pressure taps lay on a single generator on the surface, while the other fifteen were spaced circumferentially at three axial locations, X/L = 0.104, 0.445, and 0.771, for use in model adjustment. The main body of the model was made of seasoned wood, but metal nose and tail pieces, 5.08 cm and 12.70 cm in length, respectively, were used to provide accuracy and durability. The major features of the model are shown in Figure 1.

II.1.2 Model Alignment. The model was mounted in the wind tunnel by means of eight 0.84 mm diameter steel wires in tension (Figure 1). Each wire was provided with a screw coupling so that its length could be adjusted to locate the model at the desired position. Several means were employed to ascertain axial symmetry of the model in the wind tunnel:

(A) The static pressures measured along the circumference at three axial locations were used to guide the preliminary model position.

(B) Three 1.651 mm diameter Preston tubes were then mounted on the surface at X/L = 0.771 at 120-degree intervals. Further adjustments in model location were made until these tubes gave nearly equal readings.

(C) A total-head tube and a hot wire were traversed across the wake of the body at X/L = 1.10 and 1.20 as the final check on axial symmetry. Satisfactory lateral symmetry was

observed in terms of the profiles of total pressure, mean velocity and turbulence intensity.

II.1.3 Instrumentation. Basically the same traversing mechanism as the one described in Patel et al. (1974) was used for the measurements in the boundary layer and the wake of the model. Suitable extensions of the mounting rails outside the tunnel were made to continue the measurements into the wake.

Micro-manometers and probes of standard design were used for the total- and static-pressure measurements. The static probe was mounted on a fixture which enabled the probe to be aligned with the local flow direction. This method provides somewhat improved accuracy in static-pressure measurements. The wall shear stress on the body was measured by using different sizes of Preston tubes with the calibration of Patel (1965). The wall pressure taps mentioned earlier were used to measure the surface pressure distribution.

Mean-velocities and Reynolds stresses within the boundary layer and the wake were measured by means of single-wire and cross-wire probes using the two-channel, constant-temperature, "Old-Gold-Model, Type 4-2H Hot-Wire Anemometer" and "Type 2 Mean-Product Computer" (Glover, 1972). These instruments were modified to make them compatible with the gold-plated series of probes made by DISA. In order to ascertain that proper matching had been achieved and, at the same time, to establish measurement procedures to be used, a series of preliminary tests was conducted in fully-developed turbulent flow in

a 5.08 cm diameter pipe. The measurements on the low-drag body were commenced only after achieving satisfactory agreement (mean velocity within 2 percent, and turbulence intensities within 15 percent) with the data of Laufer (1954) at a pipe Reynolds number of 50,000.

II.1.4 Transition Device. The computations of Parsons and Goodson (1972) had indicated that transition on the low-drag body would occur naturally at X/L = 0.475 over a wide range of Reynolds numbers. Surface pressure distributions and other flow diagnostics on the model, at a Reynolds number ($Re = U_o L/\nu$) of 1.2×10^6, indicated that, in reality, transition occurred as a result of laminar separation followed by a turbulent reattachment, the bubble being in the neighborhood of the predicted location of transition. In order to eliminate this somewhat unsteady separation bubble and establish well-defined conditions for the subsequent development of the turbulent boundary layer, a circular trip wire of 1.664 mm diameter was wrapped around the body at X/L = 0.475. Subsequent analysis of the data revealed that the choice of such a relatively large trip wire was somewhat unfortunate since its downstream influence (say 100 diameters) may have persisted up to X/L = 0.6, where the first set of detailed measurements was made. Nevertheless, since the main body of data of interest here was collected from stations further downstream, the overall influence of the trip wire may be considered negligible.

II.2 Mean-Flow Measurements

All measurements reported here were made at a Reynolds number, based on the approach velocity U_o and the body length L, of 1.2×10^6, which corresponded to a nominal approach velocity of 15.24 m/s. U_o and the static pressure P_o at the end of the tunnel contraction were monitored throughout the experiments and have been used as reference conditions to nondimensionalize the data.

II.2.1 Surface Pressure Distribution. The static pressure distribution on the body surface is shown in Figure 2. Also shown, for comparison, is the potential-flow pressure distribution computed using the method of Landweber (1951). The close agreement between the two over most of the body indicates that the influence of wind-tunnel blockage is quite small. The departure of the measured pressure distribution from the theoretical one over the rear 25 percent of the body length is a result of the large thickness of the boundary layer in that region and its interaction with the external inviscid flow. It is seen that the influence of the increasing boundary-layer thickness is to relieve the inviscid pressure gradient.

II.2.2 Upstream Laminar Boundary Layer. A single set of measurements was made in the laminar boundary layer upstream of the trip wire at the axial location X/L = 0.433. The velocity profile obtained by means of a flattened pitot tube is shown in Figure 3 along with two members of the Pohlhausen family of profiles, the values of the

Pohlhausen parameter Λ being chosen to span the value of -1.65 estimated from the local boundary-layer thickness, which was 1.93 mm, and the local pressure gradient.

II.2.3 Static Pressure Field. Figure 4 shows the variation of static pressure across the boundary layer and the wake at several axial positions in the range $0.551 < X/L < 2.472$. The convex longitudinal curvature of the body surface in the range $0.45 < X/L < 0.76$ apparently leads to the substantial increase in static pressure along the outward normal not only within the boundary layer but also for some distance beyond the edge of the boundary layer (which was determined from the distribution of total pressure and is indicated by the dotted line $y = \delta$). As the longitudinal curvature becomes concave and the boundary layer thickens as a result of the decreasing transverse radius r_o over the rear one-quarter of the body length, the trends of the static pressure variation are reversed, indicating that the mean streamlines are concave. The data in the near wake suggest that the streamlines become nearly straight within a short distance downstream of the tail.

The axial variation of static pressure at the edge of the boundary layer inferred from these measurements is compared in Figure 2 with the surface pressure distribution. The magnitude of the pressure difference between the surface of the body and the edge of the boundary layer is apparent from Figure 2.

The present data have been used to assess the importance of the static-pressure variation across the near wake in the prediction of

the overall drag coefficient of bodies of revolution using the conventional Squire-Young-type formula (Patel and Guven, 1976). The importance of this pressure variation in the boundary-layer-prediction procedures is discussed in subsequent chapters.

II.2.4 Mean-Velocity Profiles. Figure 5 shows the mean-velocity profiles across the boundary layer and wake at several axial stations. Here U and V are the components of velocity in the directions tangent and normal to the body surface, respectively, and Q is the resultant velocity, i.e. $(U^2 + V^2)^{\frac{1}{2}}$. Q was measured by means of a single hot-wire probe and was also obtained from the separate pitot and static-probe traverses. It is seen that the two sets of data are in close agreement. The U and V components were measured by means of a cross-wire probe. It is known that this technique is not altogether satisfactory insofar as accuracy of the mean-flow quantities is concerned. Nevertheless, the data show the relative magnitude of the two components and indicate that the normal component attains maximum values in the neighborhood of X/L = 0.92, where it is roughly 12 to 13 percent of the tangential component. The implication of this with regard to the validity of the thin boundary-layer assumptions is obvious.

The velocity and shear-stress profiles measured at the most downstream station in the wake, namely X/L = 2.472, are compared in Figure 6 with the most downstream measurements of Chevray (1968) and Schetz and others (Swanson et al., 1974; Chieng et al., 1974), and with the asymptotic axisymmetric wake profile. It will be recalled

that the measurements of Chevray were made in the wake of a prolate spheroid of axis ratio 6 : 1, where the boundary layer separated some distance upstream of the tail. The measurements of Schetz and others were made in the wake of an elongated body of axis ratio 12 : 1, consisting of a parabolic nose, a cylindrical middle body and a pointed stern, and it is not clear whether boundary-layer separation was encountered before the tail. The velocity distribution in the far wake is assumed to be (Schlichting, 1968)

$$\frac{U_d}{U_{d_{max}}} = \left\{ 1 - 0.293\left(\frac{y}{y_{\frac{1}{2}}} \right)^{3/2} \right\}^2 \qquad (1)$$

where U_d (= U_o - U) is the velocity defect, $U_{d_{max}}$ is its value at the wake center, and $y_{\frac{1}{2}}$ is the radial distance to the point where U_d is one-half of the maximum value $U_{d_{max}}$. The corresponding shear-stress profile is deduced by assuming a constant mixing length across the wake. It is seen from Figure 6 that the present measurements at X/L = 2.472 may be regarded as those corresponding to a fully-developed axisymmetric far wake, where the memory of the body which generated it is almost eliminated. It is, however, known (Rodi, 1975) that the mean velocity distribution in an axisymmetric wake continues to depend on body shape for quite large axial distances.

Figure 7 shows the variations of the velocity Q_c along the centerline of the wake and the total velocity Q_δ at the edge of the boundary layer and wake. It is observed that the velocity at the edge of the wake reaches the freestream value by about X/L = 1.25. This

is roughly 2.3 initial wake diameters, or one maximum body diameter, downstream of the tail. The wake develops under the influence of a small, favorable, axial pressure gradient over this region. The maximum velocity defect in the wake, $Q_\delta - Q_c$, is also seen to decrease rapidly within this distance. On the basis of these observations it may be conjectured that the so-called near wake is confined to this region, and we may expect the measurements further downstream to conform with the asymptotic wake behavior discussed above.

II.2.5 Integral Parameters. The velocity profiles deduced from the pitot and static traverses were integrated to determine the various types of integral parameters discussed earlier in Patel et al. (1974). The overall shape of velocity profile is best described by the so-called "planar" displacement and momentum thicknesses:

$$\overline{\delta_1} = \int_o^\delta (1 - \frac{U}{U_\delta})dy \ , \qquad \overline{\delta_2} = \int_o^\delta \frac{U}{U_\delta}(1 - \frac{U}{U_\delta})dy \quad (2)$$

which do not take the axial symmetry of the flow into account. On the other hand, the physical mass- and momentum-flux deficit areas in the boundary layer and the wake are given by the integrals

$$\Delta_1 = \int_o^\delta (1 - \frac{U}{U_\delta})rdy \ , \qquad \Delta_2 = \int_o^\delta \frac{U}{U_\delta}(1 - \frac{U}{U_\delta})rdy \quad (3)$$

respectively+. Here, U_δ is the velocity component at the edge of the

---

+ In view of the inaccuracies in the direct measurements of U, the integral parameters have been determined using Q. The error is within 3 percent for the most severe case in the thick boundary layer.

boundary layer and wake ($y = \delta$), tangent to the body surface for the boundary layer and parallel to the axis for the wake, r is the radial distance from the axis of symmetry and y is measured normal to the surface of the body. Thus, $r = r_o + y\cos\theta$, where θ is the angle between the axis and the tangent to the body surface, for the boundary layer, and $r = y$ for the wake.

The variations of $\overline{\delta}_2$ and Δ_2 with X/L in the turbulent boundary layer and wake, and the corresponding shape parameters, defined by

$$\overline{H} = \frac{\overline{\delta}_1}{\overline{\delta}_2} \quad , \qquad H = \frac{\Delta_1}{\Delta_2} \tag{4}$$

are shown in Figure 8. It should be noted that the total drag coefficient C_D of the body is related to the asymptotic value $\Delta_{2\infty}$ of the momentum-deficit area in the far wake via

$$C_D = \frac{D}{\frac{1}{2}\rho U_o^2 S} = \frac{4\pi\Delta_{2\infty}}{S} \tag{5}$$

where D is the drag force, S is a representative area of the body and ρ is the density of the fluid. The measurements at X/L = 2.472 indicate that the drag coefficient, based on frontal area, of the present body (with the trip wire) is 0.0092. $\overline{\delta}_2$, on the other hand, has no special physical significance, but the parameter $\overline{H}$ indicates the shape of the velocity distributions.

Finally, the normal distance by which the external inviscid-flow streamlines are displaced outward due to the presence of the boundary

layer and the wake, i.e. the displacement thickness δ^*, may be obtained from the relation (Patel et al., 1974)

$$r_o\delta^* \left(1 + \frac{1}{2}\frac{\delta^*}{r_o}\cos\theta\right) = \Delta_1 \qquad (6)$$

for the boundary layer, and

$$\frac{1}{2}\delta^{*2} = \Delta_1 \qquad (7)$$

for the wake. The displacement surface deduced in this manner is shown in Figure 9 along with the physical edge of the boundary layer and wake. It should be emphasized here that this figure was drawn to scale without any distortion so that it clearly illustrates what is meant by a THICK BOUNDARY LAYER. It is particularly interesting to note the magnitude of the displacement effect of the boundary layer over the rear one-quarter of the body and that in the near wake. The implication of this with regard to the boundary-layer and near-wake computation is discussed later on.

II.2.6 Wall Shear Stress. As mentioned earlier, three different Preston tubes of external diameters 1.651, 1.270 and 0.711 mm were used to measure the wall shear-stress distribution on the body. Figure 10 shows the results obtained with the largest and the smallest tubes. The data from the intermediate-size tube lay between these. The use of Preston tubes, of course, presupposes the validity of the usual law of the wall even in the thick axisymmetric boundary layer.

The small but systematic variation in the wall shear stress obtained with the three tubes indicated the need for an alternative approach. The velocity profile data were therefore replotted in the form suggested by Clauser, but using the extended law of the wall proposed by Patel (1973), to determine the wall shear stress compatible with that law. These results are also shown in Figure 10. It will be seen that substantial departures from the usual law of the wall (over the distance occupied by the Preston tube) are indicated only in the neighborhood of the tail ($X/L > 0.94$, say).

II.3 Turbulence Measurements

Hot-wire traverses were made at six axial stations in the boundary layer (X/L = 0.60, 0.80, 0.88, 0.92, 0.96 and 1.00) and six stations in the wake (X/L = 1.02, 1.06, 1.20, 1.30, 1.40 and 2.47). The mean-velocity profiles obtained in this manner were discussed earlier. The distributions of the four nonzero Reynolds stresses, namely $\overline{u^2}$, $\overline{v^2}$, $\overline{w^2}$ and $\overline{uv}$, are shown in Figures 11, 12, 13 and 14, respectively. It will be observed that two sets of data are shown in each figure for the station X/L = 1.00, which corresponds to the tail of the body. The only difference between these is the direction of traverse. Initially, a traverse was made normal to the axis of the body and the wake ($\theta = 0^{\circ}$), but since the semi-angle of the body tail is 5.7 degrees, another traverse was made ($\theta = 5.7^{\circ}$) in the direction normal to the surface of the body at the tail. Figures 11, 12 and 14 show that the results of the two traverses differ appreciably in

the distributions of $\overline{v^2}$ and $\overline{uv}$, and the data in terms of boundary-layer coordinates ($\theta = 5.7^{\circ}$) are more consistent. It is obvious that this ambiguity would not have arisen had the tail been exactly cusped. However, the present data indicate the need for a very careful treatment of the flow in the neighborhood of pointed tails where the change from the boundary-layer to the wake coordinates occurs abruptly. This will be considered in Chapter V. The data corresponding to $\theta = 5.7^{\circ}$ are used in the subsequent analysis. The estimated uncertainity level in the measured Reynolds stresses is indicated in Figure 14.

Insofar as the measurements of the Reynolds stresses in the thick boundary layer are concerned, it is observed that they are qualitatively similar to those made earlier in the tail region of a modified spheroid (Patel et al., 1974). Quantitatively, however, the present data are quite different from the earlier set due to the different pressure-gradient and surface-curvature histories.

The distributions of shear stress $\overline{uv}$ were used in conjunction with the mean-velocity profiles to calculate the variation of eddy viscosity,

$$-\overline{uv} = \epsilon\left(\frac{\partial U}{\partial y}\right) \tag{8}$$

and the corresponding variation of mixing length,

$$-\overline{uv} = \ell^2\left(\frac{\partial U}{\partial y}\right)^2 \tag{9}$$

They are shown in Figures 15 and 16, respectively. The mixing-length distributions of the boundary-layer data for the modified spheroid (Patel et al., 1974) are reproduced in Figure 17 for comparison. The data indicate a substantial reduction of eddy viscosity and mixing length as the boundary layer thickens towards the tail. They increase again with axial distance in the wake. The mixing length reaches a nearly constant value in the range $0.08 < \ell/\delta < 0.10$ at the most downstream station $X/L = 2.47$, where, as indicated earlier, the wake approaches a nearly fully-developed state. The major conclusion to be drawn from these measurements is that the characteristics of the turbulence in the region where the boundary layer is thick, and in the near wake, i.e. over $0.75 < X/L < 1.25$, say, are markedly different from those of a thin turbulent boundary layer and the asymptotic far wake.

Yet another quantity that is of interest in the discussion of the characteristics of the turbulence is the so-called structure parameter $a_1 = -\overline{uv}/q^2$, where $q^2 = \overline{u^2} + \overline{v^2} + \overline{w^2}$ is twice the turbulent kinetic energy. It would be recalled that, for most thin, turbulent shear layers, a_1 is nearly constant across the flow and equal to about 0.15. The distributions of a_1 across the boundary layer and wake of the low-drag body are shown in Figure 18. The corresponding results deduced from the modified-spheroid boundary layer (Patel et al., 1974) are shown in Figure 19. From Figure 18, it is seen that a_1 remains nearly constant around 0.14 in the inner one-half of the boundary layer on the low-drag body and indicates some reduction with normal

distance over the outer half. The data in the wake, however, appear to indicate nearly constant values again. Figure 19 indicates that a_1 diminishes with both x and y through the boundary layer of the modified spheroid, the minimum values of a_1 being reached at X/L = 0.93.

The observed reductions in ℓ for both bodies and in a_1 for the modified spheroid may be explained on the basis of the joint influence of the transverse and longitudinal surface curvatures on the turbulence structure if recourse is had to the results of some recent studies. Consider first the conventional curvature parameters in the two sets of experiments shown in Figure 20.

The ratio of the boundary-layer thickness to the transverse radius of curvature, δ/r_o, is seen to be more than twice as large in the low-drag body as in the spheroid. In both cases, however, δ/r_o is less than 0.4 up to X/L = 0.75 so that the boundary layers may be regarded as thin up to that station. Over the rear one-quarter of the body length, however, the influence of transverse curvature would prevail, not only through the geometrical terms in the equation of motion, e.g. $(\Delta_2/r_o)(dr_o/dx)$ in the integral momentum equation, but also through any direct effect on the turbulence.

The longitudinal surface curvature parameter $\kappa\delta$, where κ is the longitudinal surface curvature, is seen to be quite different for the two bodies. In the case of the modified spheroid, the curvature is convex upto X/L = 0.933 and zero thereafter due to the conical tail, while that of the low-drag body is initially convex and becomes concave for X/L > 0.772.

Now, several recent studies with nominally two-dimensional turbulent boundary layers (Bradshaw, 1969, 1973; So and Mellor, 1972, 1973, 1975; Meroney and Bradshaw, 1975; Ramaprian and Shivaprasad, 1977, 1978; Shivaprasad and Ramaprian, 1977, 1978) have indicated that even mild ($\kappa\delta \sim 0.01$) longitudinal surface curvature exerts a dramatic influence on the turbulence structure. In particular, it is noted that quantities such as the mixing length ℓ, the structure parameter a_1 and the shear-stress correlation coefficient $\overline{uv}/(\sqrt{\overline{u^2}}\sqrt{\overline{v^2}})$ are influenced markedly, and experiments indicate that convex streamline curvature leads to a reduction in these, whereas concave curvature has an opposite effect. While these studies in thin boundary layers, where the streamline curvature is dictated by that of the surface, would tend to indicate that the somewhat larger reduction in ℓ (compare Figure 17 with Figure 16) and the drastic reduction in a_1 (compare Figure 19 with Figure 18) observed on the modified spheroid may be attributed to the large, prolonged, convex longitudinal curvature of the surface, it should be noted that the rapid growth of the boundary layer over the tail tends to cancel out some of the convex curvature of the steamlines. Nevertheless, in view of the fact that the longitudinal streamline curvature in both experiments is large, it is possible that a part, if not all, of the changes in parameters such as ℓ and a_1 may be due to that factor.

Bradshaw (1973) has examined a vast array of experimental data, which include surface curvature, buoyancy, compressibility, rotation and other effects, to suggest that, whenever a thin shear layer

experiences an extra rate of strain, i.e. in addition to the usual one, $\partial U/\partial y$, the response of the turbulence parameters is an order of magnitude greater than one would expect from an observation of the appropriate extra terms in the mean-flow equations of momentum and continuity. Since the convergence of the streamlines, in planes parallel to the surface, in the present axisymmetric flow introduces an extra linear rate of strain, which is proportional to dr_o/dx, we may expect to see a direct effect of the transverse curvature on the turbulence. A detailed examination of the relative magnitudes and sense of these extra rates of strain on the two bodies indeed confirmed the observed reductions in the length-scale parameter ℓ.

In conclusion, it is noted that the turbulence measurements indicate, at least qualitatively, the importance of both the longitudinal and transverse surface curvatures. The quantitative description of these effects is pursued further in Chapter IV, where a simple heuristic model, due to Bradshaw (1973), is examined in order to obtain a turbulence closure equation for the solution of the differential equations of the thick boundary layer and near wake.

The complete set of data obtained from this investigation has been presented in a report by Patel and Lee (1977).

CHAPTER III

ASSESSMENT OF THE INTEGRAL METHOD

Patel (1974) has developed a simple integral method for the calculation of the thick axisymmetric turbulent boundary layer. Nakayama et al. (1976b) extended that to calculate the near wake by making some additional assumptions. Since only limited data were available at the time those methods were proposed, it is of interest to use the data from the low-drag body to verify the assumptions made in the boundary-layer method as well as those made in its extension to wakes.

III.1 Integral Correlations

The method of Patel (1974) is based on that of Head (1958) for thin two-dimensional boundary layers. It involves the simultaneous solution of the momentum integral equation for the thick axisymmetric boundary layer (Patel, 1974; Nakayama et al., 1976b), and an equation relating the rate of mass entrainment into the boundary layer to the shape of the velocity profile, together with a number of auxiliary relations between the planar and axisymmetric integral parameters deduced from assumed velocity-profile shapes,

$$\frac{d\Delta_2}{dx} + (H + 2)\frac{\Delta_2}{U_\delta}\frac{dU_\delta}{dx} - \frac{1}{2}C_f r_o - I_k - I_p = 0 \qquad (10)$$

with $$I_k = \kappa \int_o^\delta \frac{UV}{U_\delta^2} \, r dy \qquad (11)$$

and $$I_p = \frac{1}{U_\delta^2} \int_o^\delta r \frac{\partial}{\partial x} \left(\frac{p - p_\delta}{\rho} - \frac{V_\delta^2}{2} \right) dy \qquad (12)$$

$$C_E = \frac{1}{U_\delta r_\delta h_{1\delta}} \frac{d}{dx} \left[U_\delta (r_o \delta - \Delta_1 + \frac{1}{2} \delta^2 \cos\theta) \right] \qquad (13)^+$$

with $r_\delta = r_o + \delta\cos\theta$, $h_1 = 1 + \kappa\delta$ and the quantity within the square brackets represents the mass flux within the boundary layer.

For thick axisymmetric boundary layers, the additional assumptions required are: that the empirical correlation between the entrainment shape parameter $\overline{H^*} = (\delta - \overline{\delta_1})/\overline{\delta_2}$ and the usual shape parameter $\overline{H}$, and the correlation between the entrainment coefficient C_E and $\overline{H^*}$, are the same as in two-dimensional flow, provided the shape parameters are based only on the shape of the velocity profile (i.e. planar definitions are used), and that the friction coefficient C_f is related to $\overline{H}$ and $R_{\overline{\delta_2}}$ via a two-parameter family of velocity profiles.

The assumption concerning the shape-parameter correlation was verified directly in Nakayama et al. (1976b) using the then available data from boundary layer and wakes. Figure 21 shows that the data from the low-drag body support this observation. Upon closer

---

+ This definition of C_E differs slightly from that of Patel (1974) and is in agreement with the improvement suggested by Nakayama et al. (1976b) and Granville (1975).

examination, however, it is seen that there is a systematic departure from the boundary-layer correlation, and that the data from the most downstream wake stations are in better agreement with the $\overline{H^*}$ vs. $\overline{H}$ relation deduced from the asymptotic wake profile of equation (1). Wake calculations have been performed using both correlations to demonstrate their influence.

An attempt was made to deduce the variation of C_E with $\overline{H^*}$ using equation (13) and the measured values of the quantities appearing therein. The inaccuracies associated with the differentiation in equation (13), however, masked any systematic trend, and therefore the previous assumption that the correlation of Head continues to apply in the wake has been retained. The influence of this could then be determined by the performance of the overall solutions.

The method of Patel (1974), with the modification of C_E noted earlier, was used to predict the development of the boundary layer and the wake of the low-drag body. Since the tail of the low-drag body is nearly cusped, it was not necessary to change the coordinates abruptly at the tail and make a special analysis, as in Nakayama et al. (1976b), in order to continue the calculation into the wake. The assumption of an exponential velocity-profile family in the wake, suggested in Nakayama et al. (1976b), namely

$$\frac{U}{U_\delta} = 1 - \overline{U}_c \exp\left[-\lambda\left(\frac{y}{\delta}\right)^2\right] \tag{14}$$

where

$$\overline{U}_c = 1 - \frac{U_c}{U_\delta}$$

U_c is the velocity at the wake center and λ is a parameter, was retained. The inter-relationships between the planar and the axisymmetric integral parameters were obtained in Nakayama et al. (1976b) by using $\lambda = 3.22$ in equation (14), performing the integrations in equations (2) and (3) up to $y/\delta = 1$, and curve-fitting. In the present work, this procedure has been simplified by setting the outer limit of integration equal to infinity so that the necessary relations are obtained analytically. These are

$$\left.\begin{aligned} \Delta_1 &= \frac{k_2}{\bar{U}_c(k_1 - \bar{U}_c)^2}\,\bar{\delta}_2^2 \\ \Delta_2 &= \frac{k_2 - k_3\bar{U}_c}{\bar{U}_c(k_1 - \bar{U}_c)^2}\,\bar{\delta}_2^2 \\ H &= \frac{k_2}{k_2 - k_3\bar{U}_c} \\ \text{and} \qquad \bar{H} &= \frac{k_1}{k_1 - \bar{U}_c} \end{aligned}\right\} \qquad (15)$$

where $k_1 = \sqrt{2}$, $k_2 = 4/\pi$, and $k_3 = 2/\pi$. It is of interest to note that these relations are independent of λ and therefore a particular constant value of λ is not required.

III.2 Comparison of Calculations with Experimental Data

The boundary-layer calculation on the low-drag body was started at $X/L = 0.70$, where the boundary layer has recovered from the

influence of the trip wire, and terminated at the tail. The initial conditions for the wake were provided by requiring the continuity of the physical mass- and momentum-deficits there; i.e. Δ_2 and H remain continuous in going from the boundary layer to the wake. Since the integral method is basically a two-parameter method, this leads to a discontinuity of the other parameters, such as the boundary layer thickness, δ. The calculation was terminated in the far wake, where the momentum deficit approaches a constant value.

A set of calculations was first performed using only the pressure distribution along the body surface and wake centerline (i.e. with $I_k = I_p = 0$ in equation (10), as suggested by Patel (1974)), and the two alternative shape-parameter relations $\overline{H^*}(\overline{H})$ (Figure 21) in the wake. The results of these are shown in Figure 22 and identified as curves A and B. It is seen that the method predicts most of the quantities reasonably well in the boundary layer. The performance of the method in the wake is not as good as that for the boundary layer. This is due partly to the retention of the boundary-layer entrainment correlation, and more likely to the inadequacy of the exponential velocity-profile family used to describe the velocity distribution in the near as well as the far wake. The difference between curves A and B, which correspond to the two different shape-parameter relations, clearly indicates the need for the introduction of another parameter which would govern the gradual change from the boundary-layer profile at the tail to the asymptotic profile in the far wake. Although such an additional parameter would eliminate the discontinuity

in δ (Figure 22a) and improve the prediction of the near wake, it is not entirely clear what additional equation could be used to determine its streamwise distribution within the framework of an integral method.

Another possible source of the disagreement between the calculations and experimental data is the use of the pressure distribution on the body surface and the wake centerline to compensate for the neglected static pressure and curvature integrals (I_p and I_k) in the momentum integral equation. An attempt has been made to evaluate these integrals from the experimental data. The procedure that has been adopted is described in the Appendix A. Although this involves several approximations and inaccuracies stemming from the differentiation of ill-defined quantities, such as the boundary-layer and wake thicknesses and the normal velocity at the edge of the boundary layer and the wake, it is seen from Figure 23 that the two integrals are not small in comparison with some of the other terms in the momentum integral equation. A similar conclusion was drawn by Patel and Guven (1976) from their analysis of the same data in order to explore the importance of the near wake in the calculation of the viscous resistance of axisymmetric bodies using conventional extrapolation formulae.

A second set of calculations was performed in which the momentum integral equation was solved using the estimated values of I_p and I_k and the velocity distribution measured at the edge of the boundary layer in place of that inferred from the pressure distribution on the body surface and the wake centerline. The effective value of I_k in the near wake was estimated simply by fairing the value at the tail

to zero in the far wake, as shown in Figure 23. The results of these calculations are shown in Figure 22 as curves C and D, corresponding again to the two shape-parameter relations for the wake. The relatively small differences between this and the previous set of calculations suggest that the use of the pressure distribution on the surface and wake centerline to account for the effects of I_p and I_k, as recommended by Patel (1974), is a good engineering approximation. However, the results of the calculations also indicate that such an approximation can be discarded in favor of the correct momentum integral equation, equation (10), provided the values of I_p and I_k can be determined a priori, as is the case in an interactive scheme such as that of Nakayama et al. (1976b).

CHAPTER IV

DEVELOPMENT OF THE DIFFERENTIAL METHOD

In the previous chapter, the simple integral method of Patel (1974) and its extension to the wake were re-evaluated in the light of the experimental data from the low-drag body. Although the method appears to be adequate for rapid calculations, it involves several gross assumptions and yet does not give the detailed information that is necessary to incorporate it in an iterative calculation procedure, such as that of Nakayama et al. (1976a,b), so that a complete solution can be obtained for the flow in the tail region. The difficulties of the integral method arise from the treatment of the static-pressure variation across the flow and the representation of the velocity profiles in the boundary layer and wake by a limited number of parameters. Nakayama et al. (1976b) used a simple profile family for the normal component of velocity to evaluate the integrals I_p and I_k in the momentum equation and thereby introduced additional approximations. Further complications resulted from the separate integral analysis that was required to continue the boundary-layer solution into the wake at the tail of the body. It was therefore decided to explore the possibility of using a numerical method for the direct solution of the differential equations of a thick, axisymmetric boundary layer and wake, since then the information required for the calculation of the external flow could be obtained much more directly.

IV.1 Differential Equations

On the basis of the experimental observations and order-of-magnitude considerations, it can be shown (Bradshaw et al., 1967; Nakayama et al., 1976b) that the momentum and continuity equations of a thick, axisymmetric turbulent boundary layer are

$$\frac{U}{h_1}\frac{\partial U}{\partial x} + V\frac{\partial U}{\partial y} + \frac{\kappa}{h_1}UV + \frac{1}{\rho h_1}\frac{\partial p}{\partial x} - \frac{1}{r h_1}\frac{\partial}{\partial y}\left(\frac{h_1 r \tau}{\rho}\right) = 0 \quad (16)^{+}$$

$$\frac{U}{h_1}\frac{\partial V}{\partial x} + V\frac{\partial V}{\partial y} - \frac{\kappa}{h_1}U^2 + \frac{1}{\rho}\frac{\partial p}{\partial y} = 0 \quad (17)$$

$$\frac{\partial}{\partial x}(Ur) + \frac{\partial}{\partial y}(r h_1 V) = 0 \quad (18)$$

where $h_1 = 1 + \kappa y$; $\tau = -\rho\overline{uv} + \mu\frac{\partial U}{\partial y}$, μ being the dynamic viscosity of the fluid, and the other symbols have been defined earlier. Equation (17), in which the viscous and turbulence terms have been neglected, implies that the variation of static pressure across the boundary layer is associated primarily with the curvature of the mean-flow streamlines.

Equations (16), (17) and (18) contain four unknowns, namely U, V, p and $\overline{uv}$. Even when a turbulence model is introduced for $\overline{uv}$, the resulting set of equations cannot be solved by a marching technique.

+ In Appendix B the magnitude of each term in equation (16) is analyzed on the basis of the data from the low-drag-body experiment.

This is due to the presence of the pressure as an unknown. However, one approach to the solution of this set of equations is to solve equations (16) and (18), by a marching procedure, for U and V with some assumed pressure field $p(x,y)$. The y-momentum equation can then be used to update the pressure field. This is an iteration scheme in which the solution of p and the y-momentum equation lags one iteration behind the velocity field. Since the physical problem under consideration requires the matching of the boundary layer and wake solution with the external flow, and this is accomplished by an iterative procedure, the uncoupling of the y-momentum equation from the equations for x-momentum and continuity does not pose a serious difficulty.

IV.2 Turbulence Model

Before describing the solution procedure, the turbulence model of Bradshaw, Ferriss and Atwell (1967) that has been adopted for the present problem is discussed. According to that model, the equation for the conservation of turbulent kinetic energy is transformed into one for the Reynolds stress $\tau = -\rho\overline{uv}$:

$$\frac{1}{2a_1}\left(\frac{U}{h_1}\frac{\partial \tau}{\partial x} + V\frac{\partial \tau}{\partial y}\right) - \tau\left(\frac{\partial U}{\partial y} - \kappa U\right) + \frac{1}{r}\frac{\partial}{\partial y}\left(rG\frac{\tau}{a_1^{3/2}}\sqrt{\frac{\tau_{max}}{\rho}}\right)$$

$$+ \frac{1}{\ell}\frac{\tau^{3/2}}{\rho^{1/2}} = 0 \qquad (19)$$

where $a_1 (=-\overline{uv}/q^2)$ is a constant (=0.15), $G(y/\delta)$ is a diffusion function and $\ell(y/\delta)$ is a length-scale function identified with the usual mixing

length. Bradshaw et al. (1967) have demonstrated that for a variety of thin two-dimensional boundary-layer flows, G and ℓ may be regarded as universal functions of y/δ, as shown in Figure 24, and that a_1 = constant is a realistic assumption. As discussed in Chapter II, the data from the two experiments of thick boundary layer and wake, on the other hand, suggest that a_1 is not constant across the boundary layer and that the distribution of ℓ changes markedly as the boundary layer thickens. Numerical experiments performed here and elsewhere also indicate that the overall prediction of the boundary layer is primarily dependent on the assumption concerning ℓ, but quite insensitive to the value of a_1 and the diffusion function G. In order to utilize equation (19) in the thick boundary layer and the near wake it is necessary to allow for the variation of ℓ from the universal distribution in a thin boundary layer.

Bradshaw (1973) has suggested that, for <u>thin</u> shear layers and <u>small</u> extra rates of strain, a simple linear correction formula for ℓ is adequate. Thus, he proposed

$$\frac{\ell}{\ell_o} = 1 + \frac{\alpha e}{\partial U/\partial y} \tag{20}$$

where ℓ_o is the length scale with the usual rate of strain $\partial U/\partial y$, ℓ is the length scale with the extra rate of strain e, and α is a constant of the order of 10. As noted earlier, for the axisymmetric problem being considered here, there are two extra rates of strain:

$$e_{\ell} = - \frac{\kappa U}{1 + \kappa y} \tag{21}$$

due to the longitudinal curvature, and

$$e_t = \frac{U}{1 + \kappa y} \frac{1}{r} \frac{\partial r}{\partial x} = \frac{U}{r} \frac{dr_o}{dx} \tag{22}$$

due to the convergence or divergence of the streamlines (in planes parallel to the surface) associated with the changes in the transverse curvature. The former is a shearing strain while the latter is a plain strain, and it is not certain whether the two effects can be added simply in using equation (20), as recommended by Bradshaw (1973). If this is the case, however, we would expect a greater reduction in ℓ in the tail region of the modified spheroid, where κ is positive and dr_o/dx is negative, than on the low-drag body, where κ becomes negative and would therefore tend to offset the influence of the negative dr_o/dx. Although the data shown in Figures 16 and 17 appear to bear this out to some extent, a direct comparison between equations (20), (21) and (22) and the data was not attempted, in view of Bradshaw's (Bradshaw and Unsworth, 1976) assertion that equation (20) should be used in conjunction with a simple rate equation which accounts for the upstream extra rate-of-strain history. He proposed

$$\frac{\ell}{\ell_o} = 1 + \frac{\alpha e_{eff}}{\partial U/\partial y} \tag{23}$$

and

$$\frac{d}{dx} (e_{eff}) = \frac{e - e_{eff}}{10\delta} \tag{24}$$

where e is the actual rate of strain, e_{eff} is its effective value and 10δ represents the "lag length" over which the boundary layer responds to a change in e. In order to determine the merit of this proposal, it is of course necessary to incorporate it in an actual calculation and make a comparison between the prediction and measurement. Such an attempt has been made here.

IV.3 Method of Solution

A numerical method available for the solution of equations corresponding to equations (16), (18) and (19) for a thin two-dimensional boundary layer was modified to introduce the longitudinal- and transverse-curvature terms. Changes were made such that a prescribed variation, across the boundary layer, of the pressure gradient $\partial p/\partial x(y)$ could be used. This implies that the pressure field is known a priori. The solution of equations (16), (18) and (19) together with equations (21), (22), (23) and (24) can then be obtained through step-by-step integration by marching downstream from some initial station where the velocity and shear-stress profiles are prescribed. A staggered-mesh, explicit numerical scheme, similar to that used by Nash (1969), was used to integrate the equations in the domain between the first mesh point away from the surface (or the wake centerline) to some distance, typically 1.25δ outside the boundary layer and the wake. The fifteen mesh points across the boundary layer are distributed nonuniformly to provide a greater concentration near the wall and the wake centerline. Instead of carrying out the

integration of the equations up to the wall, i.e. through the viscous sublayer and the blending zone, the numerical solution at the first mesh point, located in the fully turbulent part of the boundary layer, is matched to the wall using the law of the wall.

In the extension of the method to the wake, the matching between the first mesh point and the wake centerline is accomplished by using the conditions $\partial U/\partial y = 0$ and $\tau = 0$ on the centerline. The main differences between the boundary-layer and wake calculation procedures are therefore the treatment of the flow between the first mesh point and the wall or the wake centerline, and the change in ℓ_o at the tail (see Figure 24). Note that the local value of ℓ in the boundary layer as well as the wake is different from ℓ_o due to the lag equation (23). However, the length scale recovers the reference distribution ℓ_o asymptotically in the far wake. Since the near-wake data from the low-drag body indicated that most of the adjustment from the boundary layer to the far wake is accomplished over roughly five initial wake thicknesses, the lag length for the wake calculation was taken to be 5δ, rather than 10δ used for the boundary-layer calculation on the basis of Bradshaw's (1973) suggestion. Since the extra rates of strain vanish at the tail ($\kappa = 0$, $dr_o/dx = 0$), the length scale approaches the ℓ_o distribution within about five wake radii downstream of the tail.

IV.4 Comparison with Experimental Data

Preliminary calculations performed with the differential method described above quickly indicated that the extra rates of strain in

both experiments were much larger than those examined by Bradshaw (1973) in support of the linear length-scale correction formula of equation (23). In fact, the use of the linear formula led to a rapid decrease in ℓ and indicated almost total destruction of the Reynolds stress across the boundary layer in the tail region and the near wake. In view of this, recourse was had to the nonlinear correction formula in the form suggested earlier by Bradshaw (1969), namely

$$\frac{\ell}{\ell_o} = \left\{1 - \frac{\alpha e_{eff}}{\partial U/\partial y}\right\}^{-1} \qquad (23a)$$

which reduces to the linear one, equation (23), for small extra rates of strain. Equations (16), (18) and (19), together with (21), (22), (23a) and (24), were then solved with the following inputs:

A. the measured wall pressure distribution C_{pw} (i.e. no normal pressure variation) and $\ell(y/\delta) = \ell_o(y/\delta)$

B. the measured C_{pw} with $\ell(y/\delta)$ corrected for only the longitudinal curvature ($e = e_\ell$)

C. the measured C_{pw} with $\ell(y/\delta)$ corrected for only the streamline convergence ($e = e_t$)

D. as above, but with $e = e_\ell + e_t$

E. using $e = e_\ell + e_t$ in equations (23a) and (24), and a variable $\partial p/\partial x$ across the boundary layer evaluated by assuming a linear variation in $\partial p/\partial x$ from $y = 0$ to $y = \delta$ and using the measured values of C_{pw}, $C_{p\delta}$ and δ.

Thus, case A corresponds to an axisymmetric boundary layer with thin,

two-dimensional boundary-layer physics. The other cases enable the evaluation of the relative influence of the extra rates of strain as well as the static-pressure variation through the boundary layer. The calculations were started with the velocity and shear-stress profiles measured at X/L = 0.662 on the modified spheroid and at X/L = 0.601 on the low-drag body.

The major results of the calculations are summarized in Figure 25(a-m) for the low-drag body and in Figure 26(a-i) for the modified spheroid. However, in the latter case the calculations are restricted to the boundary layer since detailed measurements were not made in the wake. Both figures contain comparisons between the experimental and calculated velocity, shear-stress and mixing-length profiles at a few representative axial stations as well as the development of the integral parameters $\overline{\delta_2}$, Δ_2, $\overline{H}$, H and C_f with axial distance. In the interest of clarity, the results of all the calculations (cases A through E) are shown only at one axial station (Figures 25c and 26c), those at other stations being qualitatively similar.

Considering the most detailed figures, 25c and 26c, first, it is clear that the predictions are rather poor when the length scale ℓ is assumed to be the same as that in a thin boundary layer (case A). This is particularly evident in the prediction of the shear-stress profiles across the boundary layer and the near wake. Incorporation of the correction to ℓ to account for the extra rate of strain due to longitudinal curvature (cae B) leads to a marginal improvement in the case of the low-drag body and a dramatic improvement for the

modified spheroid. This is to be expected in view of the grossly different surface-curvature histories of the two bodies as noted earlier (Figure 20). Nevertheless, it is clear that this correction by itself is not sufficient to account for the differences between the data and the calculations with thin boundary-layer turbulence models (case A). The application of the correction for the extra rate of strain due to the transverse curvature (case C) appears to account for a major portion of these differences for both bodies. The influence of transverse curvature is in fact seen to be somewhat larger for the low-drag body, as would be expected from the fact that δ/r_o is greater in that case (Figure 20). The simple addition of the effects of the two rates of strain (case D) leads to a significant improvement in the prediction of both the velocity profiles and the shear stress profiles. The incoporation of a variable pressure gradient across the boundary layer (case E), which is an attempt to account for the normal pressure gradients, appears to make a significant improvement in the prediction of the velocity profile in the case of the modified spheroid, but its influence is small, and confined to the outer part of the boundary layer, in the case of the low-drag body.

Examination of the velocity and shear-stress profiles at several axial stations shown in Figures 25(b-g) and 26(b-d) suggests that the incorporation of the nonlinear length-scale correction of equation (23a), the associated rate equation (24) and the static-pressure variation in the equations of the thick boundary layer, which already

include the direct longitudinal- and transverse-curvature terms, leads to satisfactory overall agreement with the data for both bodies. It is particularly noteworthy that the velocity and shear-stress distributions in the far wake (X/L = 2.472) of the low-drag body are predicted with good accuracy. The level of agreement can obviously be improved further by appropriate modifications in the empirical functions in the turbulent kinetic-energy equation and changes in the lag-length used in the length-scale equation. The predictions of the shear-stress profiles are consistent with those of the mixing-length distributions shown in Figures 25(h,i) and 26e insofar as lower shear stresses correspond to an over-correction in the mixing length. These comparisons provide further insight into the manner in which the length scale must be modified to improve the correlation between the calculation method and experiment. It is apparent that the consistent discrepancy between the calculated and measured velocity and shear-stress profiles near the outer edge of the boundary layer and wake stems from a poor representation of the length-scale distribution.

It is interesting to note that, for both bodies, the calculation procedure predicts normal components of mean velocity which are of the same order of magnitude as those measured. The relatively close agreement between the predictions and experiment for both components of velocity is perhaps a good indication of the axial symmetry achieved in the experiments. The large values of the normal velocity and the influence of static-pressure variation noted above would appear to indicate that incorporation of the y-momentum equation in

the calculation procedure would be worthwhile. Note that this has been avoided in the present calculations by using the measured pressure distributions at the surface and the outer edge of the boundary layer.

Finally, the comparisons made in Figures 25(j-m) and 26(f-i) with respect to the integral parameters show several interesting and consistent features. It is observed that the prediction of the physical thickness of the boundary layer and the wake is insensitive to the changes in ℓ as well as the inclusion of static-pressure variation. The underestimation of the thickness is associated with the discrepancy, noted earlier, in the velocity profile near the outer edge of the boundary layer and wake. The planar momentum thickness $\overline{\delta}_2$ and the momentum-deficit area Δ_2 are also insensitive to changes in ℓ. The variation of static pressure across the boundary layer appears to make a small but noticeable contribution to the development of Δ_2 in both cases. However, it is not large enough to account for the differences between the calculations and experiment. The predictions of the shape parameters $\overline{H}$ and H, presented in Figures 25l and 26h, appear to be satisfactory, especially in view of the rather large scale of the plots. Nevertheless, there is a systematic difference between the data and the calculation in the tail region and wake of the low-drag body. As indicated earlier, this can be improved by modifications in the empirical functions and the lag length. The predictions of the wall shear stress, shown in Figures 25m and 26i, indicate that the present method gives acceptable results for both bodies.

CHAPTER V

VISCOUS-INVISCID FLOW INTERACTION

The differential method for the calculation of the boundary layer and wake was described in the previous chapter. Note that the method involves the solution of the x-momentum, continuity and turbulent kinetic-energy equations to determine the velocity and shear-stress distributions. Thus far, it has been assumed that the variation of pressure, $p(x,y)$, along and across the boundary layer and wake is known, so that the y-momentum equation is not required. The performance of the method has been assessed by using the measured pressure distribution.

In order to solve the problem completely, however, it is necessary to include the pressure as an unknown and therefore incorporate the y-momentum equation into the solution procedure. Since the pressure boundary condition at the outer edge of the boundary layer and wake is not known a priori, it is also necessary to solve for the irrotational flow exterior to the boundary layer and wake, and match the inner and outer solutions at a prescribed fixed boundary just outside $y = \delta$, i.e. at $y_M = 1.25\delta$, where δ is the boundary-layer thickness from the first boundary-layer and wake solution. The overall solution strategy is therefore similar to that proposed by Nakayama et al. (1976a,b). The main difference lies in the method of

solution of the boundary layer and wake, since it is proposed to use the differential method in place of the integral approach.

Assume that the shape of the body, the Reynolds number and the location of transition are all prescribed. The objective of the complete solution is then to determine (a) the pressure distribution on the surface of the body and along the centerline of the wake, and (b) the characteristics of the boundary layer and wake. The latter would include velocity and shear-stress profiles and the variation of static pressure across the flow. This information can then be used to obtain the resistance of the body. The solution involves the following steps:

(A) Calculation of the inviscid flow past the body with the boundary layer and wake neglected.

(B) An approximate solution of the boundary layer and wake, using only the surface pressure distribution obtained in step (A), to determine $y_M(x)$ and $\psi_M(x)$, where ψ_M is the stream function at the boundary y_M.

(C) Solution of the exterior irrotational flow ($y > \delta$) using the $\psi_M(x, y_M)$ obtained in step (B) or step (E). This yields the pressure distribution $p_M(x)$ along y_M.

(D) Integration of the y-momentum equation (17) from y_M to $y = 0$ using the velocity field determined in the previous boundary layer and wake calculation. This yields $p(x,y)$ within the boundary layer and wake. Differentiation yields $\partial p/\partial x(y)$.

(E) A recalculation of the boundary layer and wake using $\partial p/\partial x(y)$ to determine the velocity field as well as $\psi_M(x)$.

(F) Repetition of steps (C) through (E) until convergence is obtained within a specified tolerance level.

In what follows some of the peculiarities of the calculations in the various steps for the low-drag body and the modified spheroid are described briefly.

V.1 Initial Inviscid Solution

The initial inviscid-flow solution may be obtained by one of several well known methods. Here the method of Landweber (1951), based on an integral equation of the first kind, has been used. The results of such a calculation for the low-drag body are shown in Figure 2. When a rear stagnation point is present (as in the case of the modified spheroid), the subsequent boundary layer calculation would predict separation ahead of the tail, although there is no separation in reality due to the relief of the pressure gradient by the viscous-inviscid interaction. This difficulty is then overcome by arbitrarily prescribing a lower tail pressure and fairing it to the inviscid solution over a short distance upstream of the tail. An initial guess for the variation of pressure along the centerline of the wake, required in the calculation of the wake, is also made by providing an exponential reduction in pressure from the tail to that in the approach stream over a distance, 0.5L, from the tail.

V.2 First Solution of the Boundary Layer and Wake

This calculation is started from the nose of the body. The laminar boundary layer is calculated by an axisymmetric-flow version of the method of Thwaites (Schlichting, 1968). This calculation is terminated at laminar separation or the prescribed transition location, whichever occurs first.

The initial velocity profile for the turbulent boundary layer is constructed by using Coles' profile family because the boundary layer is still thin immediately after transition. The parameters C_f and δ required to determine the profile are obtained through iteration on known values of $\bar{H}$ and $\bar{\delta}_2$. With natural transition, $\bar{\delta}_2$ is known from the laminar solution and the corresponding $\bar{H}$ is obtained by using the equilibrium boundary-layer relations of Nash (1965). However, since artificial turbulent stimulators were used in the two experiments, the above option in the computer program was not exercised. Instead, the values of C_f and δ downstream of the transition devices were obtained by trial and error, i.e. by matching the calculations and experiment at the first measuring station on the two bodies. Special care was needed for the modified spheroid due to the rather long distance between the transition device and the first measuring station. Known results from the iteration scheme of Nakayama et al. (1976a,b) were used in order to avoid lengthy calculations in the trial and error process.

The turbulent boundary-layer and wake calculations are performed using the differential method described in Chapter IV. Note that this

method is applicable to thin as well as thick boundary layers. In the first boundary-layer and wake solution, the pressure distribution obtained from the initial inviscid solution, with the modification near the tail, is used, and the variation of pressure across the flow is ignored.

V.3 Solution of the Flow Exterior to the Boundary Layer and Wake

The method of Nakayama et al. (1976a) has been used for the calculation of the potential flow in the semi-infinite region exterior to the boundary layer and wake. It was found that the solution for the velocity distribution at the edge of the boundary layer and wake is very sensitive to the input boundary conditions, namely the values of $\psi_M(x)$ and $y_M(x)$. This difficulty was alleviated by smoothing the distributions of ψ_M and y_M obtained from the boundary-layer and wake calculations in the interval $0.8 < X/L < 1.2$, prior to their use in the inviscid solution.

V.4 Integration of the y-Momentum Equation

With the introduction of the continuity equation, the y-momentum equation (17) can be written

$$\frac{\partial}{\partial y}\left(\frac{p}{\rho}\right) = \frac{UV\sin\theta + V^2\cos\theta}{r} + \frac{1}{h_1}\left\{\kappa(U^2 + V^2) + 2V\frac{\partial U}{\partial x} - \frac{\partial(UV)}{\partial x}\right\} \quad (17a)$$

This can be integrated to obtain the pressure field $p(x,y)$ by using

the previously calculated velocity field $U(x,y)$ and $V(x,y)$. This form is to be preferred over the original form involving $\partial V/\partial x$, since the differentiation of UV with respect to x is somewhat better behaved than that of V with respect to x. Nevertheless, the last term in equation (17a) leads to unavoidable inaccuracies. A central-difference formula was used to approximate it, and since $V\frac{\partial U}{\partial x}$ is calculated as part of the previous solution, the integration itself is quite simple. However, owing to the rapid growth of the boundary layer and the use of the staggered-mesh scheme in the boundary-layer solution, there is a substantial loss in the accuracy with which the pressure field could be determined. This became more apparent when the calculated pressure field was differentiated with respect to x to determine $\partial p/\partial x(y)$. Since the accuracy of this part of the solution could not be improved without a complete revision of the numerical scheme for the boundary-layer calculation, which is an immense task, two simplifications were adopted: (a) The y-momentum equation was integrated up to $y = 0$, i.e. the surface of the body or the wake centerline, to determine $p_w(x)$, and $\partial p/\partial x(y)$ was assumed to vary linearly between $\partial p_\delta/\partial x$ and $\partial p_w/\partial x$. (b) This variation of the pressure gradient across the boundary layer and wake was introduced into the interaction procedure only after performing three iterations with the constant pressure assumption. The first of these represents an approximation, but the measured pressure distributions (see Figure 4) indicate that it is realistic. The second assumption simply recognizes the inaccuracies occurring in the integration of the y-momentum equation and

postpones its introduction into the iteration procedure to avoid an accumulation of errors.

When the above procedure was used on the modified spheroid, the discontinuity in the surface curvature produced a jump in $p_w(x)$. Since the variation of the pressure across the flow is associated with the curvature of the streamlines within the boundary layer rather than that of the surface, recourse was had, in this case, to the curvature of the displacement surface. In fact, it is felt that this procedure is more realistic in all cases since the curvature of the displacement surface is more representative of the mean streamline curvature.

V.5 Incorporation of the Differential Method

The differential method developed in Chapter IV was incorporated into the present solution procedure but with a more thorough consideration of the coordinate discontinuity at the tail of the body. When the tail angle is nonzero, the coordinate system, which follows the surface of the body and the centerline of the wake, has to be changed abruptly at the tail. To account for this, Nakayama et al. (1976b) performed a separate analysis in a conical region beyond the tail (see Figure 1 in Nakayama et al., 1976b) and used the conservations of mass and momentum to obtain the initial conditions for the wake calculation a short distance downstream of the tail. More recently, Bradshaw (1978) has suggested the use of interpolation techniques to resolve the velocity components and Reynolds stresses

calculated at the trailing edge in boundary-layer coordinates into those in the wake coordinates. The former neglects the most important region in the near wake and is restricted to the integral approach. The latter is sound theoretically, but the associated numerics leads to inaccuracies. A new approach has therefore been adopted in the present work.

The region of interest is shown in Figure 27. The boundary layer calculation is continued in the usual coordinates up to station A so that the velocity and shear stress along AO are known. In order to start the calculation, however, it is necessary to calculate the velocity components U_{wake} and V_{wake} along OC, where C is the tail. This is accomplished as follows. The distance AC, which can be determined readily from AO and the tail angle θ_o (AC is usually of the order of one-half the local boundary-layer thickness) is divided into two equal intervals. The boundary-layer solution is then advanced from AO to BO and then to CO by using the necessary unequal longitudinal step size $\Delta x(y)$. The associated program logic is simple and will not be described here. After the velocities U and V along CO are found, the components U_{wake} and V_{wake} are determined by simple coordinate rotation. Note that the Reynolds stress $\overline{uv}$ calculated along CO does not change with the coordinate rotation since, according to the present turbulence model, it represents the scalar, turbulent kinetic energy.

V.6 Convergence

The iterative interaction procedure was performed for the low-drag body as well as the modified spheroid. In each case, converged solutions were obtained with five to six iterations. The primary results are presented in Figures 28(a,b) and 29(a,b). The initial pressure distribution is shown by the zeroth iteration curve labelled 0, and the successive solutions are indicated by the iteration numbers 1 through 6.

From Figure 28a it is seen that the pressure distribution along the edge of the boundary layer and wake of the low-drag body converges rapidly and that the converged solution is in good agreement with the data. The pressure distribution on the surface of the body and along the wake centerline, shown in Figure 28b, is the same as that shown in Figure 28a for the first three iterations due to the initial neglect of the static-pressure variation. The introduction of the y-momentum equation after the third iteration rapidly changes the solution and brings it into satisfactory agreement with the experimental data within two further iterations. However, small changes continue to occur in the solution. These are attributed to the inaccuracies in the integration of the y-momentum equation noted earlier. Figure 28c shows the fixed boundary along which the boundary-layer solution is matched with the inviscid solution, and the value of the stream-function, ψ_M, obtained from the successive iterations of the potential flow. The good agreement with the experimental ψ_M indicates the reliability of the present method.

The behavior of the solutions for the modified spheroid, shown in Figure 29(a,b) is qualitatively similar to that of the low-drag body. The nearly constant pressure at the edge of the wake, predicted in the range $1.1 < X/L < 1.2$, and the somewhat abrupt change in $C_{p\delta}$ and C_{pw} around $X/L = 1.2$ is, however, surprising. An examination of the boundary conditions used for the calculation of the external flow, namely $\psi_M(x)$ and $r_M(x)$ (see Figure 29c) does not indicate any abnormal behavior of the solution. Furthermore, the data in this region are sparse and restricted to the pressure along the wake centerline. The fact that the solution indicates negligible static-pressure variation in the near wake (compare $C_{p\delta}$ and C_{pw} distributions of Figures 29 a and b), in spite of the large tail angle, appears to suggest that the source of the discrepancy may lie again in the accuracy of the integration of the y-momentum equation in this region. The changes in C_{pw} occurring between iterations 4, 5 and 6 (Figure 29b), in spite of the rapid convergence of the solution with respect to $C_{p\delta}$ and ψ_M (Figures 29a,c), also suggest that the procedure used for the integration of the y-momentum equation to obtain C_{pw} from $C_{p\delta}$ may not be altogether satisfactory.

CHAPTER VI

SUMMARY AND CONCLUSIONS

The achievements of the present investigation may be summarized as follows:

(1) The data from the present experiments have been documented (see Patel and Lee, 1977) in as much detail as possible so that they can be used by others to further investigate the various aspects of the thick, axisymmetric, turbulent boundary layer and near wake of a body of revolution.

(2) The data from the low-drag body and the modified spheroid have been analyzed to indicate the relative importance of longitudinal and transverse surface curvatures, and the interaction between the external inviscid flow and the thick boundary layer and near wake in the tail region.

(3) A manual describing the computer program for calculating the thick, turbulent boundary layer on a body of revolution will be available as a report of the Iowa Institute of Hydraulic Research.

The major conclusions from the present study are as follows:

(1) The overall reliability of the simple integral method of Patel (1974) for the prediction of the thick boundary layer has been demonstrated. Its extension to the wake is not

altogether satisfactory. This method is, however, ideally suited for rapid calculations to determine the state of the boundary layer in the tail region for some applications.

(2) The present experimental data indicate that both the length scale and the Reynolds stresses are much less in a thick axisymmetric boundary layer than in a thin boundary layer.

(3) Systematic study of the parameters involved indicates that the structure of turbulence in the boundary layer is affected significantly by the presence of both longitudinal and transverse surface curvatures. These effects can be reasonably well predicted by using the present differential method with (i) the measured pressures at both the wall and edge of the boundary layer, (ii) incorporation of Bradshaw's correlations for the extra rates of strain introduced by the longitudinal and transverse curvatures, and (iii) consideration of the transverse pressure gradient in the boundary layer.

(4) The differential method has been applied with reasonable success into the interaction calculation procedure of Nakayama et al. (1976a,b) except matching between the interior and the exterior is made at a fixed, predetermined boundary a short distance beyond $y = \delta$. It is shown that this procedure gives convergent solutions in reasonably good agreement with available data.

Several suggestions can be made for further research:

(1) The rapid changes in the mixing length observed in the thick boundary layer and the near wake indicate that the so-called two-equation turbulence models, i.e. providing an extra equation for the length-scale of the turbulence, may be desirable. However, the recent work of Launder, Priddin and Sharma (1977) and Chambers and Wilcox (1977) shows that even two-equation models require further modifications to account for the extra rates of strain stemming from such effects as streamline curvature, streamline convergence and rotation, two of which are present in the flow examined here.

(2) The solutions of the differential equations presented here were carried out by a modification of an available numerical method. The experience gained with the method suggests that a better numerical scheme is required if the difficulties associated with the integration of the y-momentum equation, and the changes in the coordinate system at the tail, are to be avoided. One possibility is to use an implicit finite-difference method in conjunction with a nonorthogonal coordinate system (e.g. (x,r) coordinates, where x is along the body and wake axis while r is the radial distance).

(3) In continuing the boundary-layer calculation into the wake, the abrupt change in the inner boundary condition has been

handled somewhat arbitrarily. A more detailed study of the response of the inner region of the boundary layer to the surface discontinuity at the tail is required to make improvement in this procedure.

(4) The solution of the potential flow exterior to the boundary layer and wake may be improved by formulating a method based on the integral equation of the second kind.

(5) In the interaction scheme, an alternative would be to use a displacement-thickness surface as a means for deriving the outer potential flow. Since a displacement-thickness surface is also well-defined, a smooth matching between the exterior inviscid flow and the boundary layer would be expected. This alternative has been considered by Preston (1945) and Lighthill (1958) who have proposed formulas for the displacement effect suitable for thin boundary layers. An extension of their results to second order, recently given by Landweber (1978), may be applicable to a thick boundary layer and wake.

APPENDIX A

ESTIMATION OF INTEGRALS I_k AND I_p FROM DATA

These integrals are defined in the text by the following equations:

$$I_k = \kappa \int_o^\delta \frac{UV}{U_\delta^2} \, r dy \tag{11}$$

and

$$I_p = \frac{1}{U_\delta^2} \int_o^\delta r \frac{\partial}{\partial x} \left(\frac{p - p_\delta}{\rho} - \frac{V_\delta^2}{2} \right) dy \tag{12}$$

The evaluation of I_k is straightforward since both U and V have been measured in the boundary layer and the wake. Since κ is the curvature of the surface, I_k becomes zero everywhere in the wake.

From physical considerations, it may be argued that I_k represents the influence of the curvature of the streamlines in the boundary layer rather than that of the surface. It may therefore be preferable to use a representative streamline curvature for κ. For example, an appropriate choice may be the longitudinal curvature of the displacement surface shown in Figure 9. In the calculations presented in the text, however, the original difinition of I_k has been retained and an "effective" value has been assigned in the near wake simply by reducing I_k to zero, from its value at the tail, exponentially over a distance X/L = 0.20 from the tail.

In order to simplify the evaluation of I_p, it is first observed that the measured static-pressure variations across the boundary layer and wake (Figure 4) may be approximated by linear distributions, viz

$$p - p_\delta = (p - p_w)(1 - \frac{y}{\delta}) \tag{A-1}$$

where p_w is the pressure at the body surface or the wake centerline. Substitution of this into equation (12) and integration leads to

$$\begin{aligned} I_p U_\delta^2 = {} & \frac{\delta^2}{12} \left(\frac{3r_o}{\delta} + \cos\theta\right) \frac{d}{dx} \left(C_{pw} - C_{p\delta}\right) \\ & + \frac{\delta}{12} \left(\frac{3r_o}{\delta} + 2\cos\theta\right) \frac{d\delta}{dx} \left(C_{pw} - C_{p\delta}\right) \\ & - \frac{\delta^2}{4} \left(\frac{2r_o}{\delta} + \cos\theta\right) \frac{d}{dx} \left(V_\delta^2\right) \end{aligned} \tag{A-2}$$

Using the Bernoulli equation, V_δ can be related to $C_{p\delta}$ and U_δ as follows

$$\frac{V_\delta^2}{U_o^2} = 1 - C_{p\delta} \frac{U_\delta^2}{U_o^2} \tag{A-3}$$

I_p can now be evaluated using the measured values of δ, U_δ, $C_{p\delta}$ and C_{pw}.

The estimated values of I_k and I_p are shown in Figure 23, along with the axial variation of the terms $d\Delta_2/dx$ and $\frac{1}{2}C_f r_o$ appearing in the momentum integral equation. It is seen that both I_k and I_p make a substantial contribution to the rate of growth of the momentum

deficit area. It should be noted that the accuracy of the solutions of the momentum equation using I_k and I_p is limited due, not only to the approximations that are involved in the estimation of these integrals, but also because they are large and of opposite signs over a substantial axial distance.

APPENDIX B

ORDERS-OF-MAGNITUDE OF THE TERMS IN THE x-MOMENTUM EQUATION

In equation (16), the streamwise derivative of the normal stress $\overline{u^2}$, i.e. $\frac{\partial}{\partial x}(\overline{u^2})$, is omitted. In order to support this, the data from the low-drag body are reexamined. In Table 1, each term in equation (16) is evaluated at both the inner and outer regions of stations X/L =0.92 and 0.96, which are in the thick boundary-layer region. Owing to lack of accuracy in differentiations, these figures only provide rough magnitudes for each term. The analyses indicate that, in the inner layer, the curvature term, $\frac{\kappa}{h_1}UV$, and $\frac{1}{h_1}\frac{\partial}{\partial x}(\overline{u^2})$ are both negligible when compared with the other terms. But, in outer layer, both the normal-stress and shear-stress terms are smaller than the convective acceleration terms. This implies that, for the entire boundary-layer calculation, the normal-stress term may be neglected.

TABLE 1

APPROXIMATE MAGNITUDE OF EACH TERM IN THE
x-MOMENTUM EQUATION FOR THE LOW-DRAG BODY

X/L	0.92		0.96	
y/L	0.005	0.040	0.005	0.040
$\frac{U}{h_1}\frac{\partial U}{\partial x}$	-0.1474	-0.3406	-0.0733	-0.4286
$V\frac{\partial U}{\partial y}$	0.0603	0.6344	0.0653	0.5289
$\frac{\kappa}{h_1}UV$	-0.0001	-0.0741	-0.0027	-0.0816
$\frac{1}{\rho h_1}\frac{\partial p}{\partial x}$	-0.0750	-0.1138	-0.2000	-0.2250
$-\frac{1}{rh_1}\frac{\partial}{\partial y}(\frac{h_1 r\tau}{\rho})$	0.0606	-0.0212	0.0839	-0.0244
$\frac{1}{h_1}\frac{\partial}{\partial x}(\overline{u^2})$	-0.0125	0.0090	-0.0101	0.0166

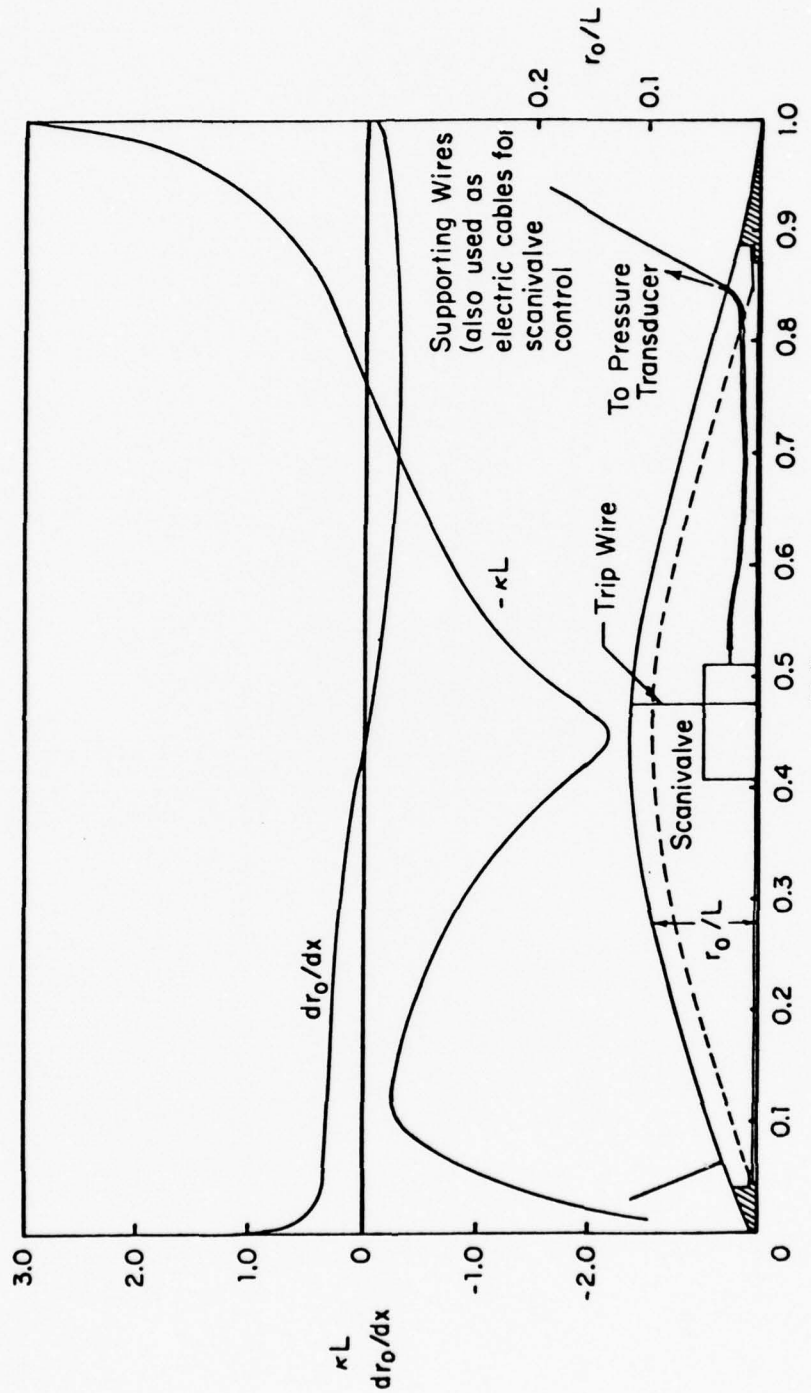

FIGURE 1. DETAILS OF THE LOW-DRAG BODY

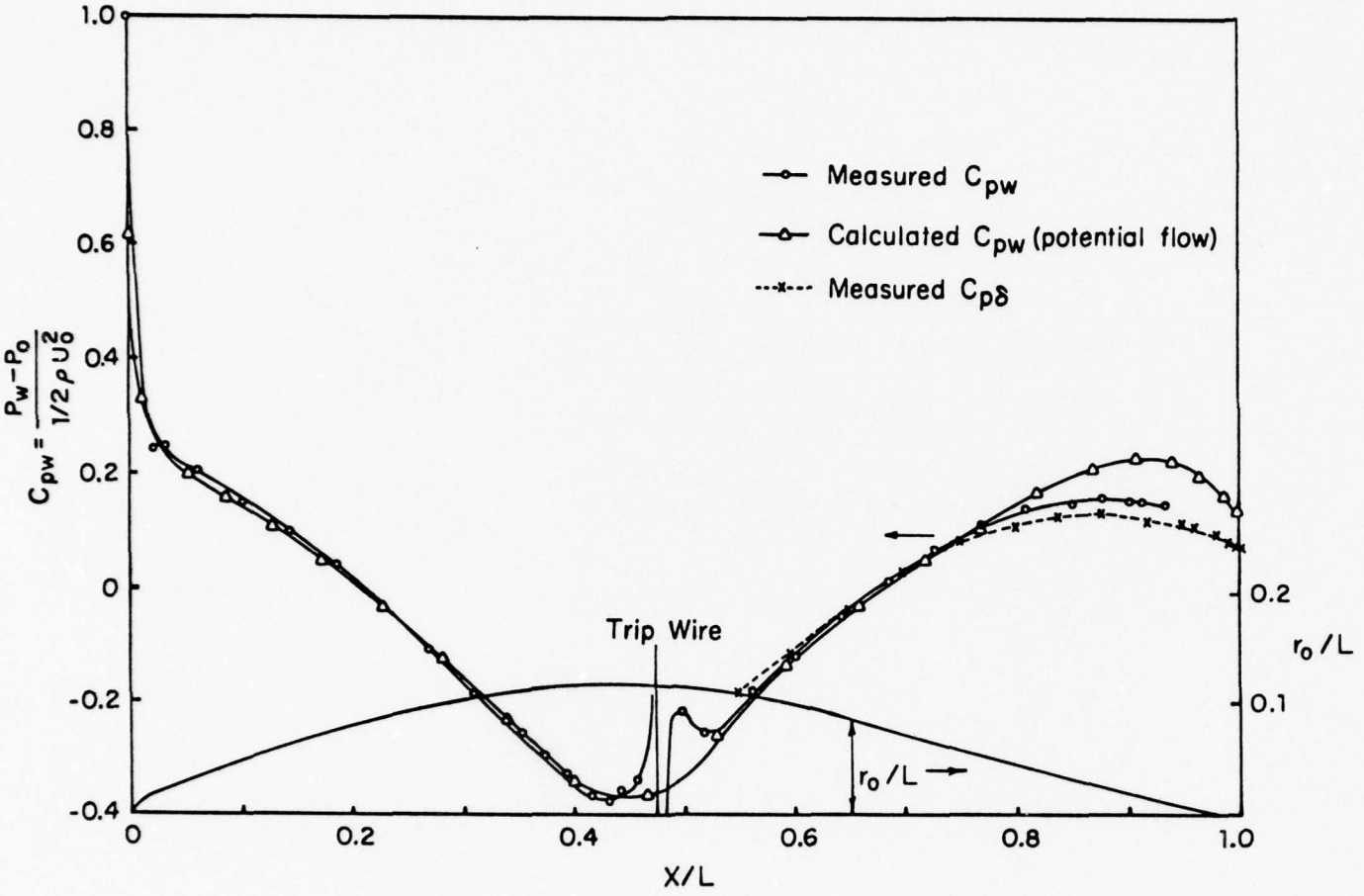

FIGURE 2. PRESSURE DISTRIBUTIONS ON THE LOW-DRAG BODY

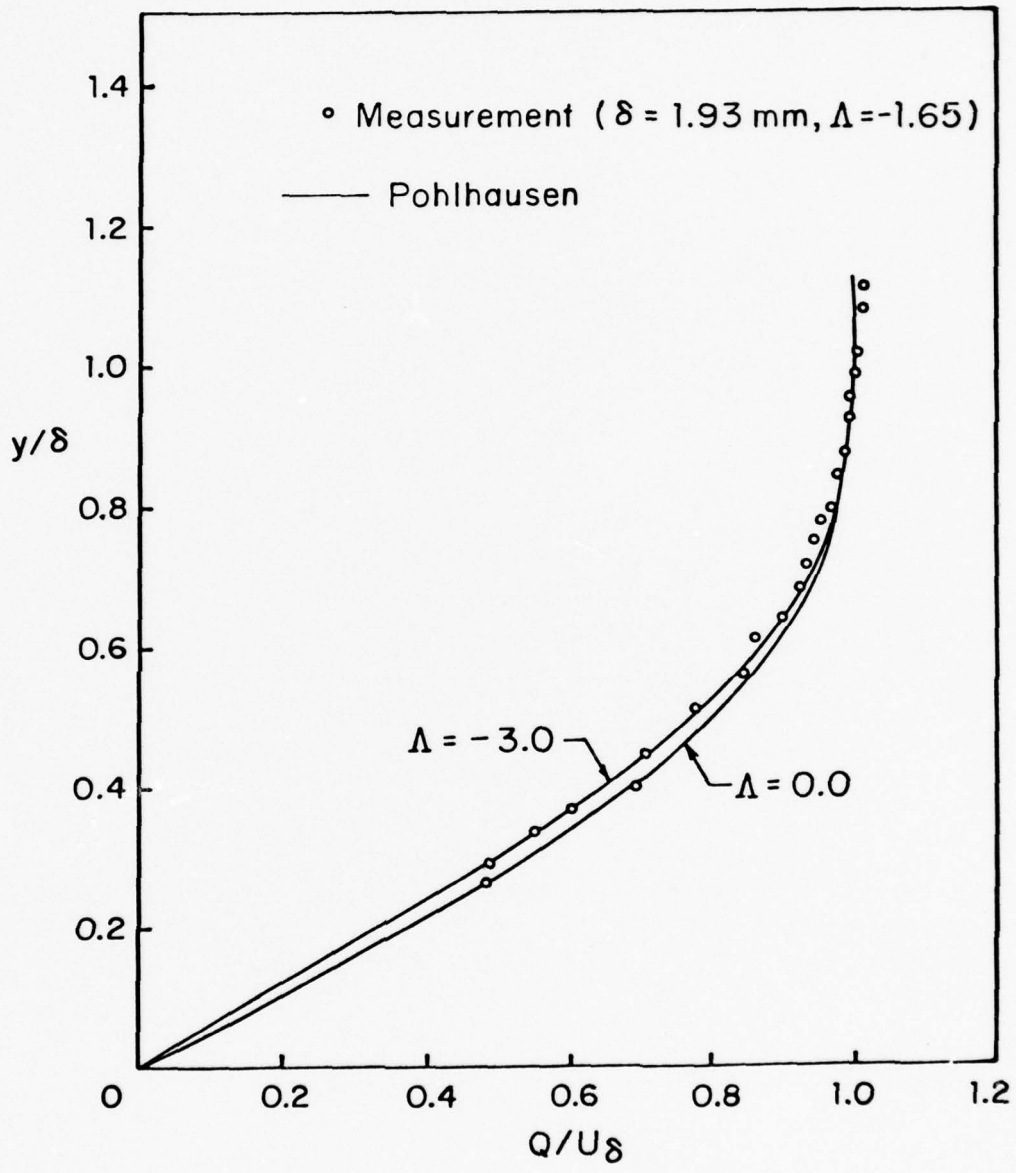

FIGURE 3. VELOCITY PROFILE AT X/L = 0.433

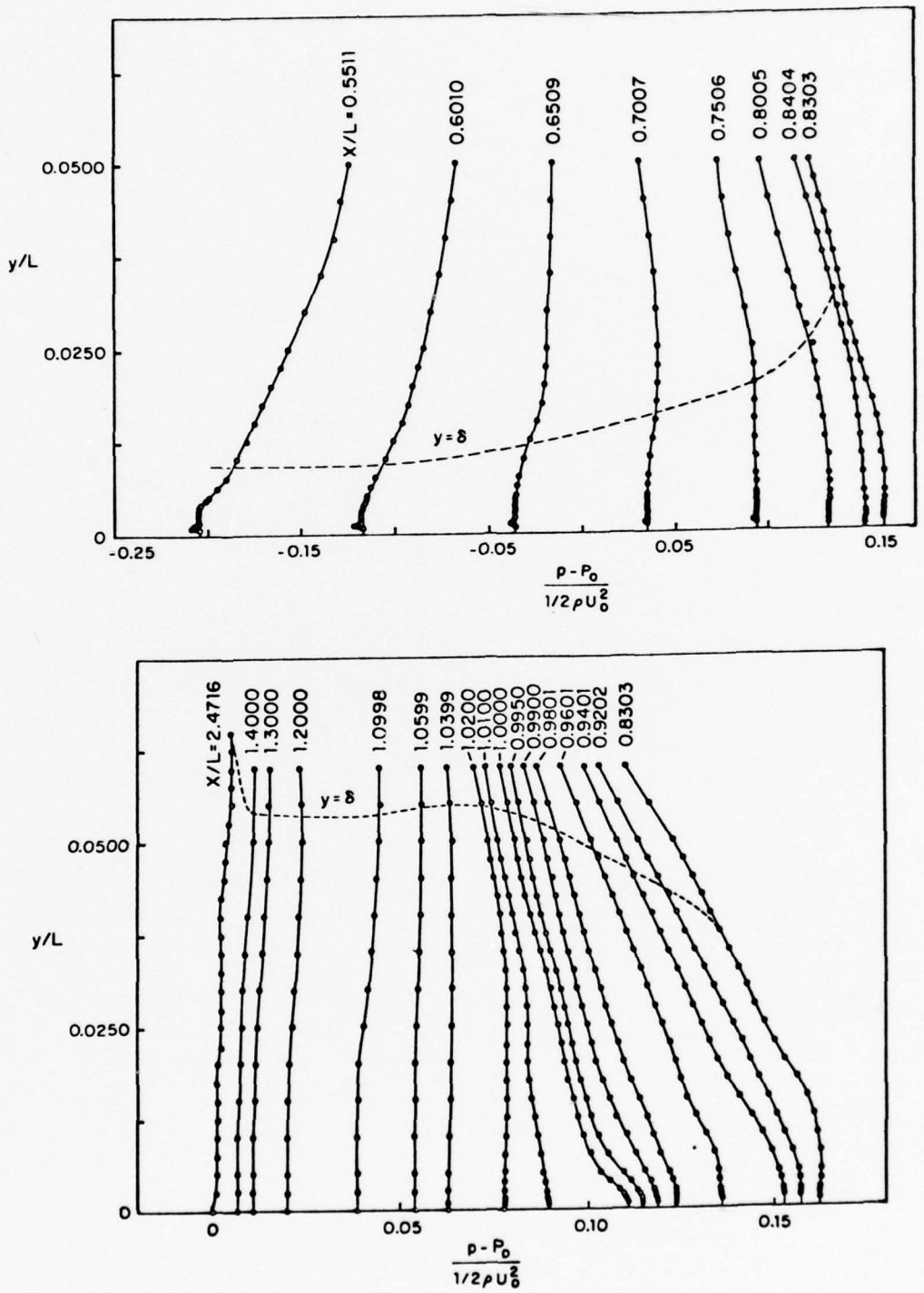

FIGURE 4. STATIC PRESSURE DISTRIBUTIONS

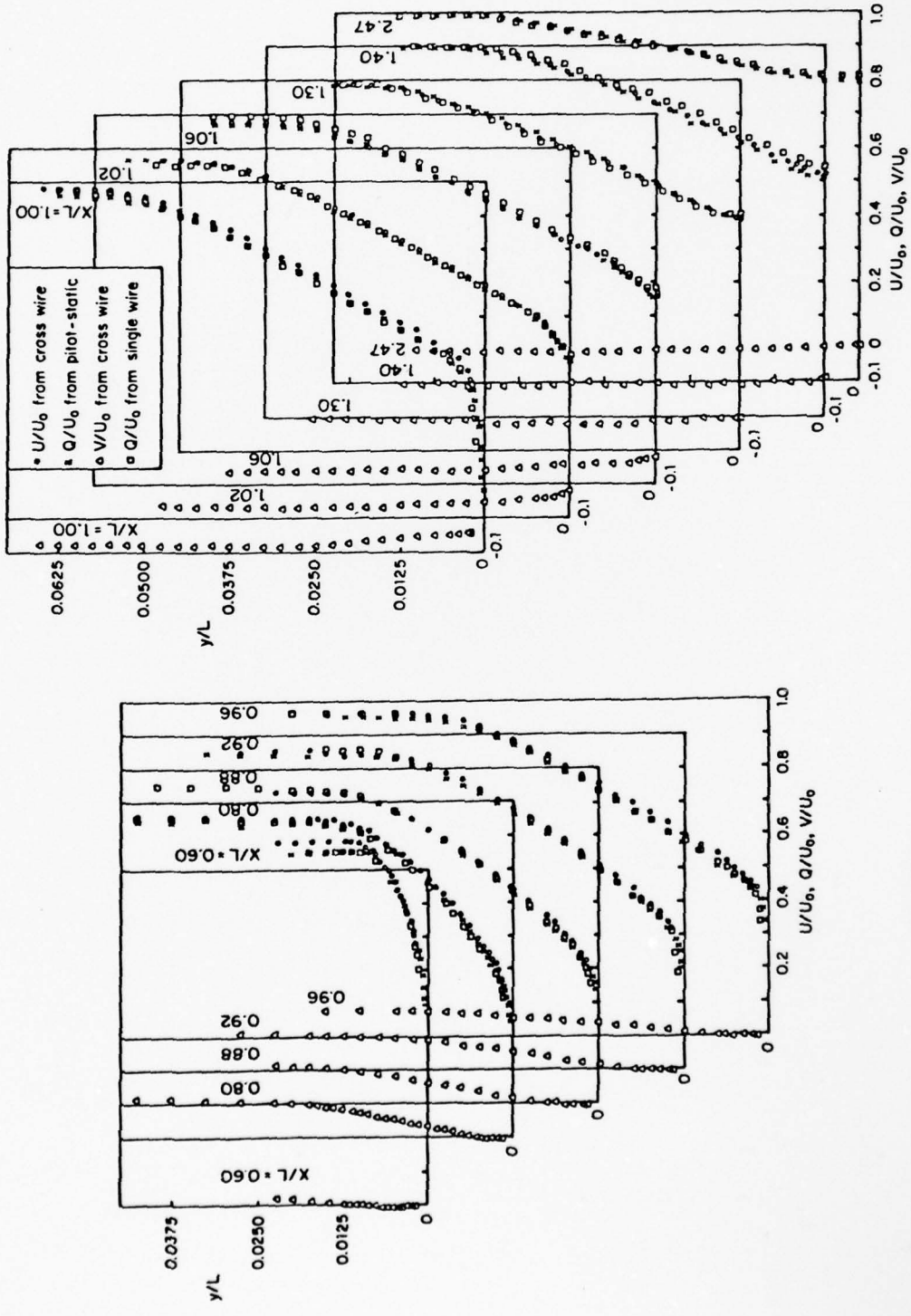

FIGURE 5. MEAN-VELOCITY PROFILES

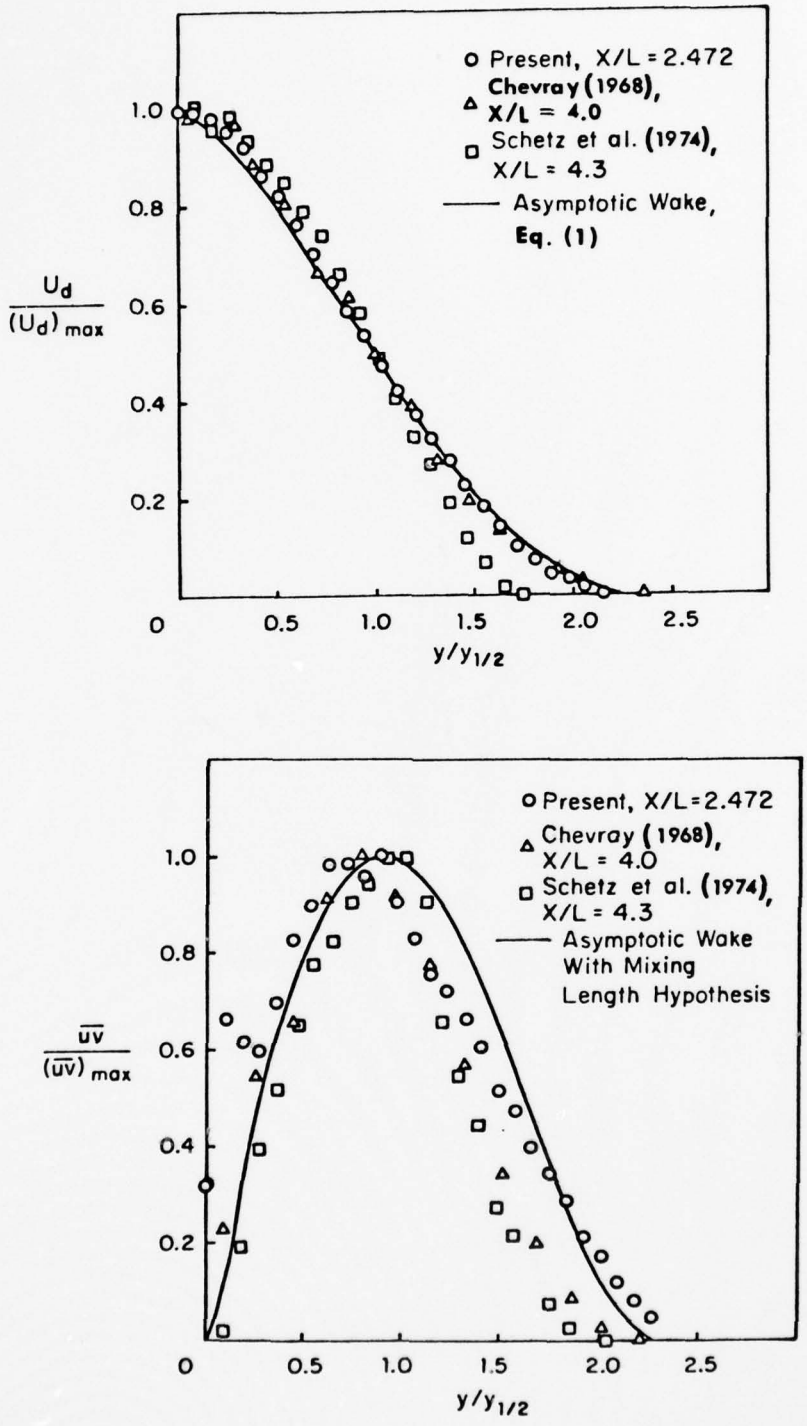

FIGURE 6. ASYMPTOTIC VELOCITY AND SHEAR-STRESS PROFILES IN THE WAKE

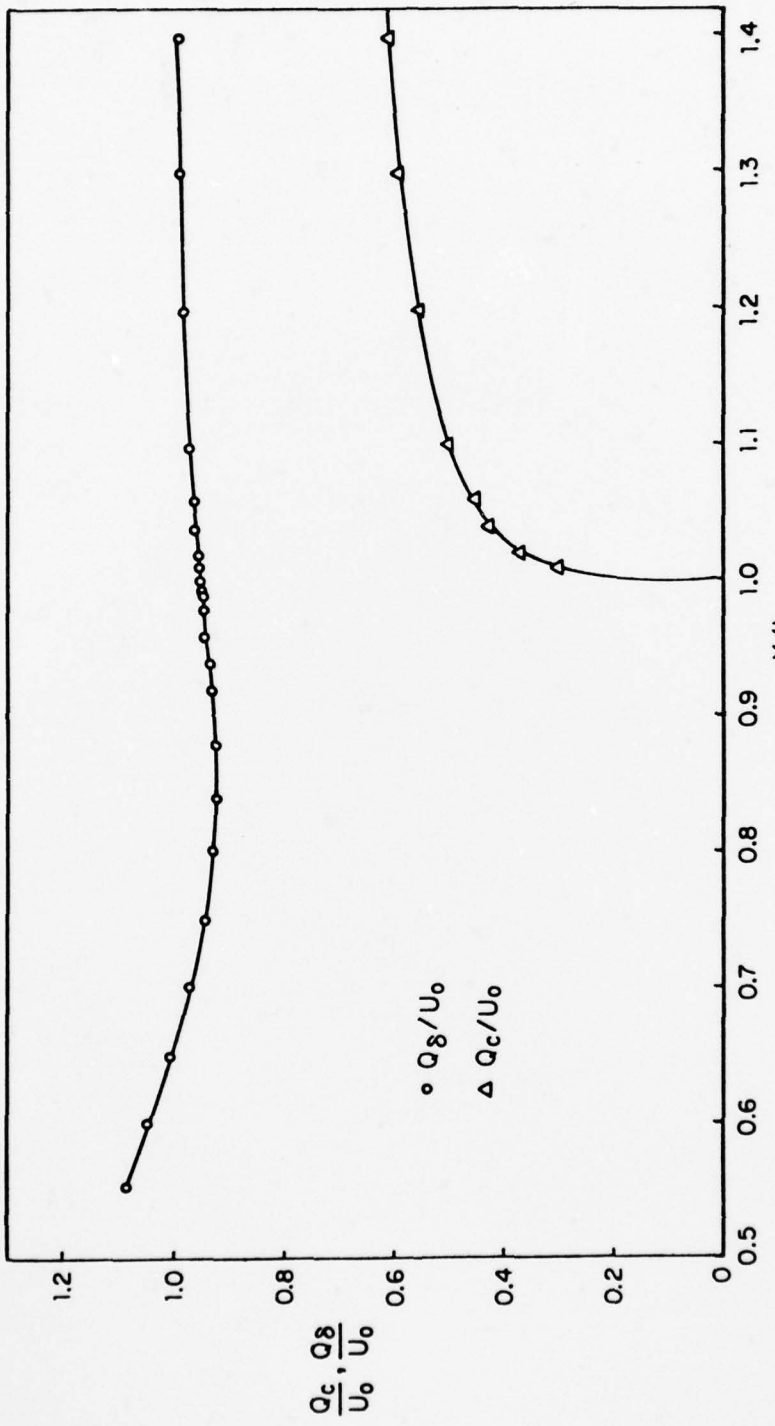

FIGURE 7. VELOCITY AT $y = \delta$ AND WAKE CENTERLINE

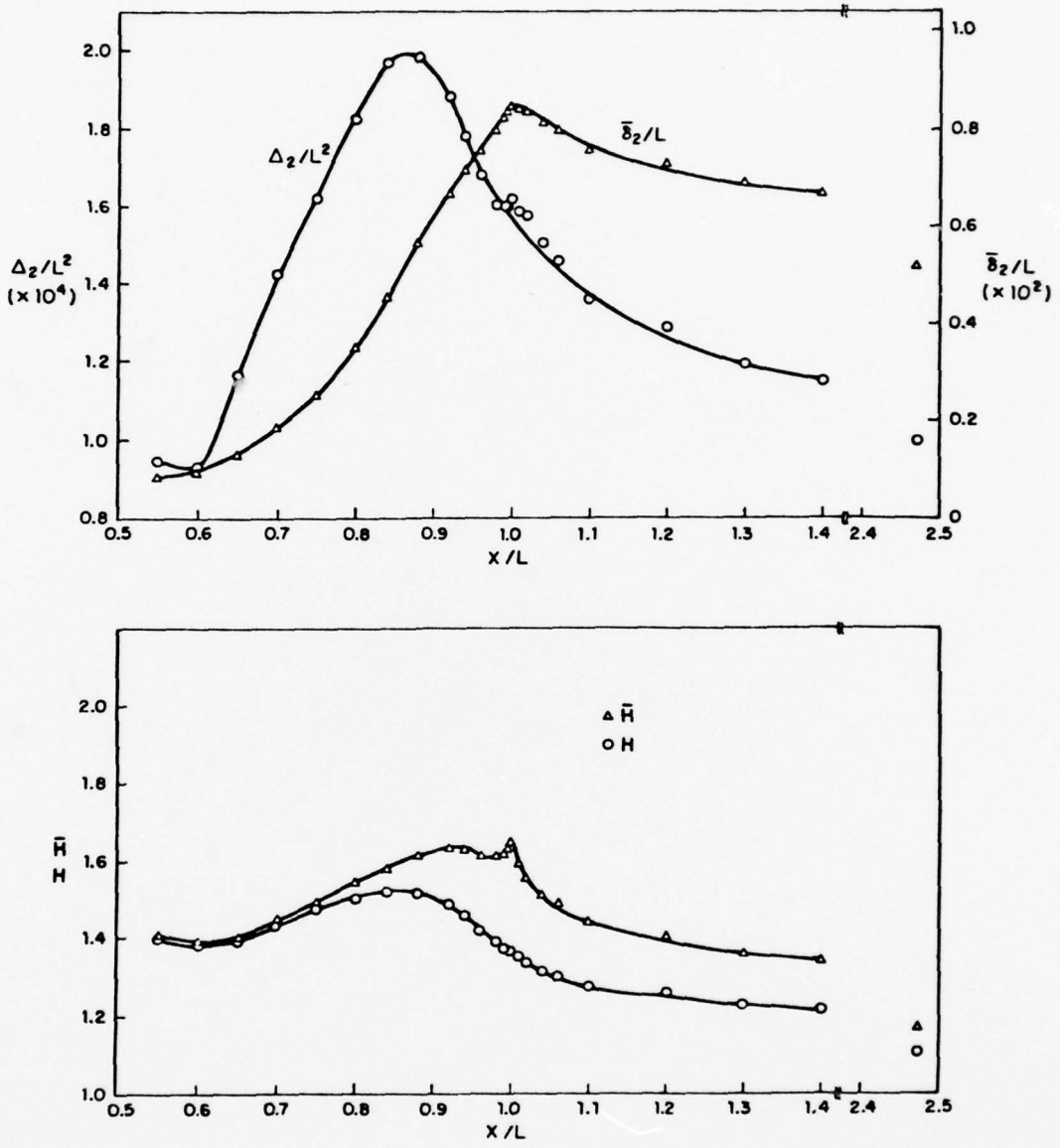

FIGURE 8. INTEGRAL PARAMETERS

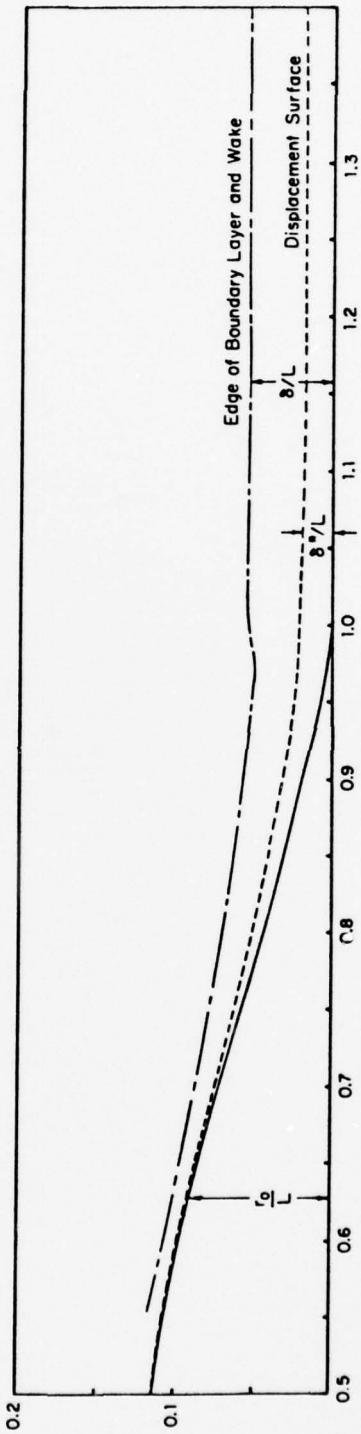

FIGURE 9. DISPLACEMENT SURFACE

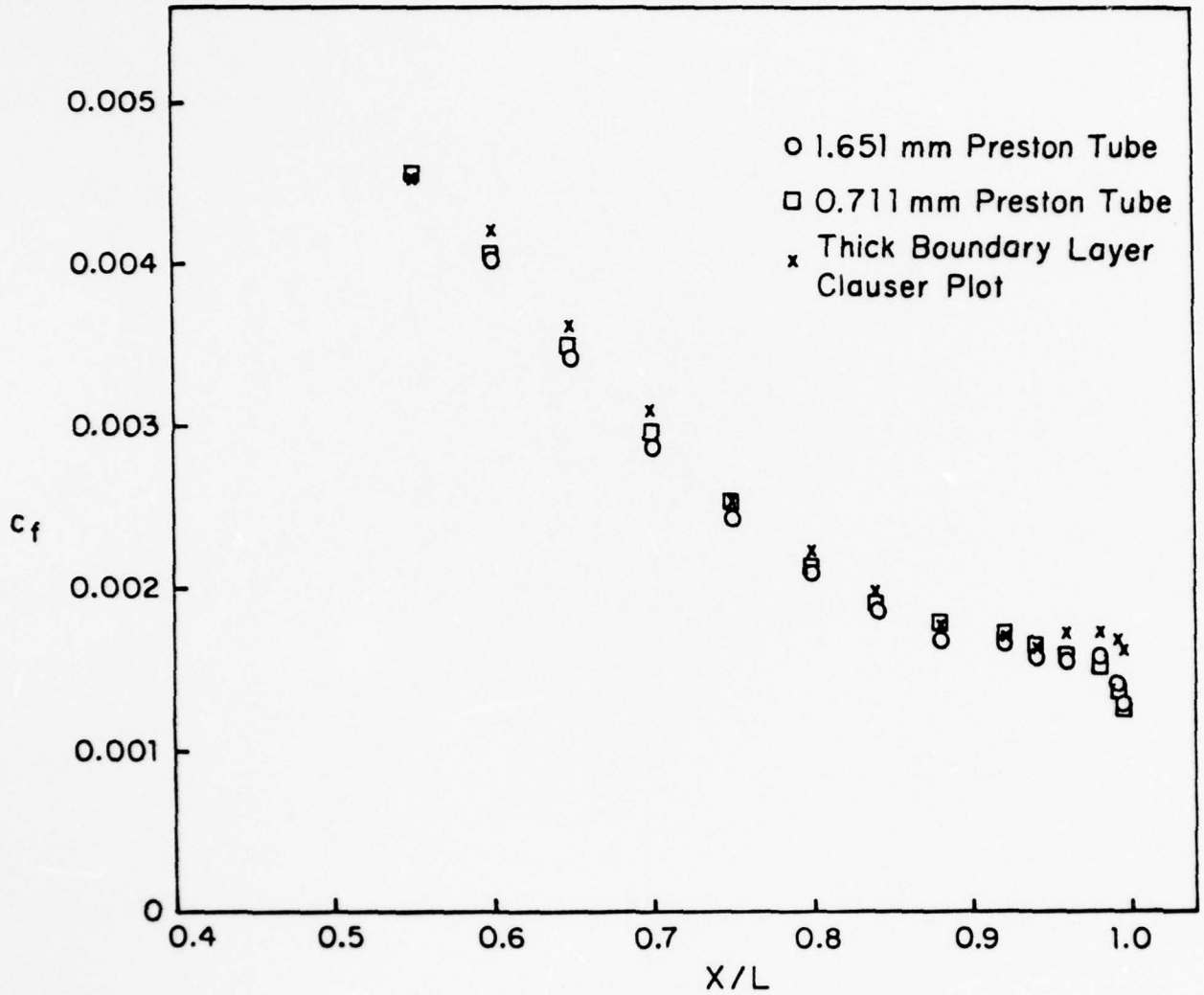

FIGURE 10. WALL SHEAR STRESS

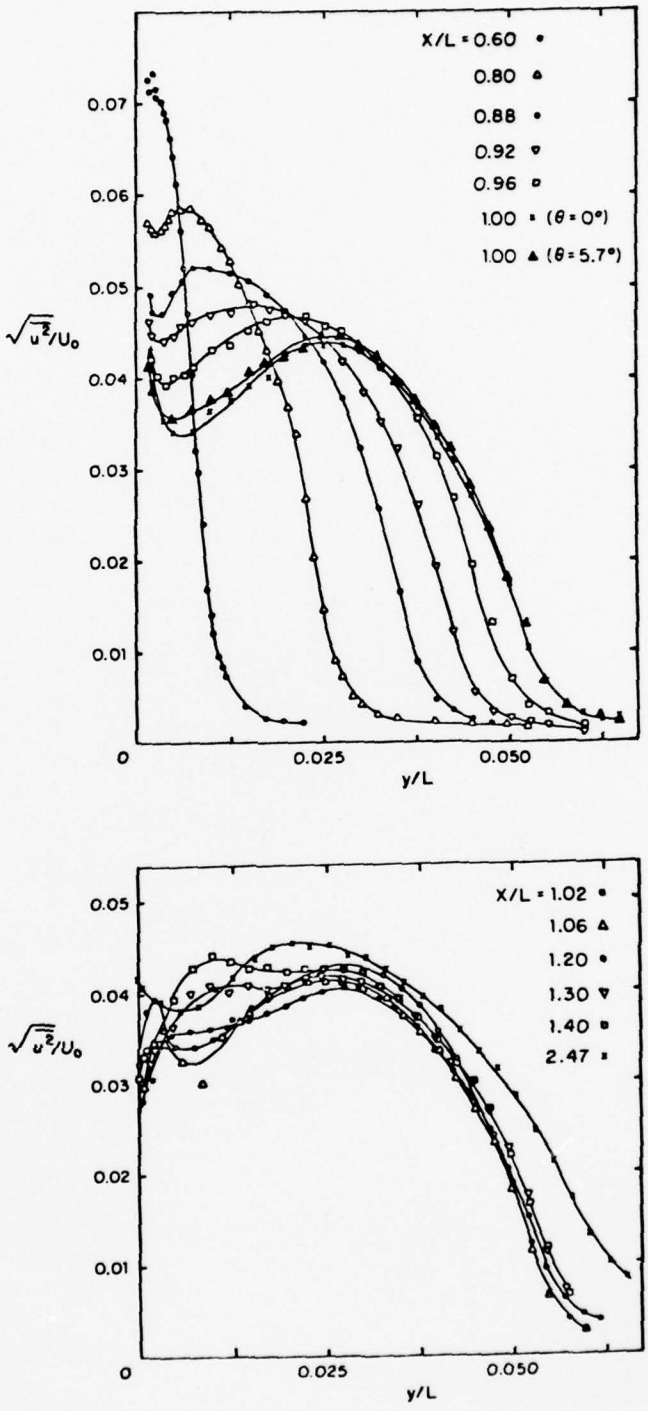

FIGURE 11. DISTRIBUTIONS OF REYNOLDS STRESS $\sqrt{\overline{u^2}}/U_o$

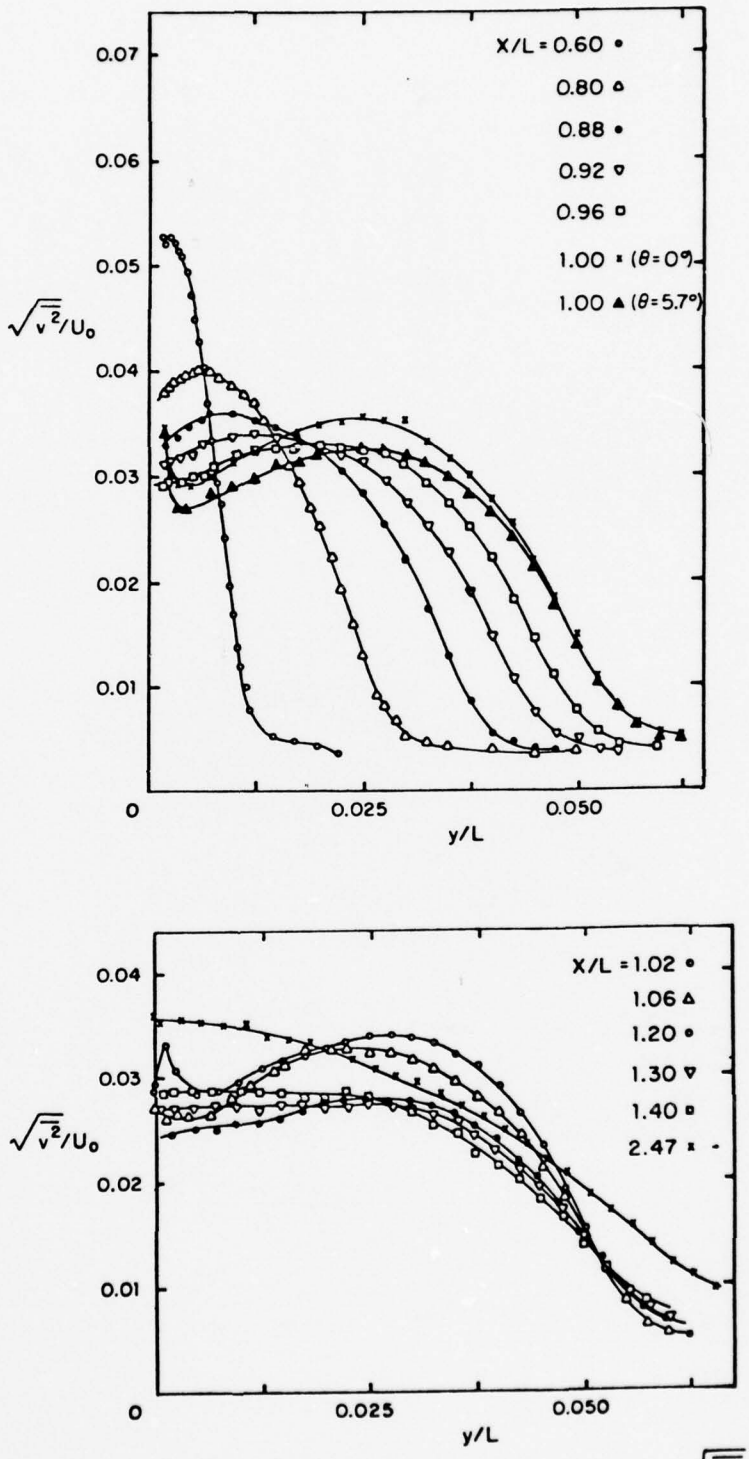

FIGURE 12. DISTRIBUTIONS OF REYNOLDS STRESS $\sqrt{\overline{v^2}}/U_o$

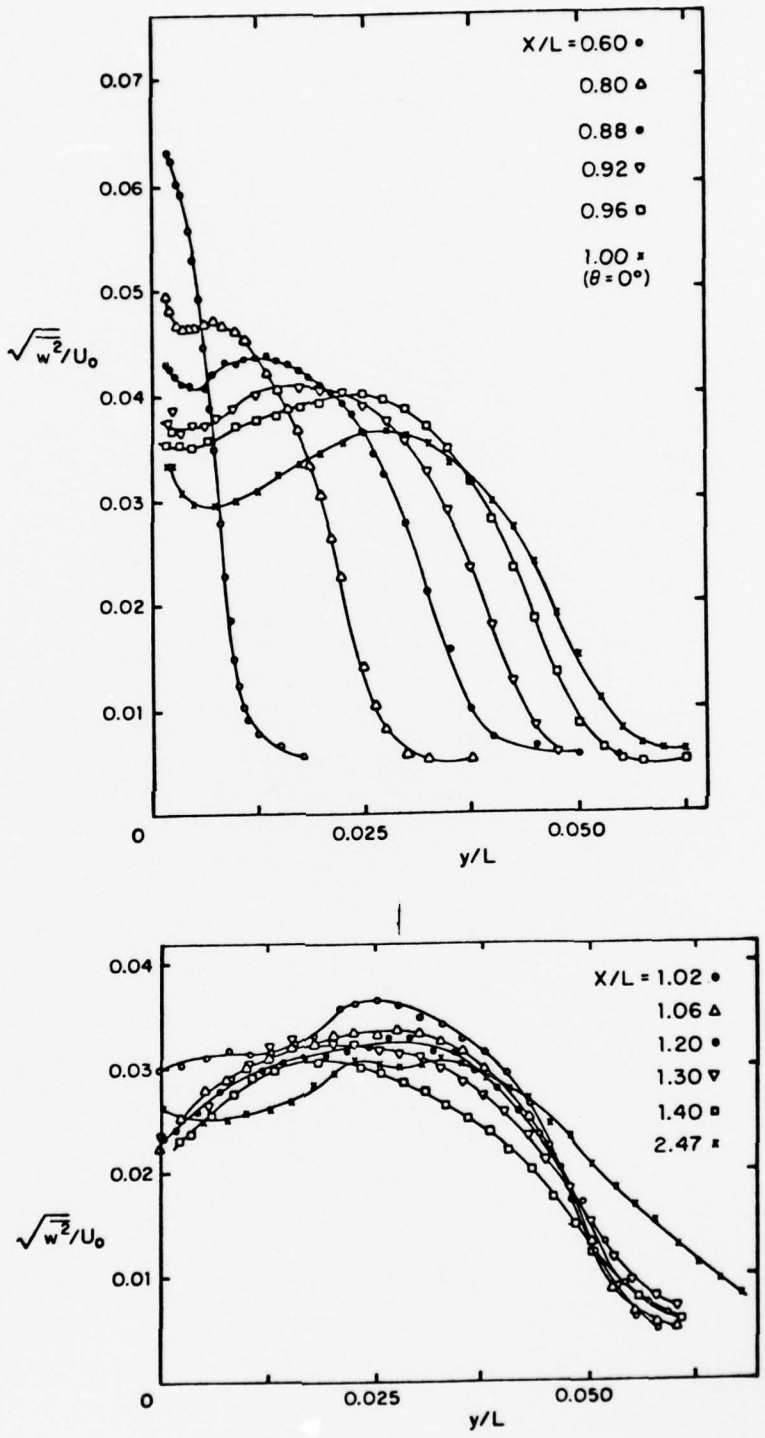

FIGURE 13. DISTRIBUTIONS OF REYNOLDS STRESS $\sqrt{\overline{w^2}}/U_o$

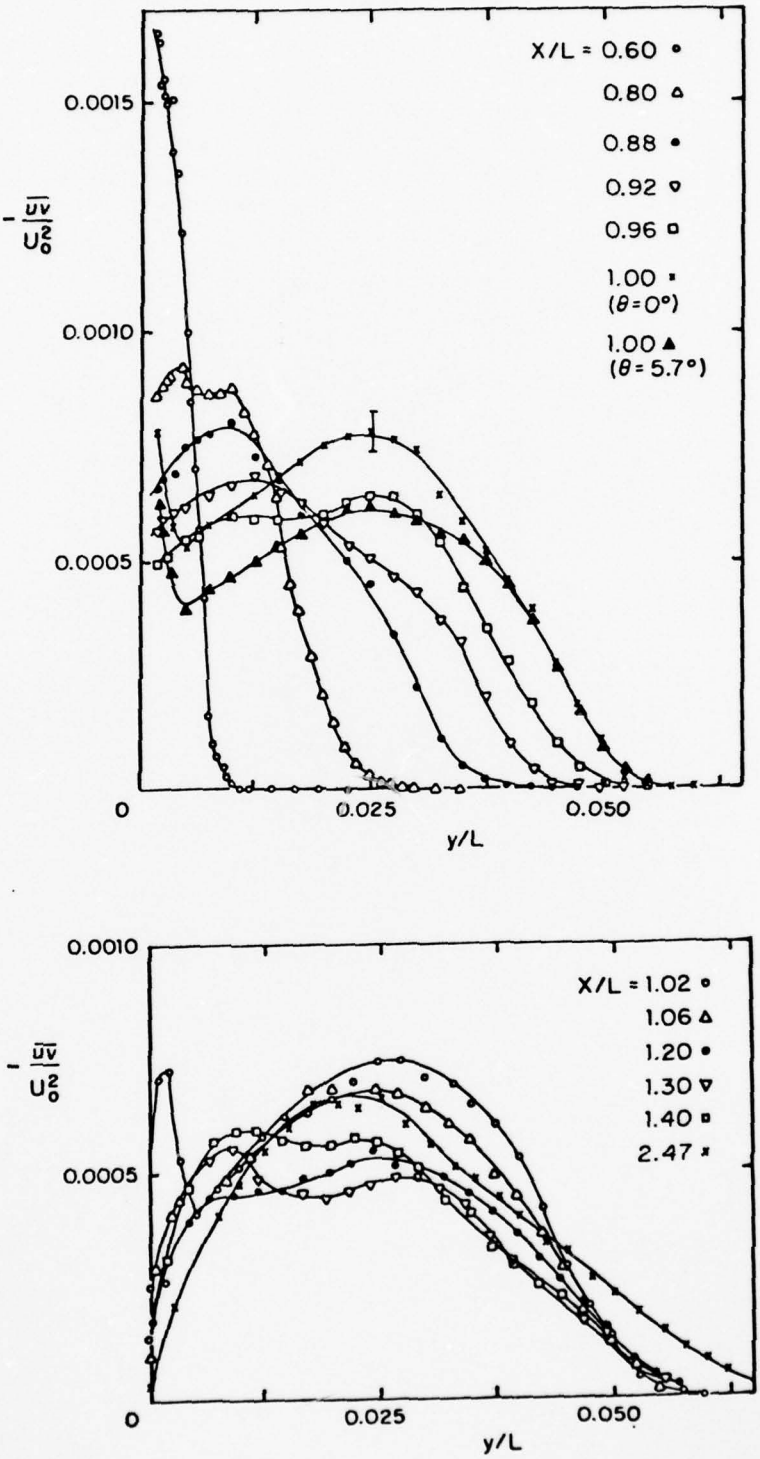

FIGURE 14. DISTRIBUTIONS OF REYNOLDS SHEAR STRESS $-\overline{uv}/U_o^2$

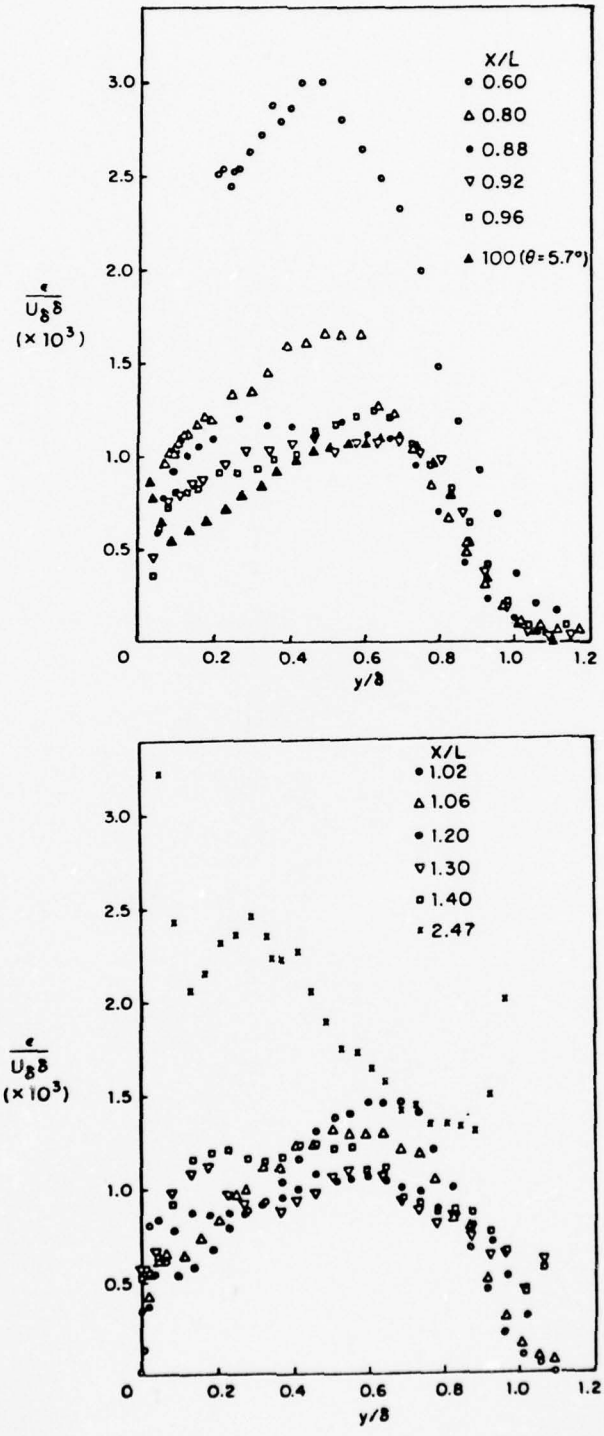

FIGURE 15. EDDY-VISCOSITY PROFILES, LOW-DRAG BODY

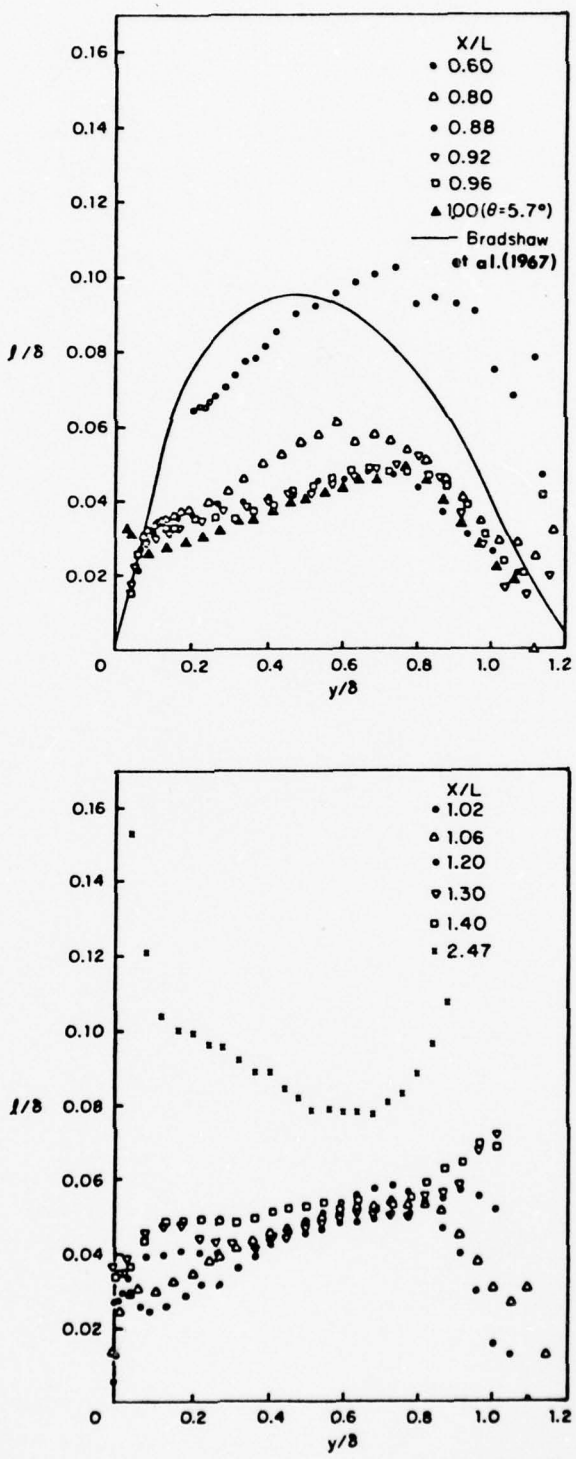

FIGURE 16. MIXING-LENGTH PROFILES, LOW-DRAG BODY

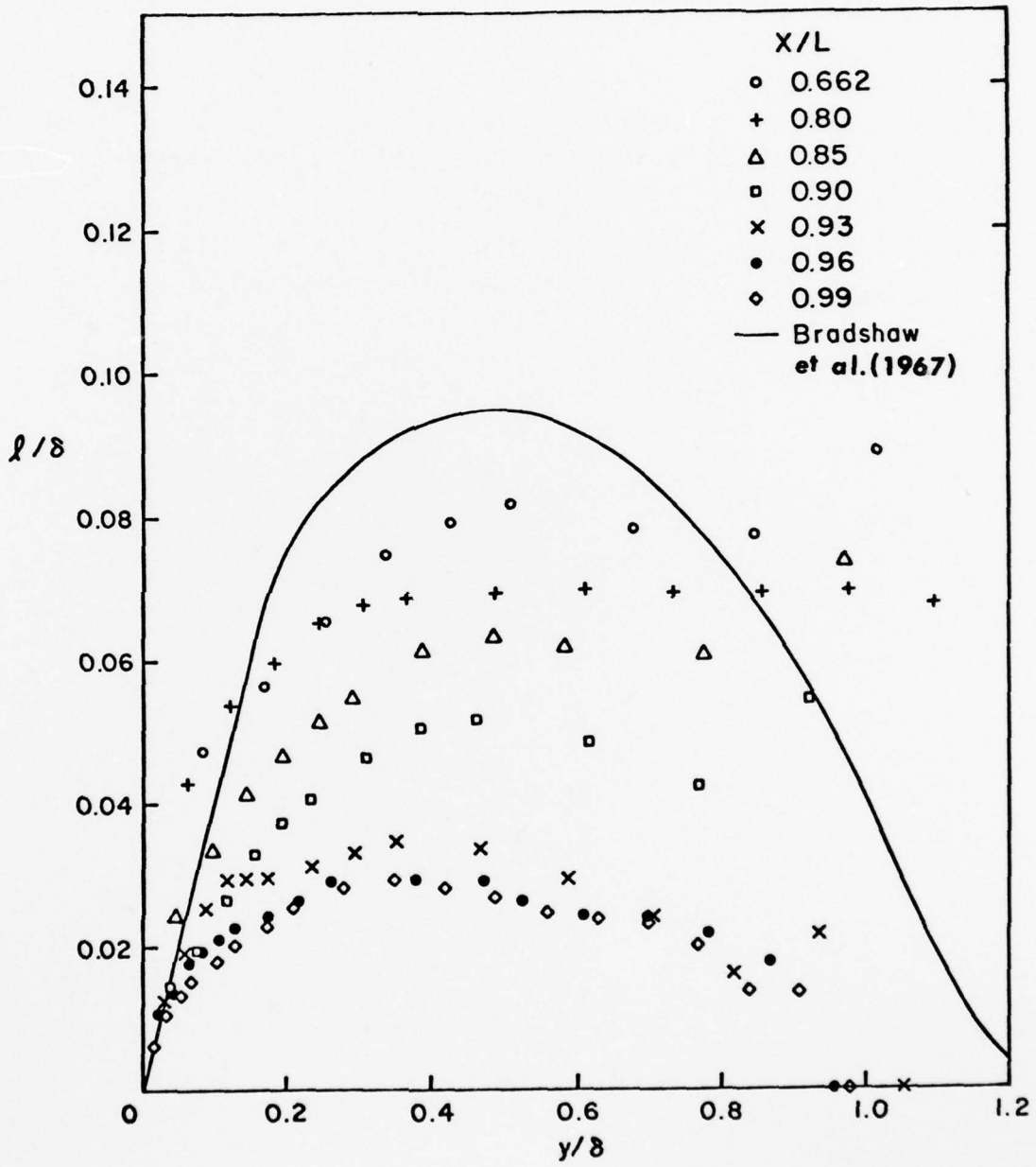

FIGURE 17. MIXING-LENGTH PROFILES, MODIFIED SPHEROID

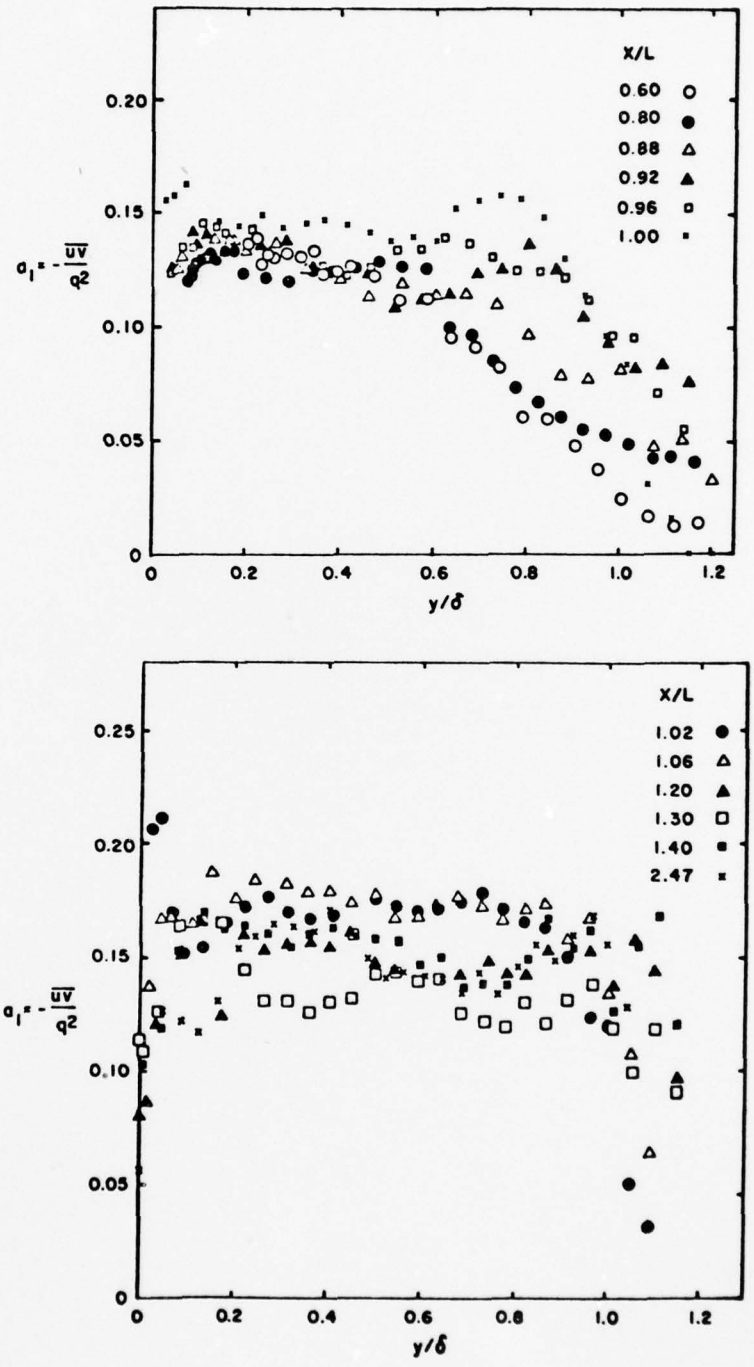

FIGURE 18. VARIATION OF THE STRUCTURE PARAMETER a_1, LOW-DRAG BODY

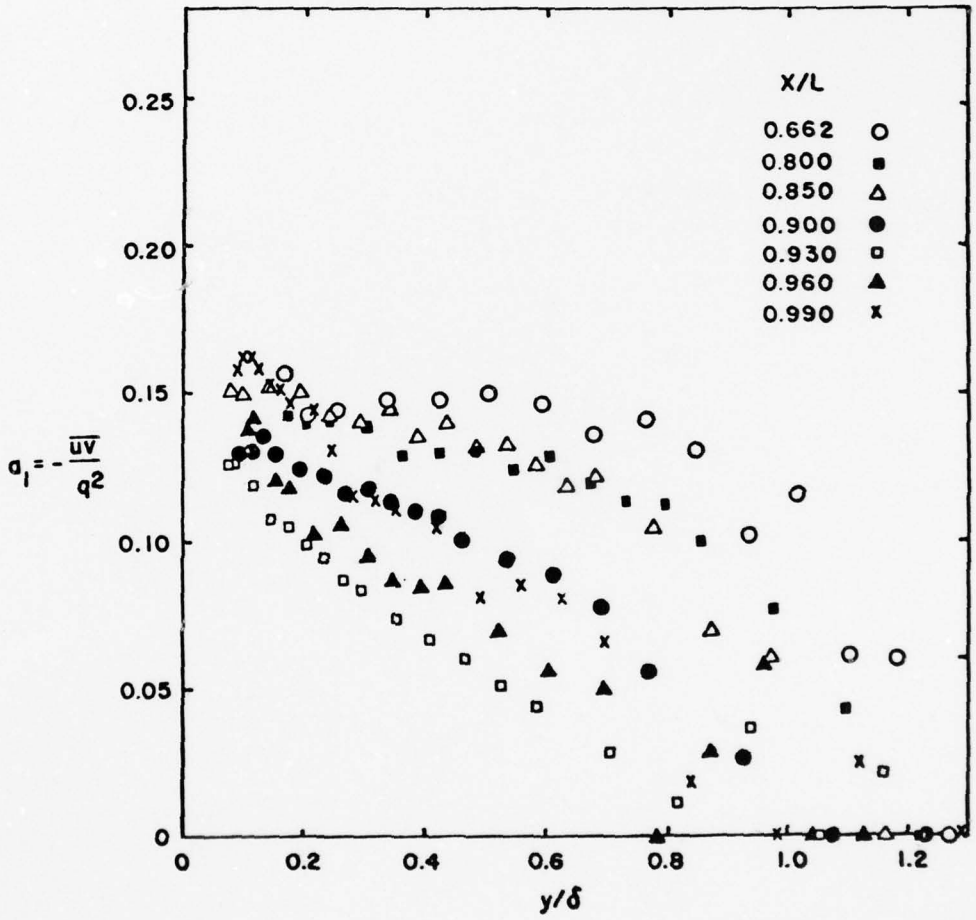

FIGURE 19. VARIATION OF THE STRUCTURE PARAMETER a_1, MODIFIED SPHEROID

AD-A064 921 IOWA INST OF HYDRAULIC RESEARCH IOWA CITY F/G 20/4
THICK AXISYMMETRIC TURBULENT BOUNDARY LAYER AND WAKE OF A LOW-D--ETC(U)
DEC 78 Y LEE N00014-75-C-0273
UNCLASSIFIED NL

2 OF 2
AD A064921

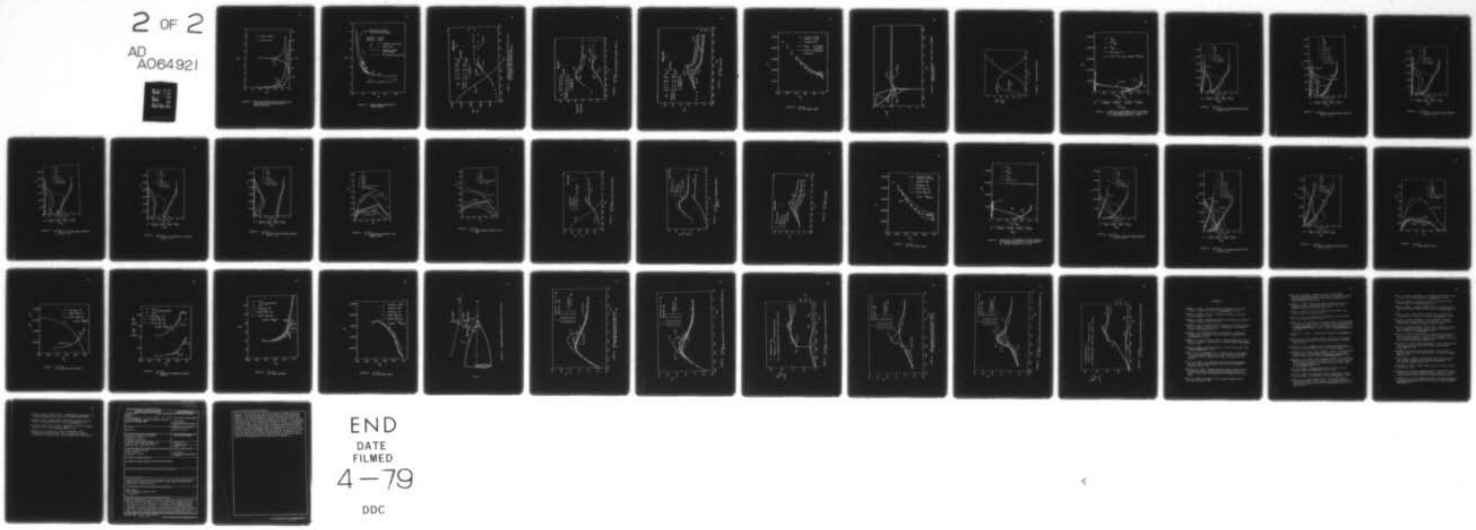

END
DATE FILMED
4-79
DDC

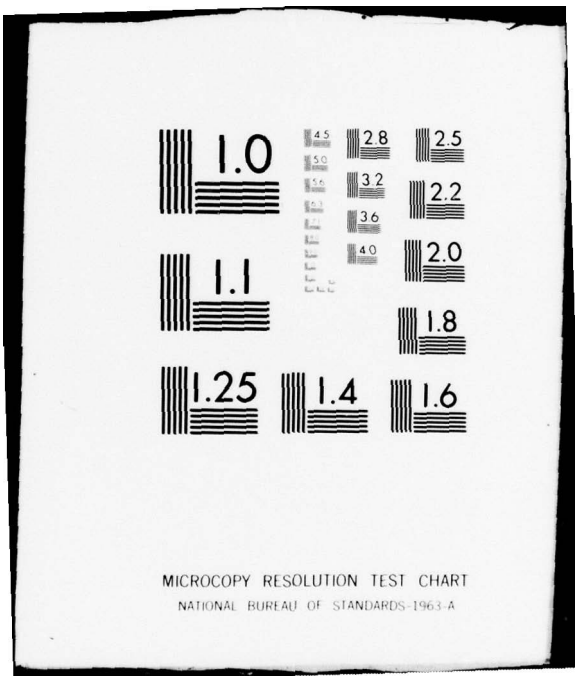
1.0
1.1
1.25
1.4
1.6
1.8
2.0
2.2
2.5
2.8
3.2
3.6
4.0
4.5
5.0
5.6
MICROCOPY RESOLUTION TEST CHART
NATIONAL BUREAU OF STANDARDS-1963-A

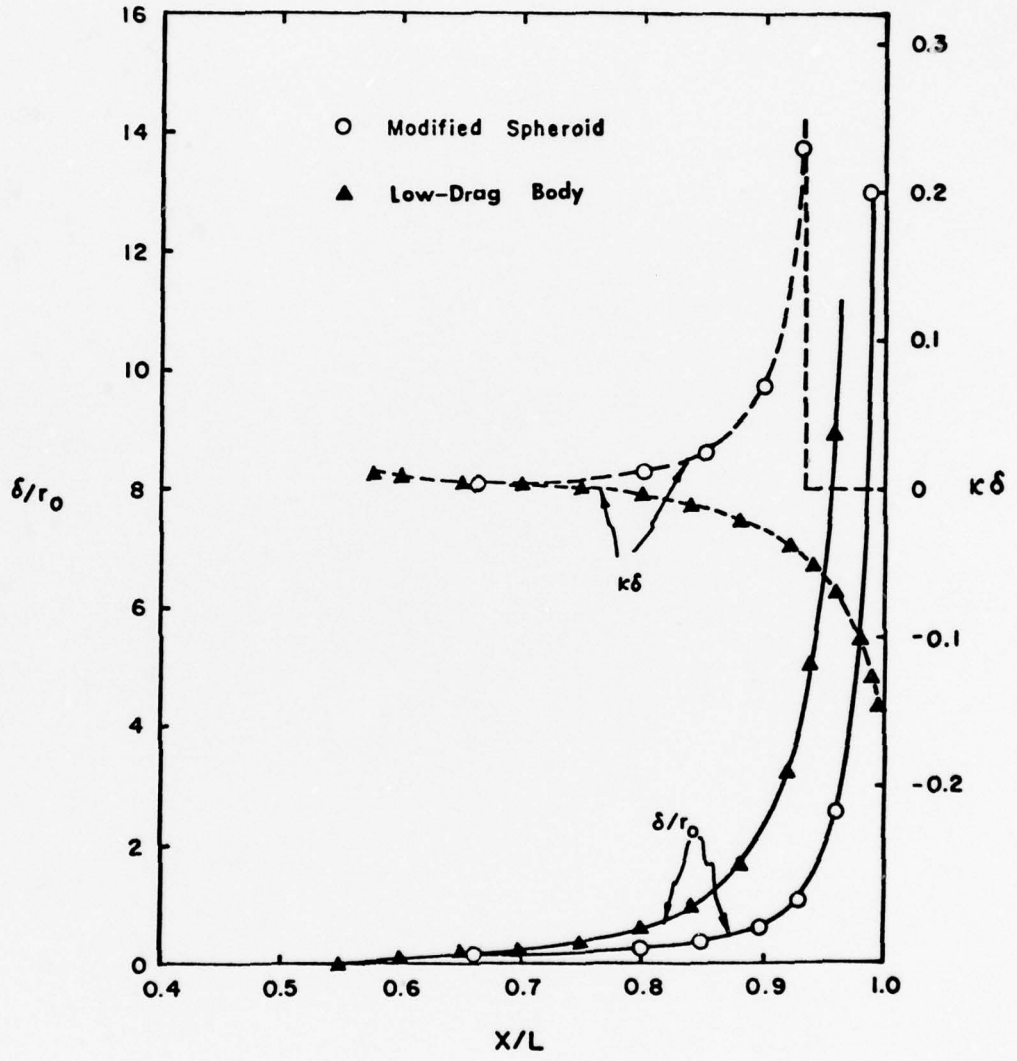

FIGURE 20. RATIOS OF BOUNDARY-LAYER THICKNESS TO THE LONGITUDINAL AND TRANSVERSE RADII OF SURFACE CURVATURE

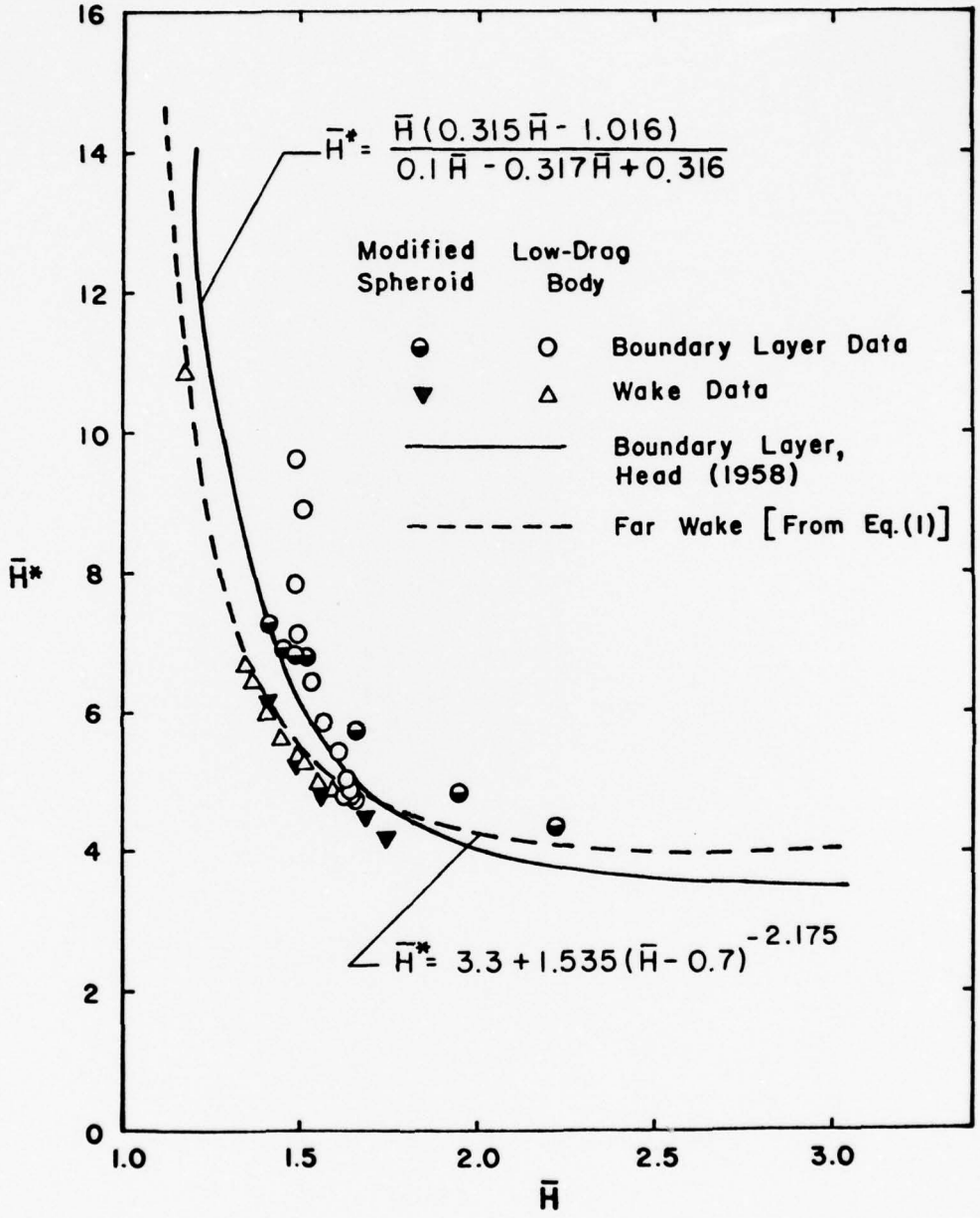

FIGURE 21. SHAPE-PARAMETER RELATIONS IN INTEGRAL METHOD

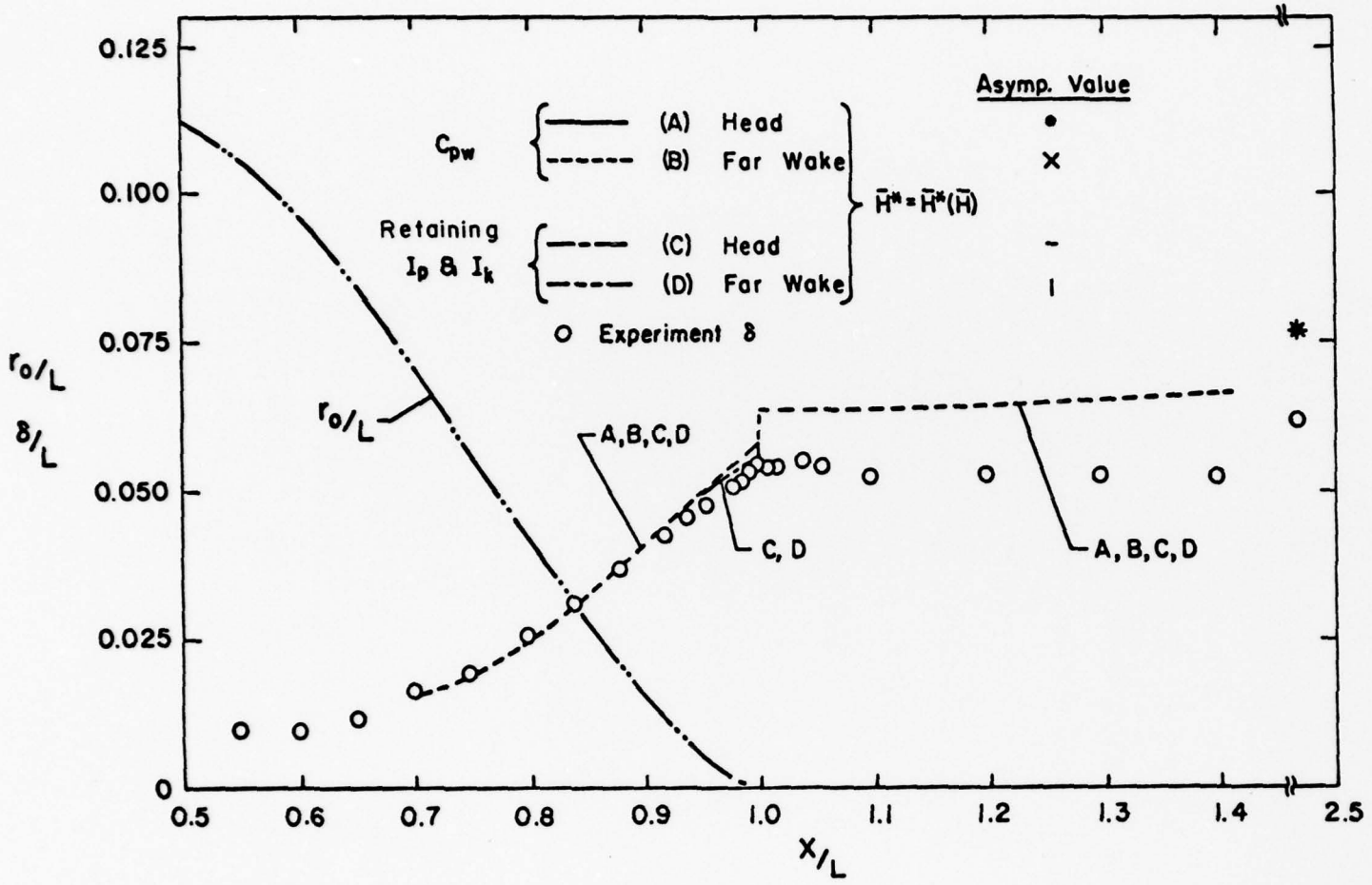

FIGURE 22. COMPARISON OF EXPERIMENTS WITH THE SOLUTION OF THE INTEGRAL EQUATIONS, LOW-DRAG BODY
(a) BOUNDARY-LAYER AND WAKE THICKNESS

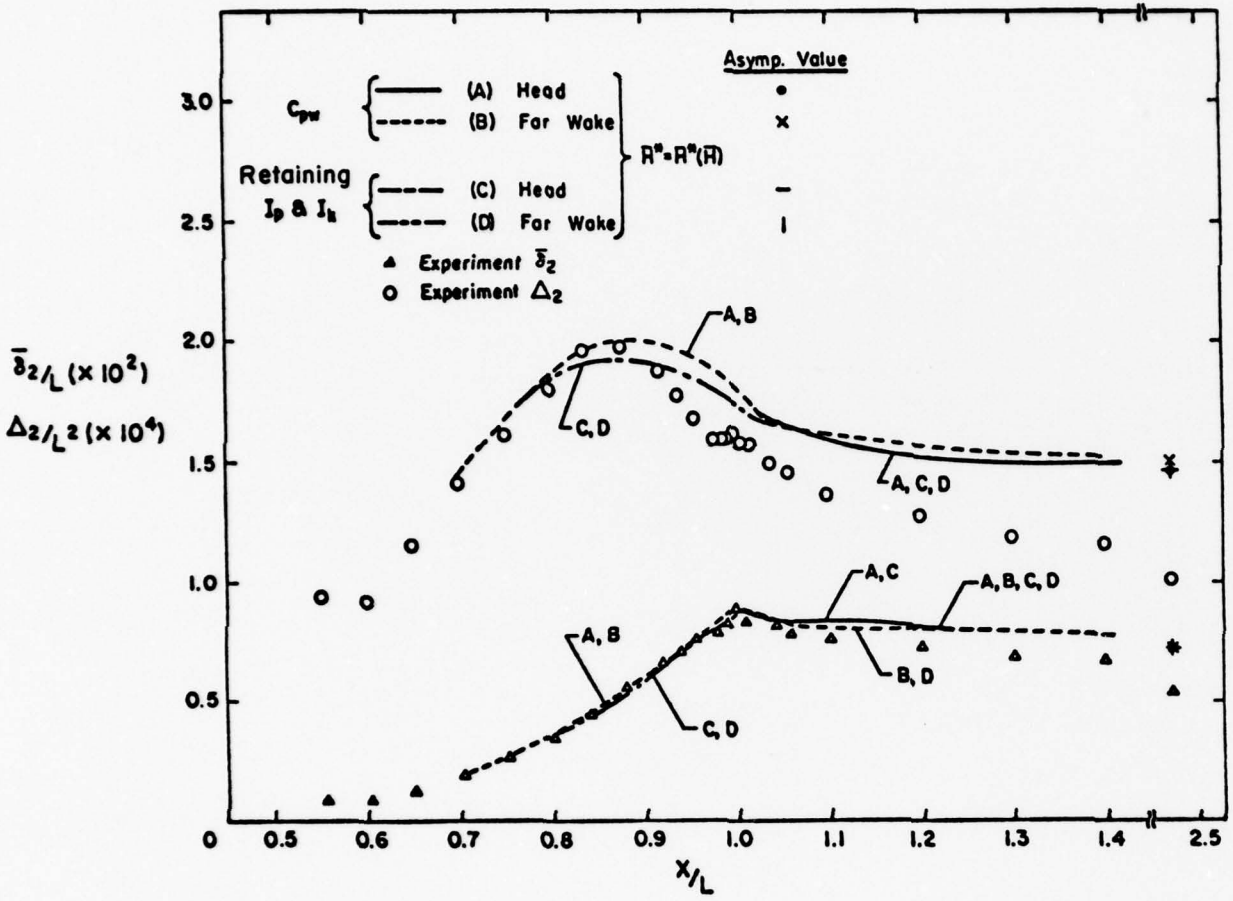

FIGURE 22. (cont'd.)
(b) PLANAR AND AXISYMMETRIC MOMENTUM DEFICITS

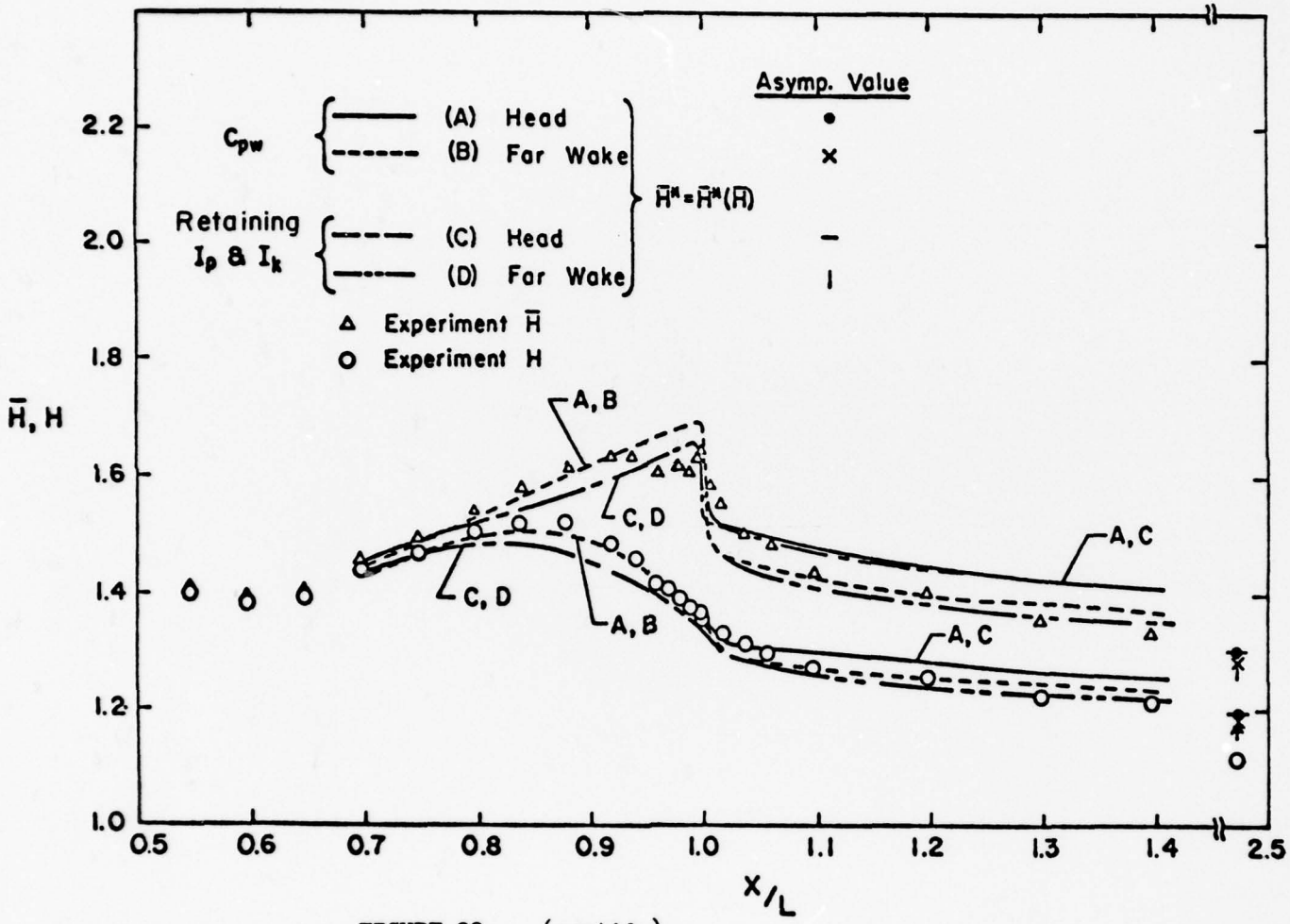

FIGURE 22. (cont'd.)
(c) SHAPE PARAMETER

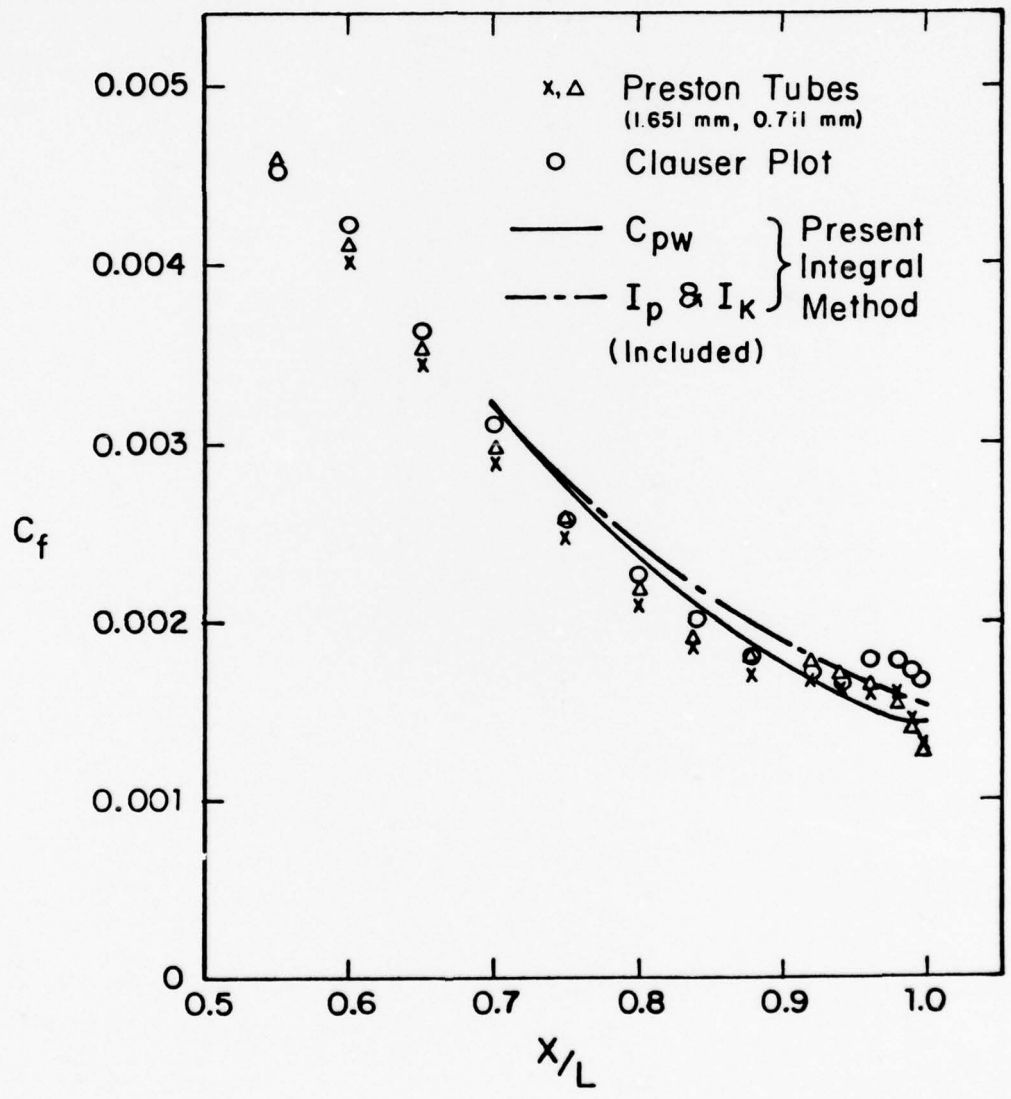

FIGURE 22. (cont'd.)
(d) WALL SHEAR STRESS

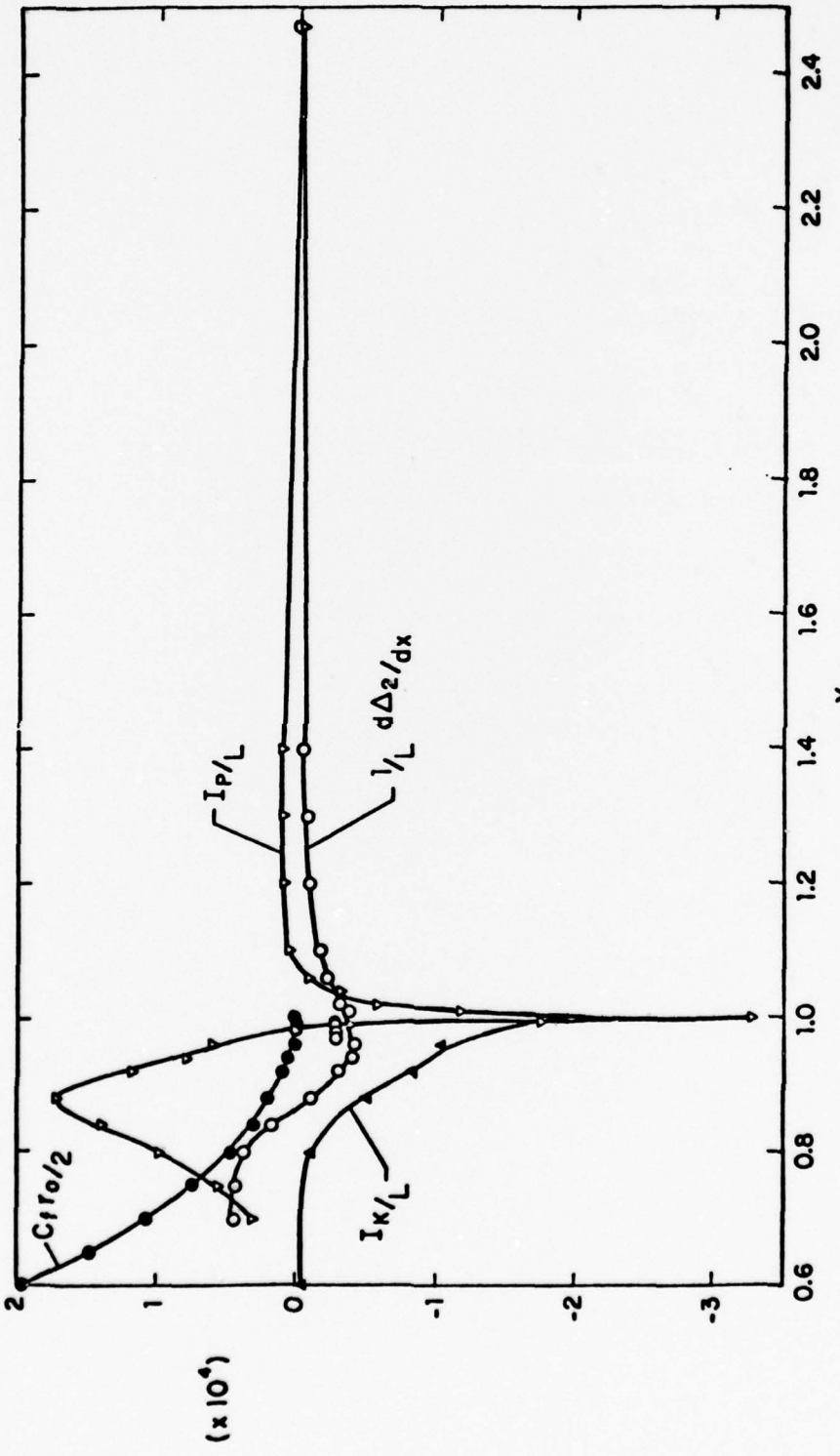

FIGURE 23. RELATIVE MAGNITUDES OF SOME TERMS IN THE MOMENTUM INTEGRAL EQUATION

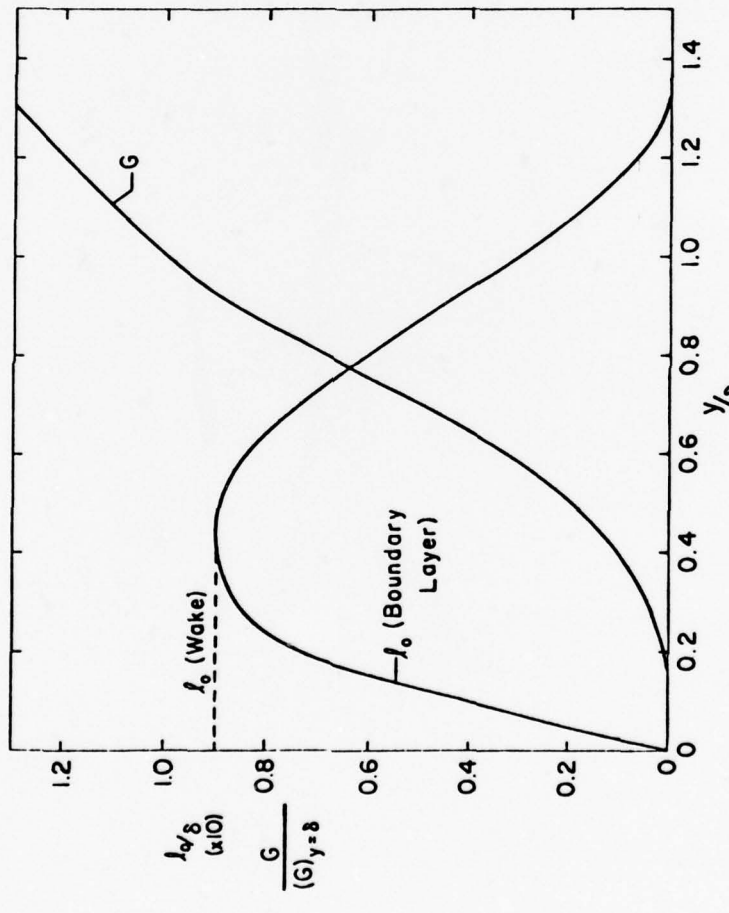

FIGURE 24. THE EMPIRICAL FUNCTIONS

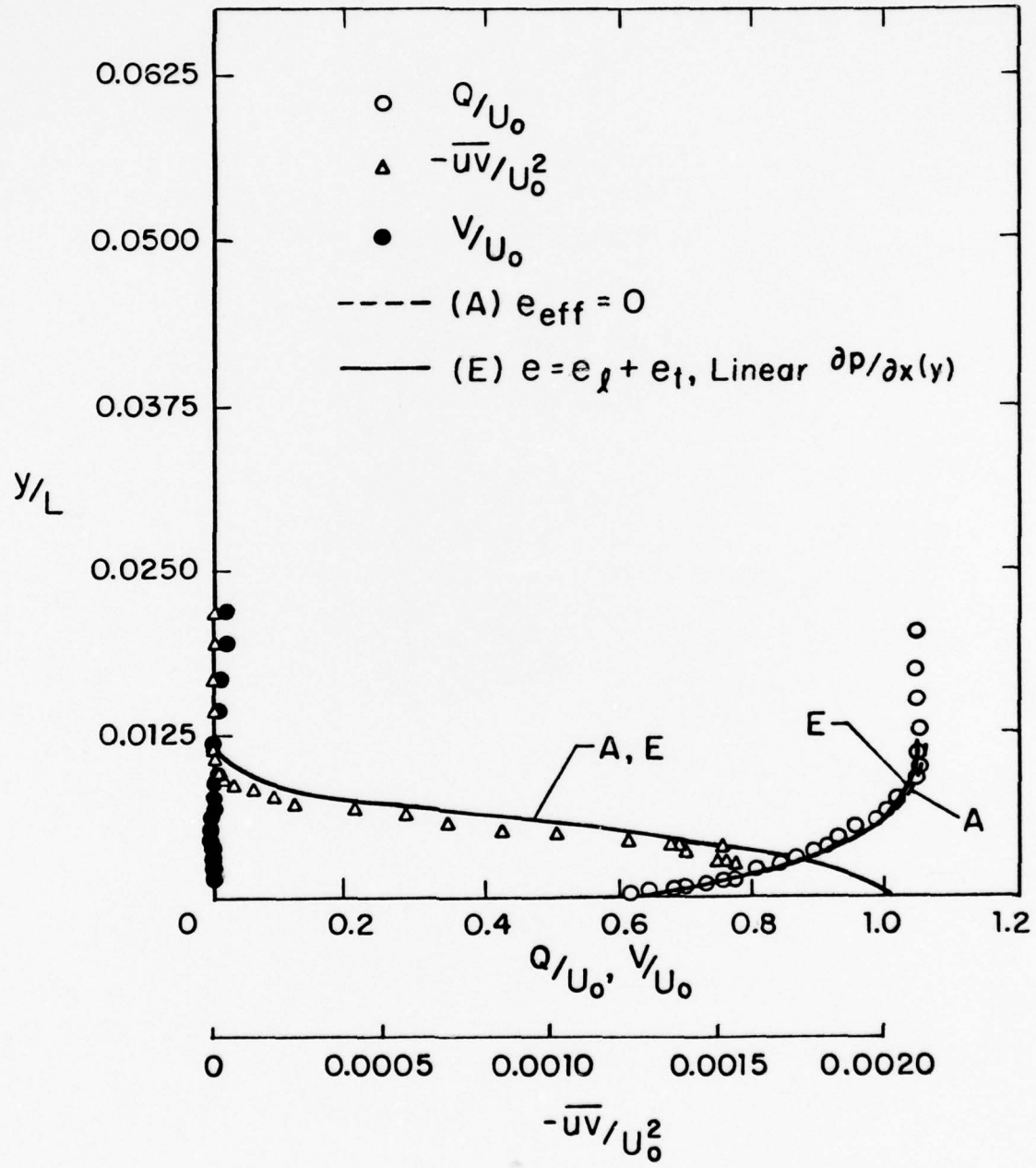

FIGURE 25. COMPARISON OF MEASUREMENTS WITH THE SOLUTION OF THE DIFFERENTIAL EQUATIONS, LOW-DRAG BODY
(a) INITIAL PROFILES AT X/L = 0.601

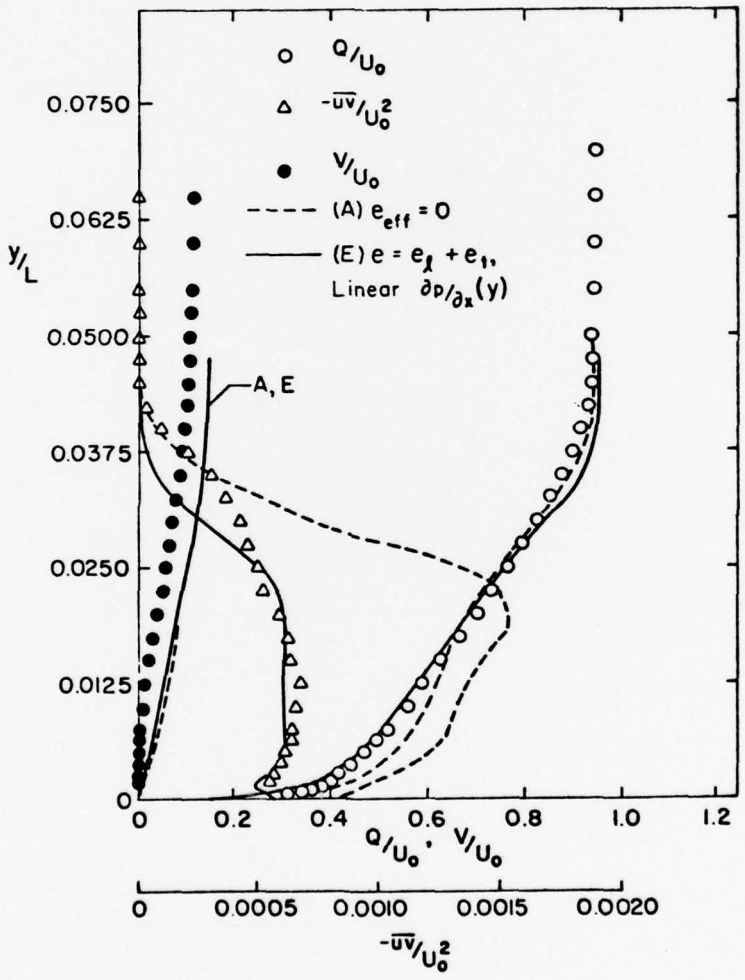

FIGURE 25. (cont'd.)
(b) VELOCITY AND SHEAR-STRESS PROFILES AT X/L = 0.92

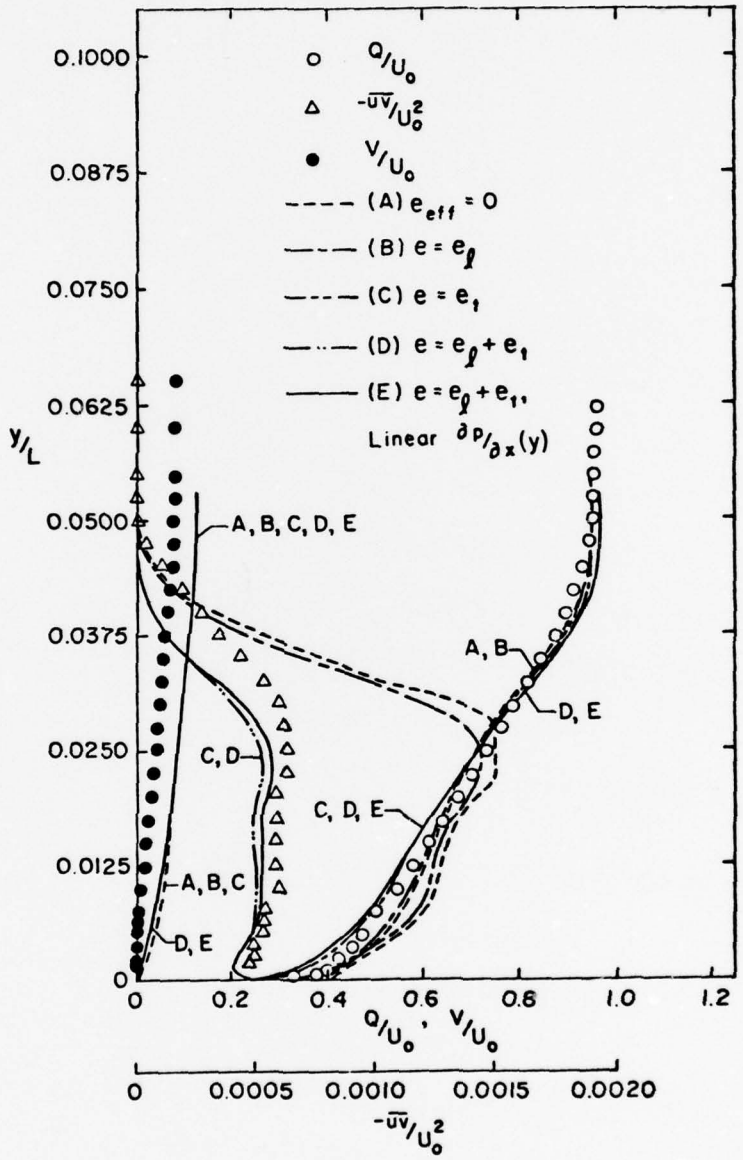

FIGURE 25. (cont'd.)
(c) VELOCITY AND SHEAR-STRESS PROFILES AT X/L = 0.96

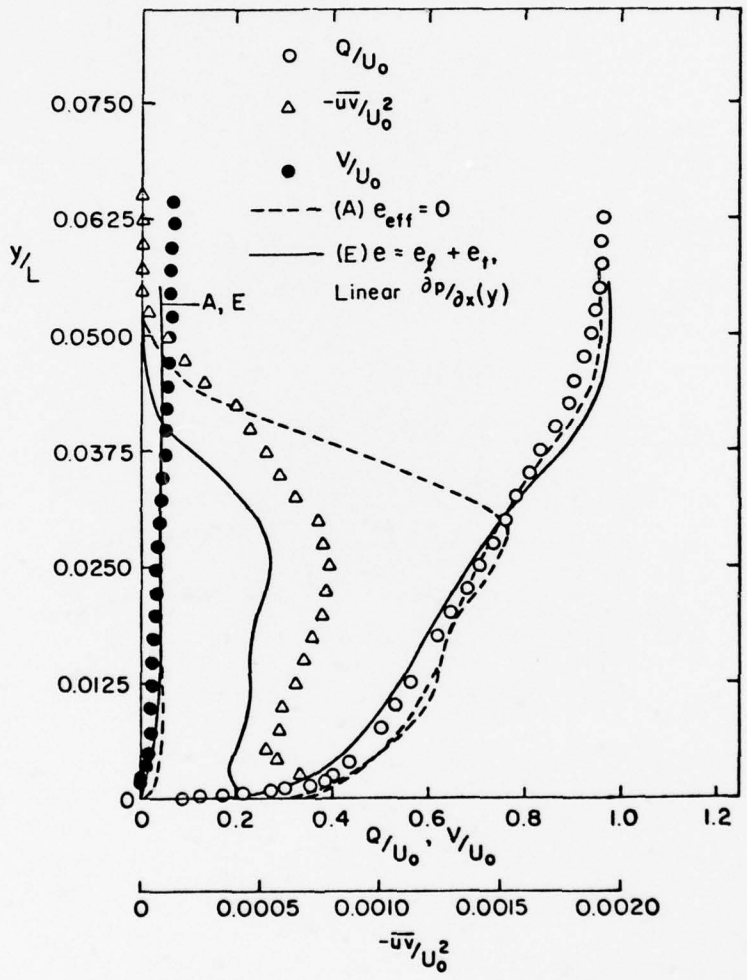

FIGURE 25. (cont'd.)
(d) VELOCITY AND SHEAR-STRESS PROFILES AT X/L = 1.00

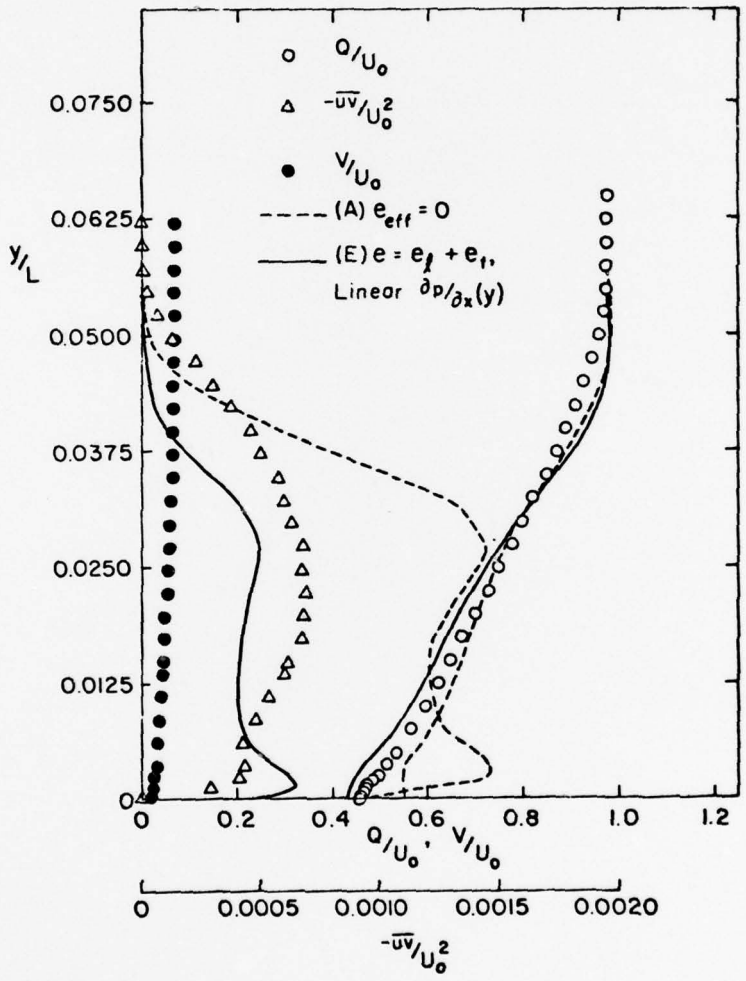

FIGURE 25. (cont'd.)
(e) VELOCITY AND SHEAR-STRESS PROFILES AT X/L = 1.06

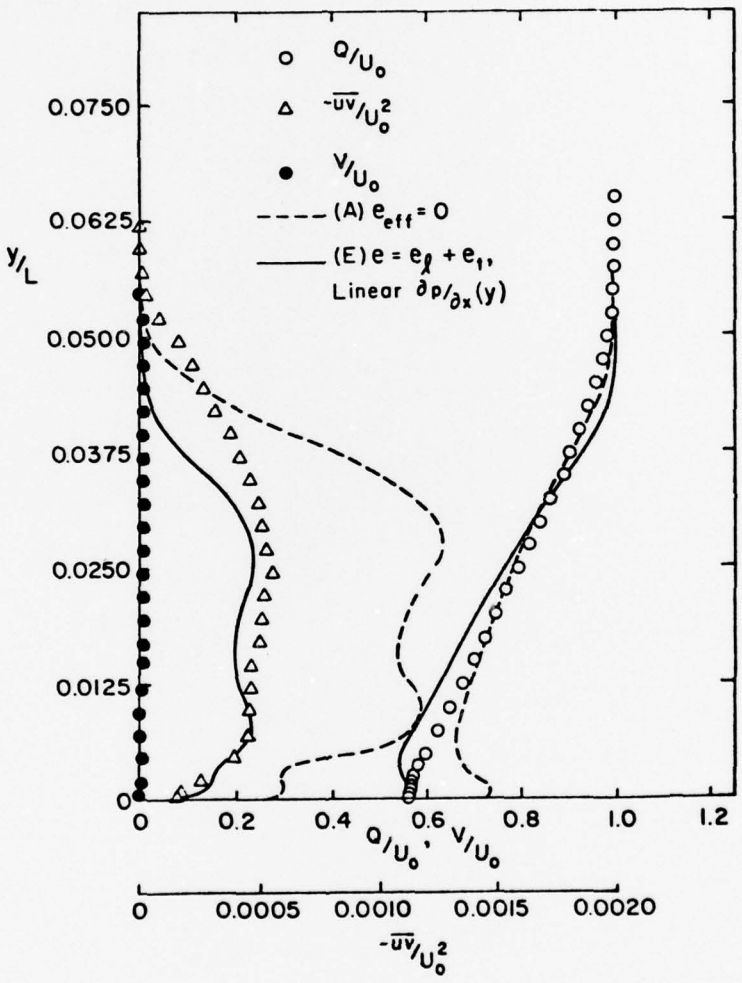

FIGURE 25. (cont'd.)
(f) VELOCITY AND SHEAR-STRESS PROFILES AT X/L = 1.20

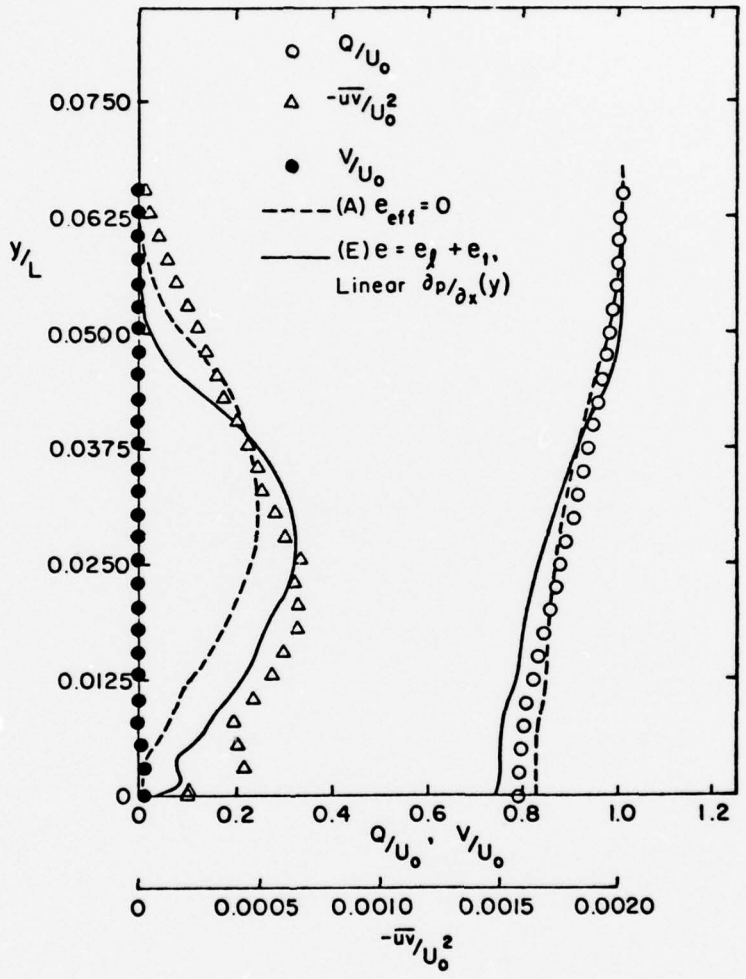

FIGURE 25. (cont'd.)
(g) VELOCITY AND SHEAR-STRESS PROFILES AT X/L = 2.47

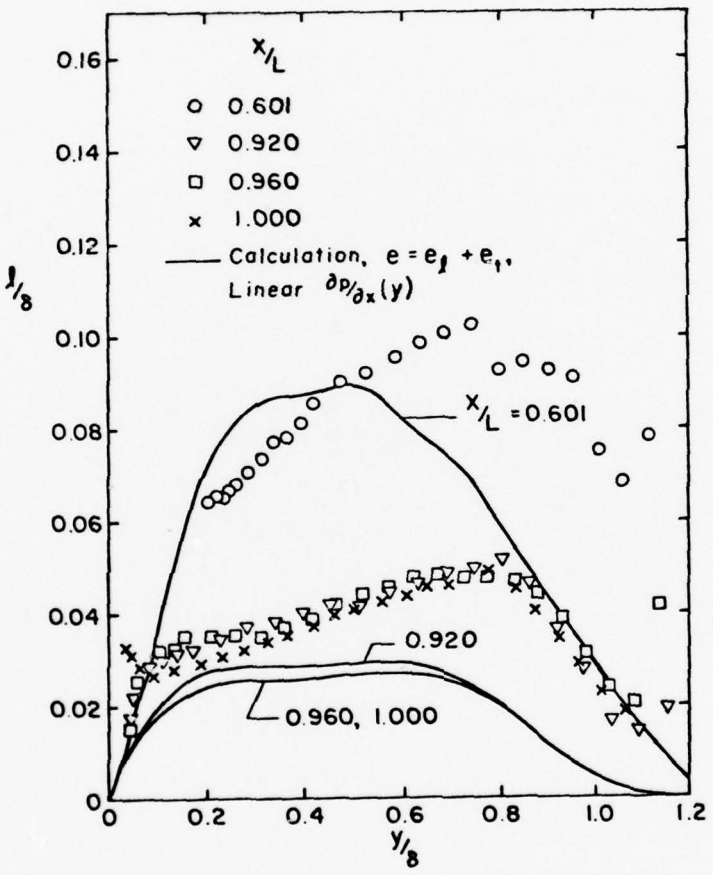

FIGURE 25. (cont'd.)
(h) MIXING-LENGTH PROFILES IN THE BOUNDARY LAYER

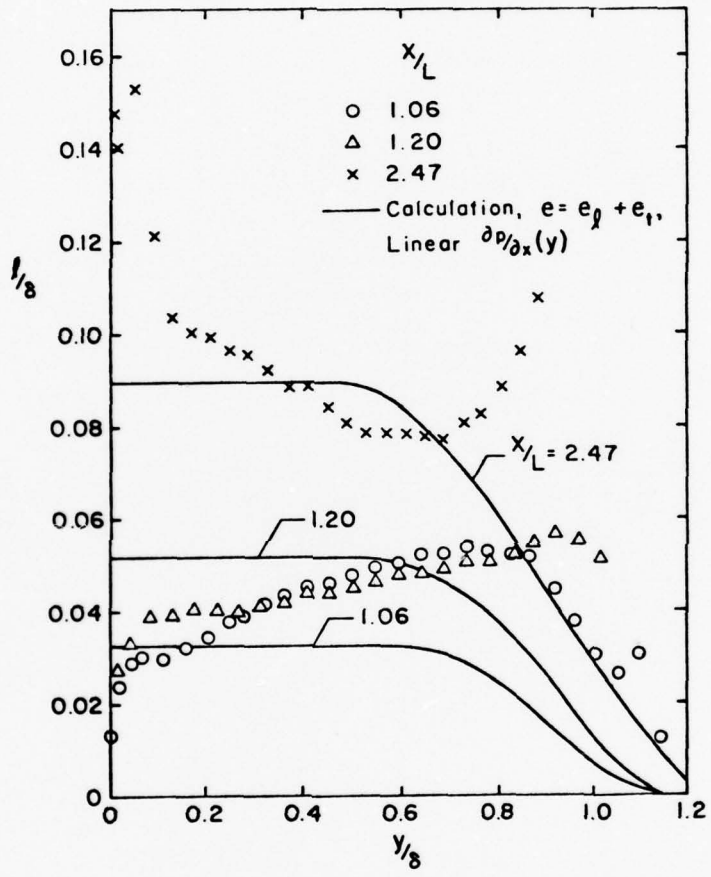

FIGURE 25. (cont'd.)
(i) MIXING-LENGTH PROFILES IN THE WAKE

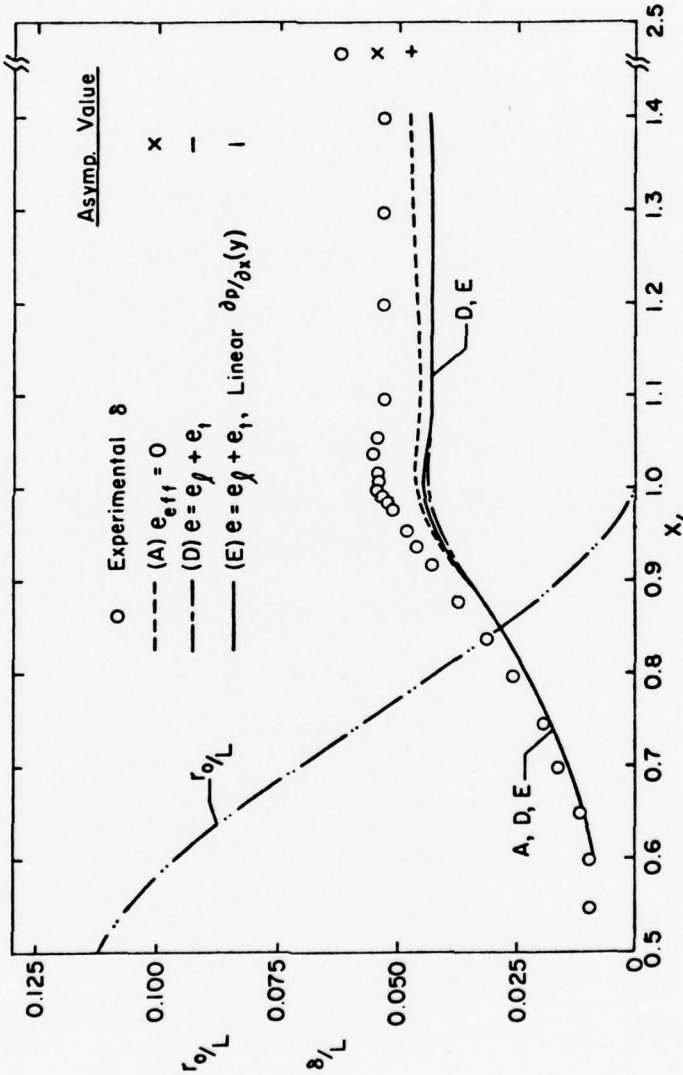

FIGURE 25. (cont'd.)
(j) BOUNDARY-LAYER AND WAKE THICKNESS

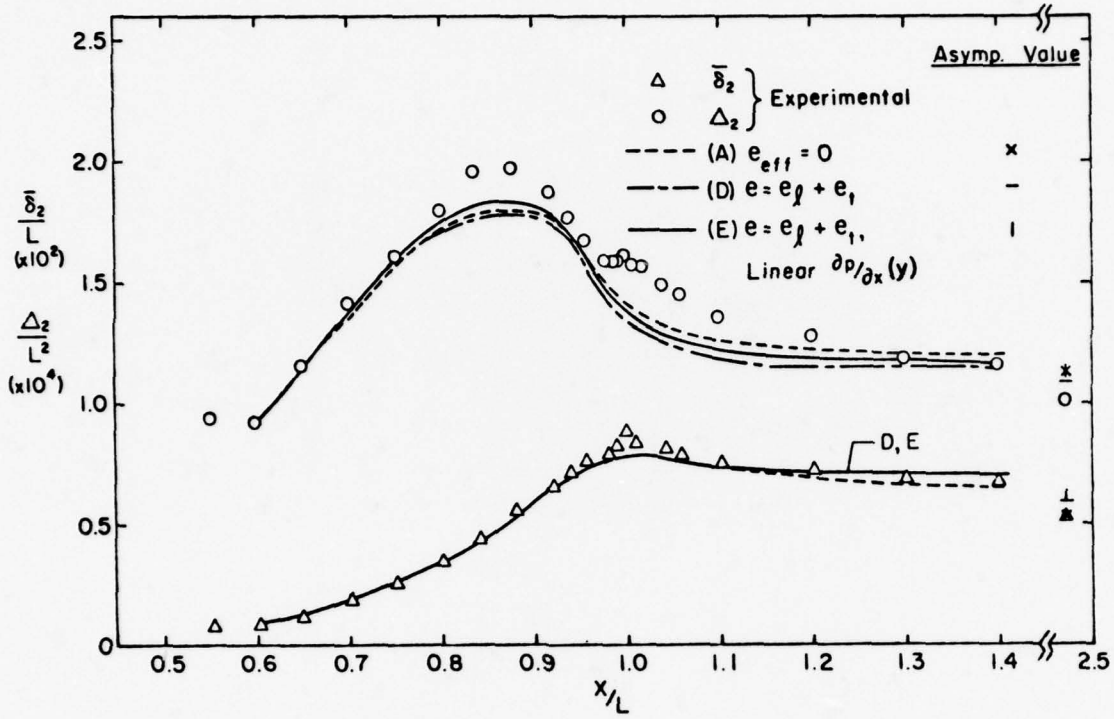

FIGURE 25. (cont'd.)
(k) PLANAR AND AXISYMMETRIC MOMENTUM DEFICITS

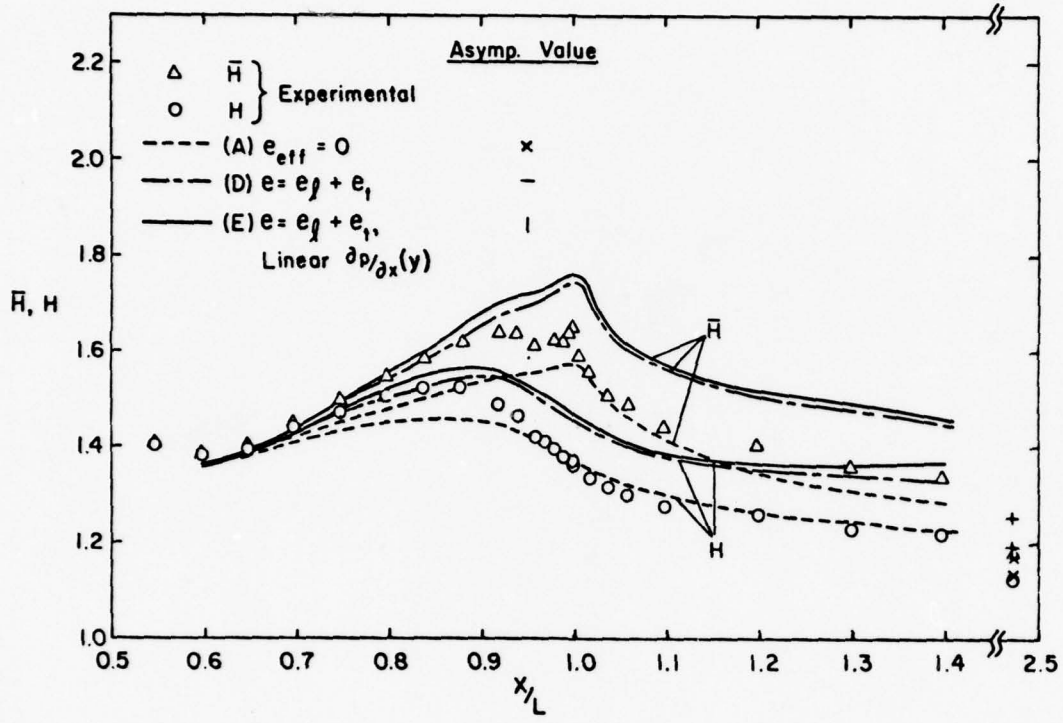

FIGURE 25. (cont'd.)
(1) SHAPE PARAMETER

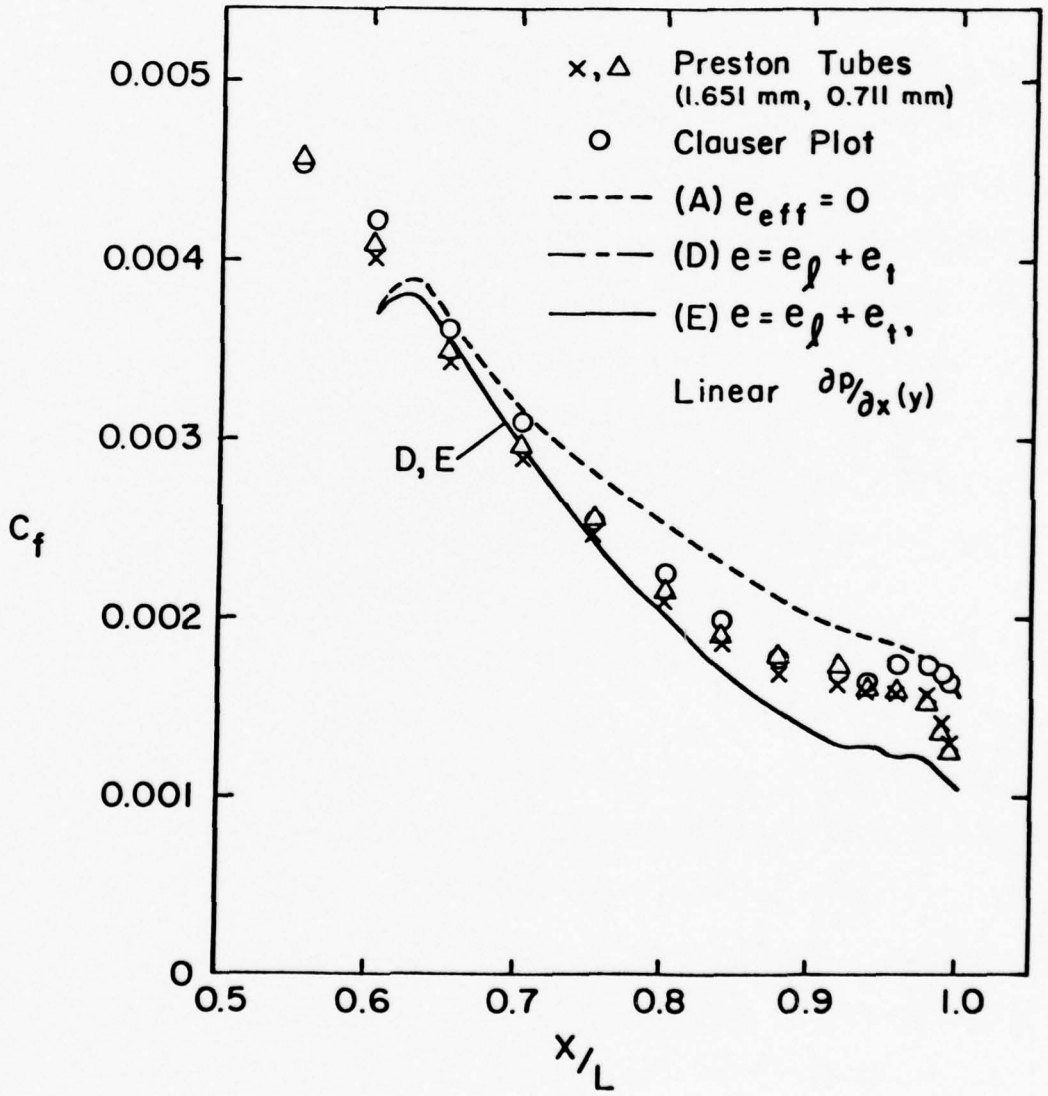

FIGURE 25. (cont'd.)
(m) WALL SHEAR STRESS

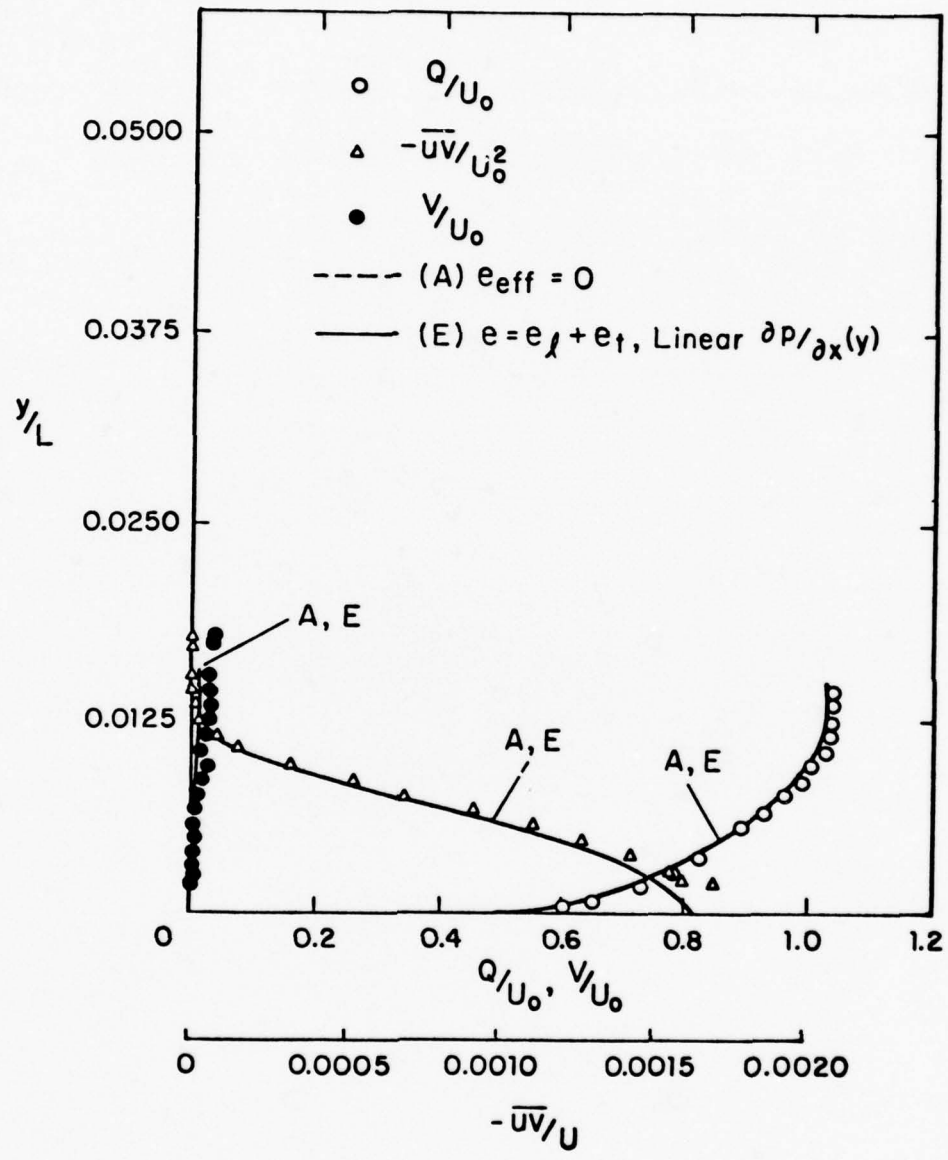

FIGURE 26. COMPARISON OF MEASUREMENTS WITH THE SOLUTION OF THE DIFFERENTIAL EQUATIONS, MODIFIED SPHEROID
(a) INITIAL PROFILES AT X/L = 0.662

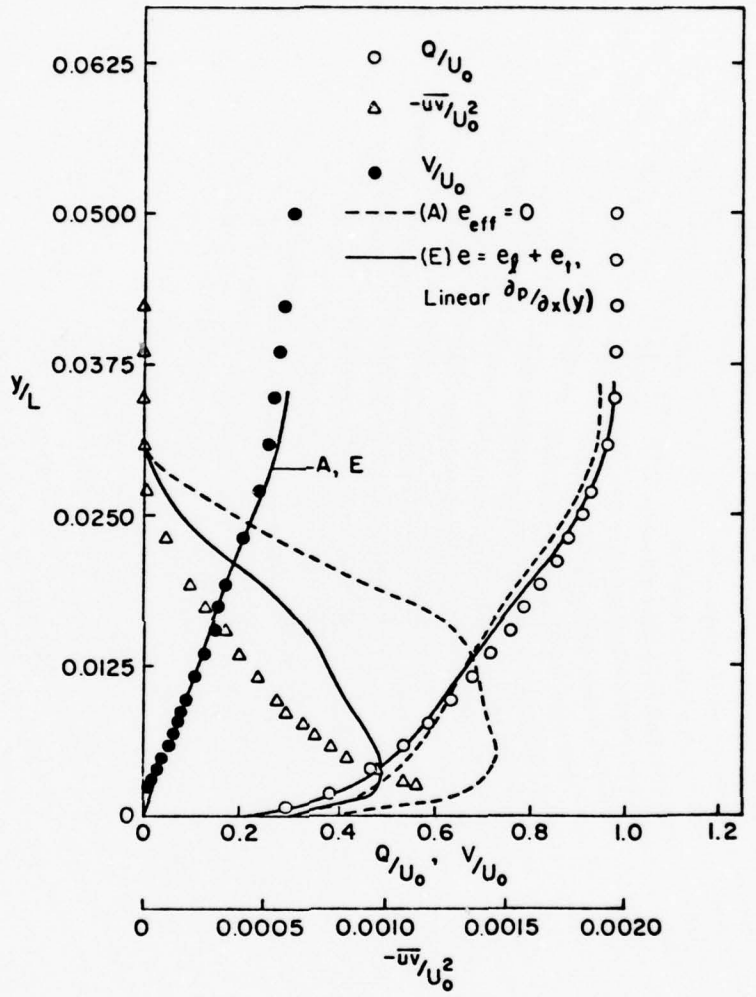

FIGURE 26. (cont'd.)
(b) VELOCITY AND SHEAR-STRESS PROFILES AT X/L = 0.93

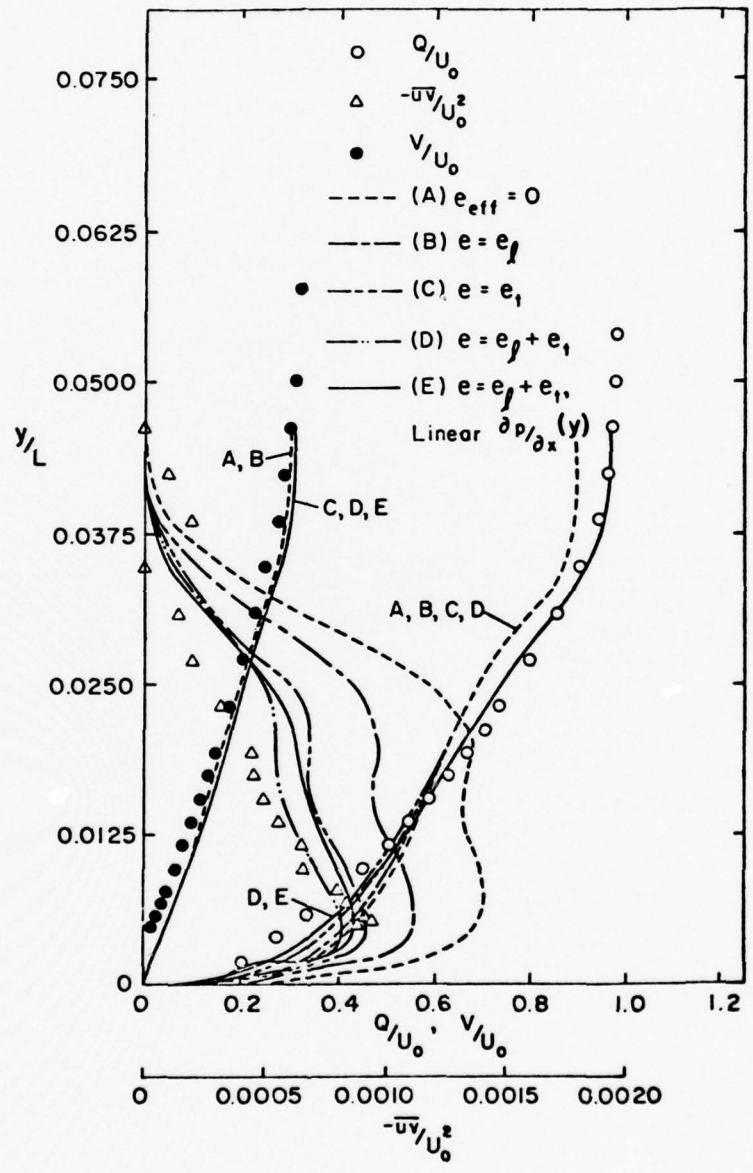

FIGURE 26. (cont'd.)
(c) VELOCITY AND SHEAR-STRESS PROFILES AT X/L = 0.96

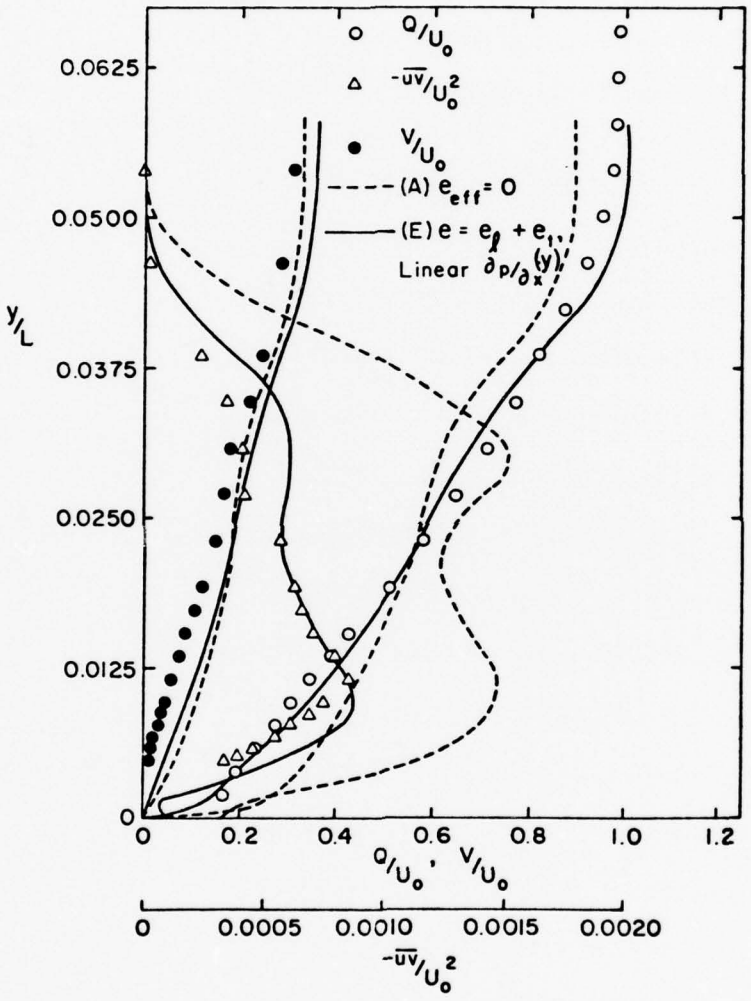

FIGURE 26. (cont'd.)
(d) VELOCITY AND SHEAR-STRESS PROFILES AT X/L = 0.99

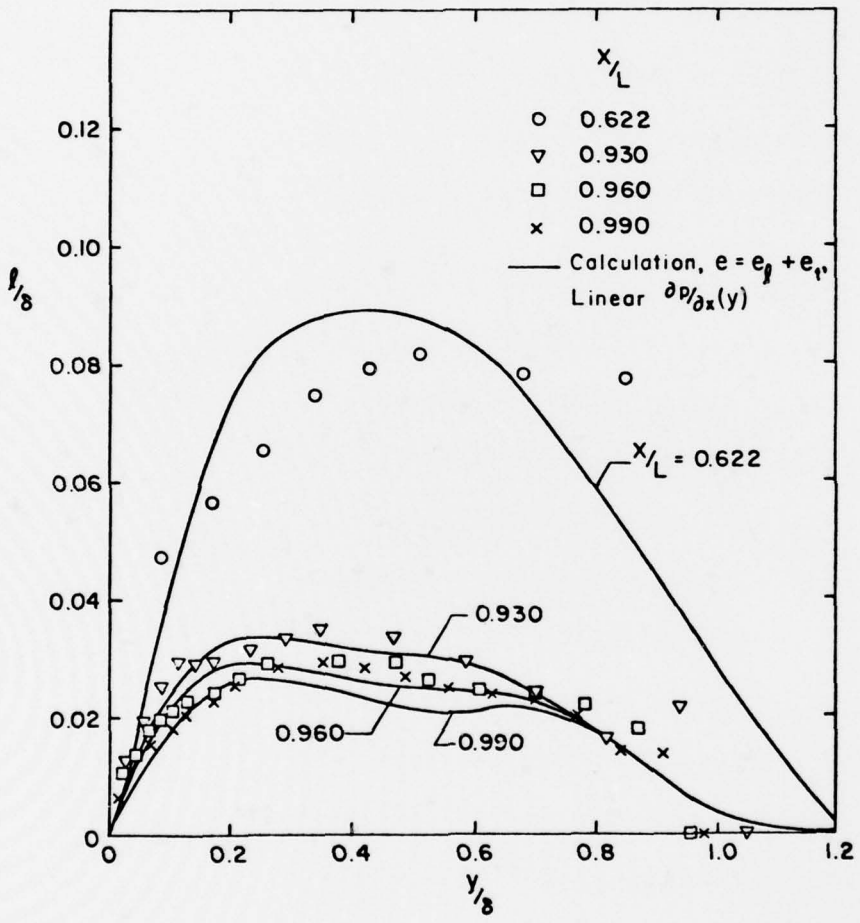

FIGURE 26. (cont'd.)
(e) MIXING-LENGTH PROFILES

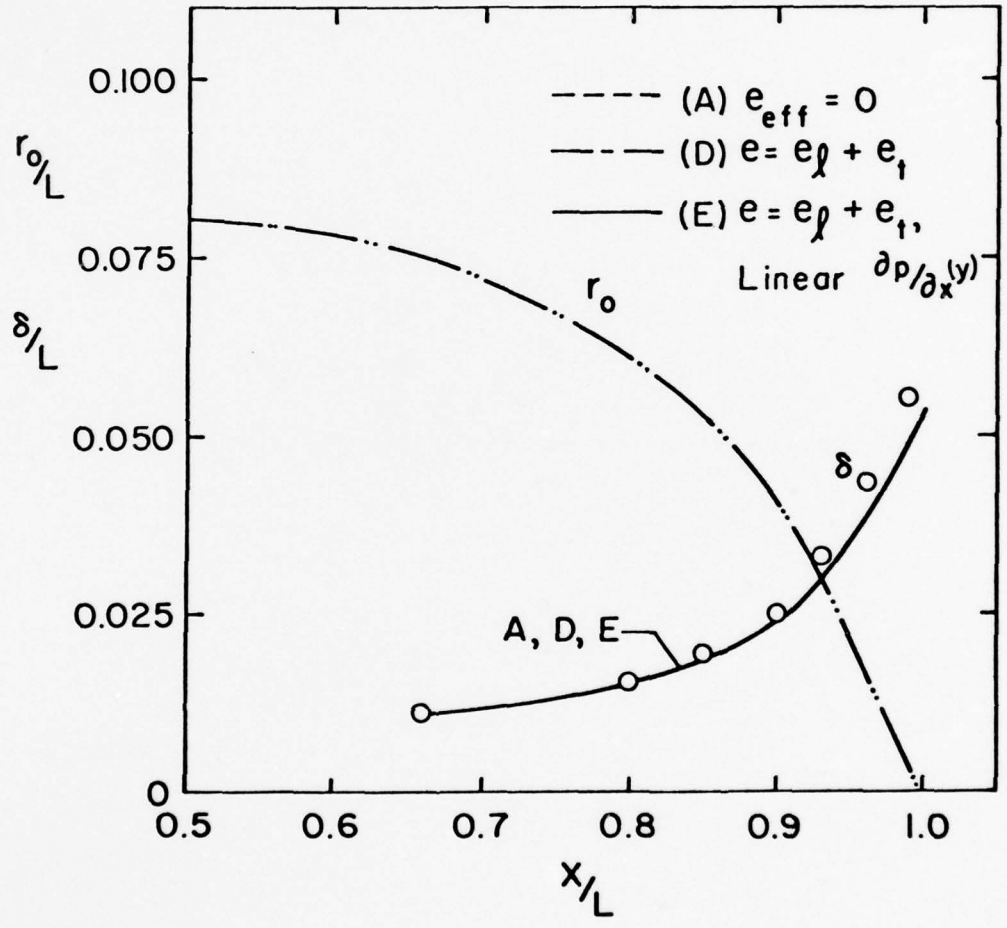

FIGURE 26. (cont'd.)
(f) BOUNDARY-LAYER THICKNESS

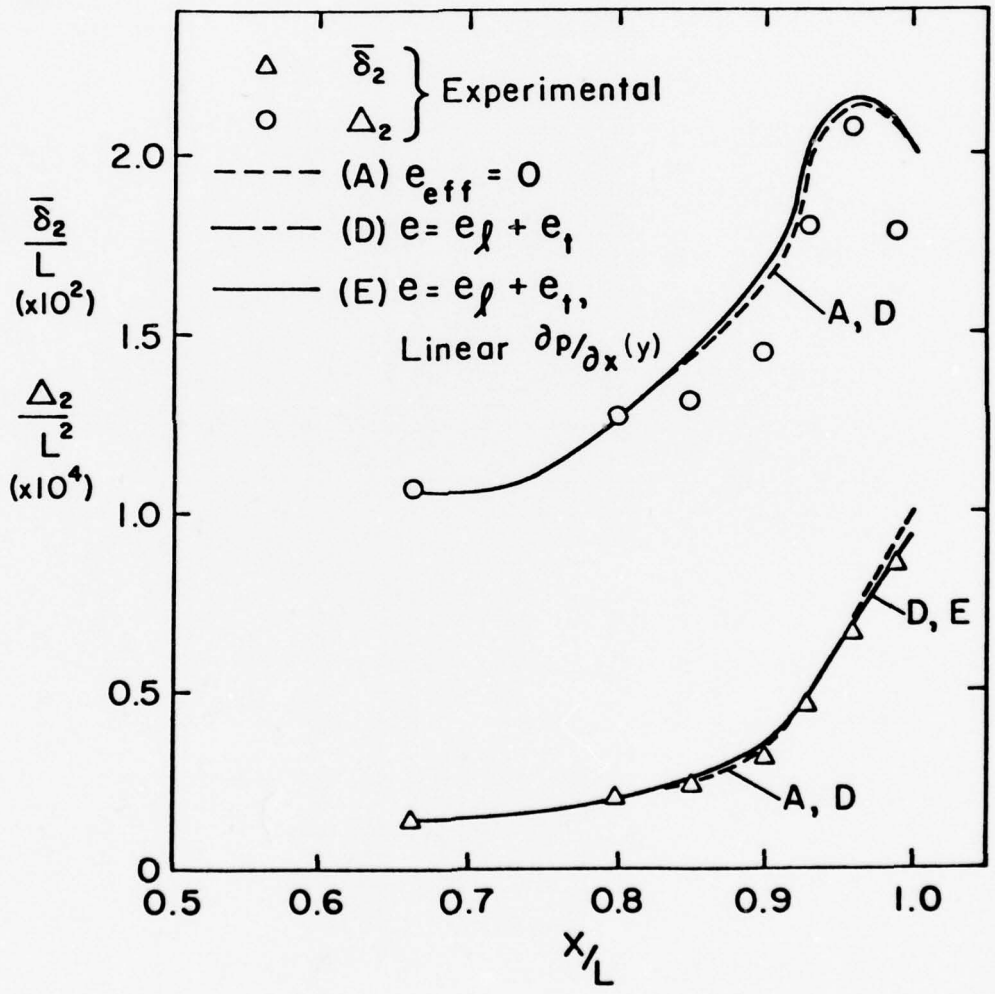

FIGURE 26. (cont'd.)
(g) PLANAR AND AXISYMMETRIC MOMENTUM DEFICITS

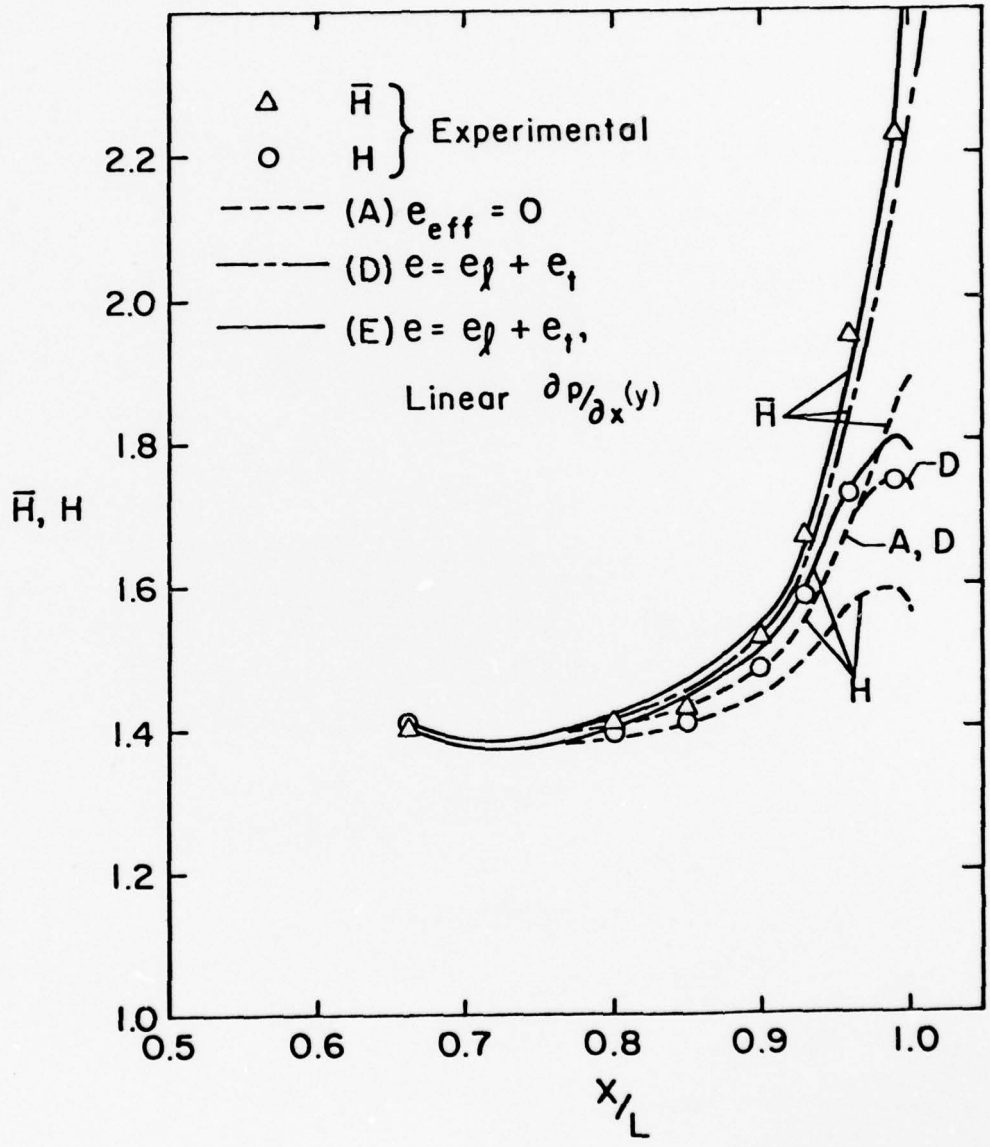

FIGURE 26. (cont'd.)
(h) SHAPE PARAMETER

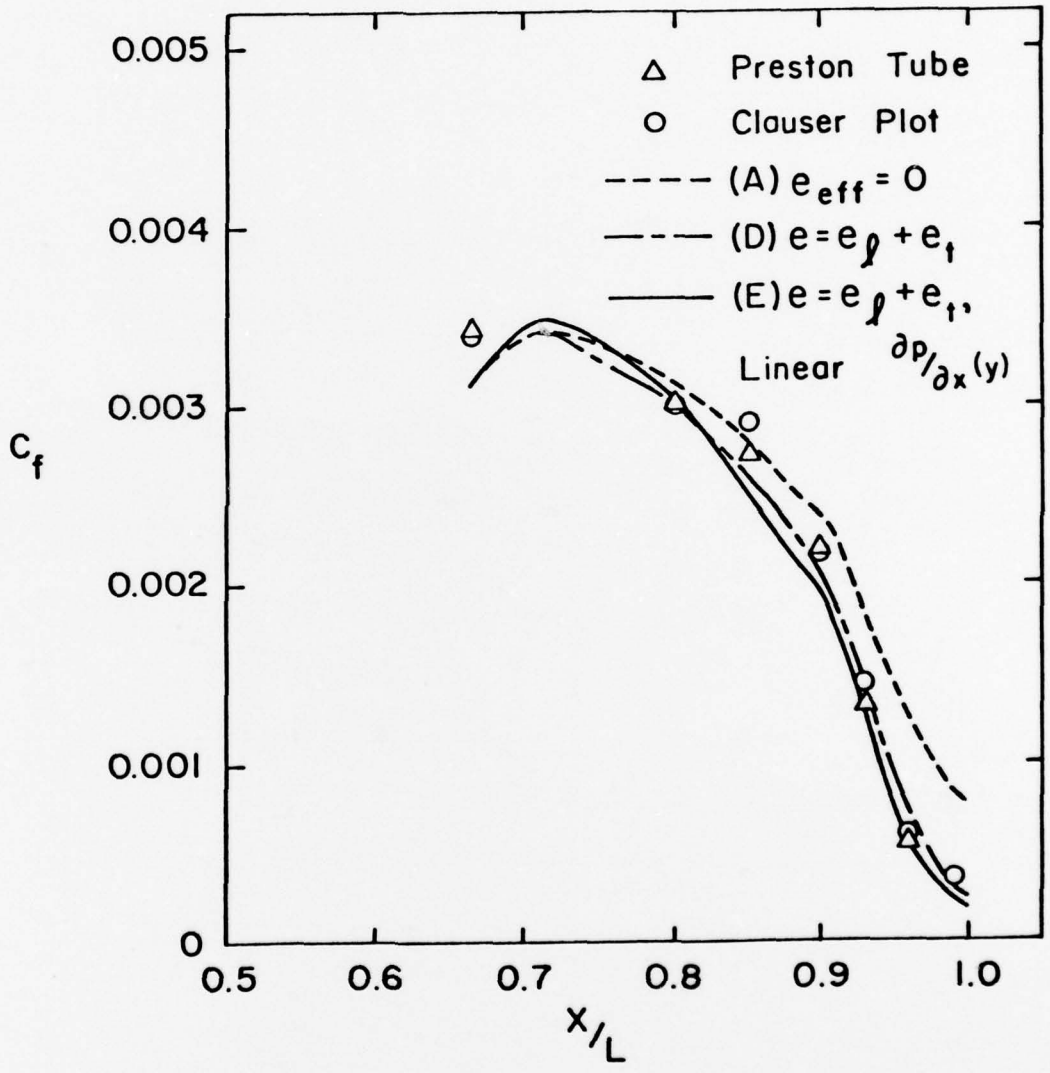

FIGURE 26. (cont'd.)
(i) WALL SHEAR STRESS

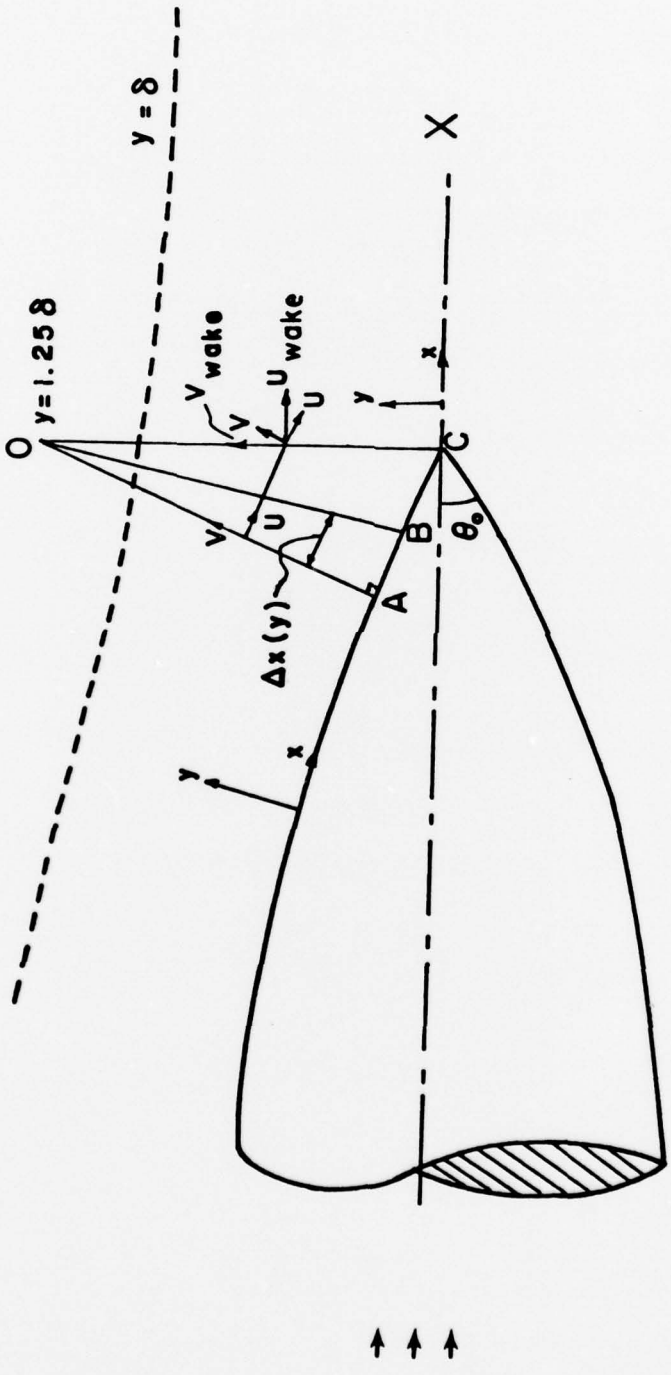

FIGURE 27. COORDINATE TRANSFORMATION AT THE TAIL OF THE BODY

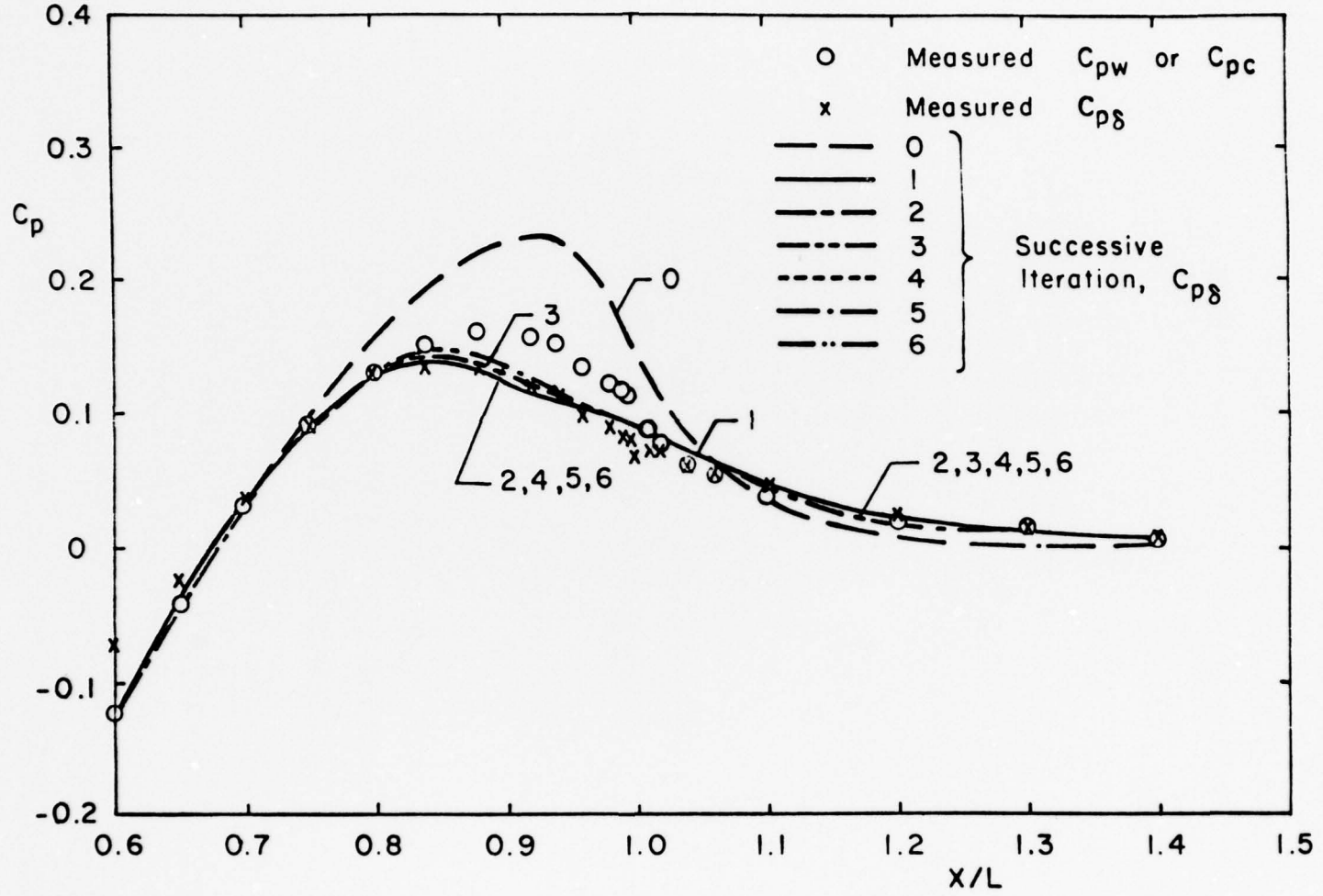

FIGURE 28. ITERATION RESULTS FOR THE LOW-DRAG BODY
(a) PRESSURE DISTRIBUTION ALONG $y = \delta$, $C_{p\delta}$

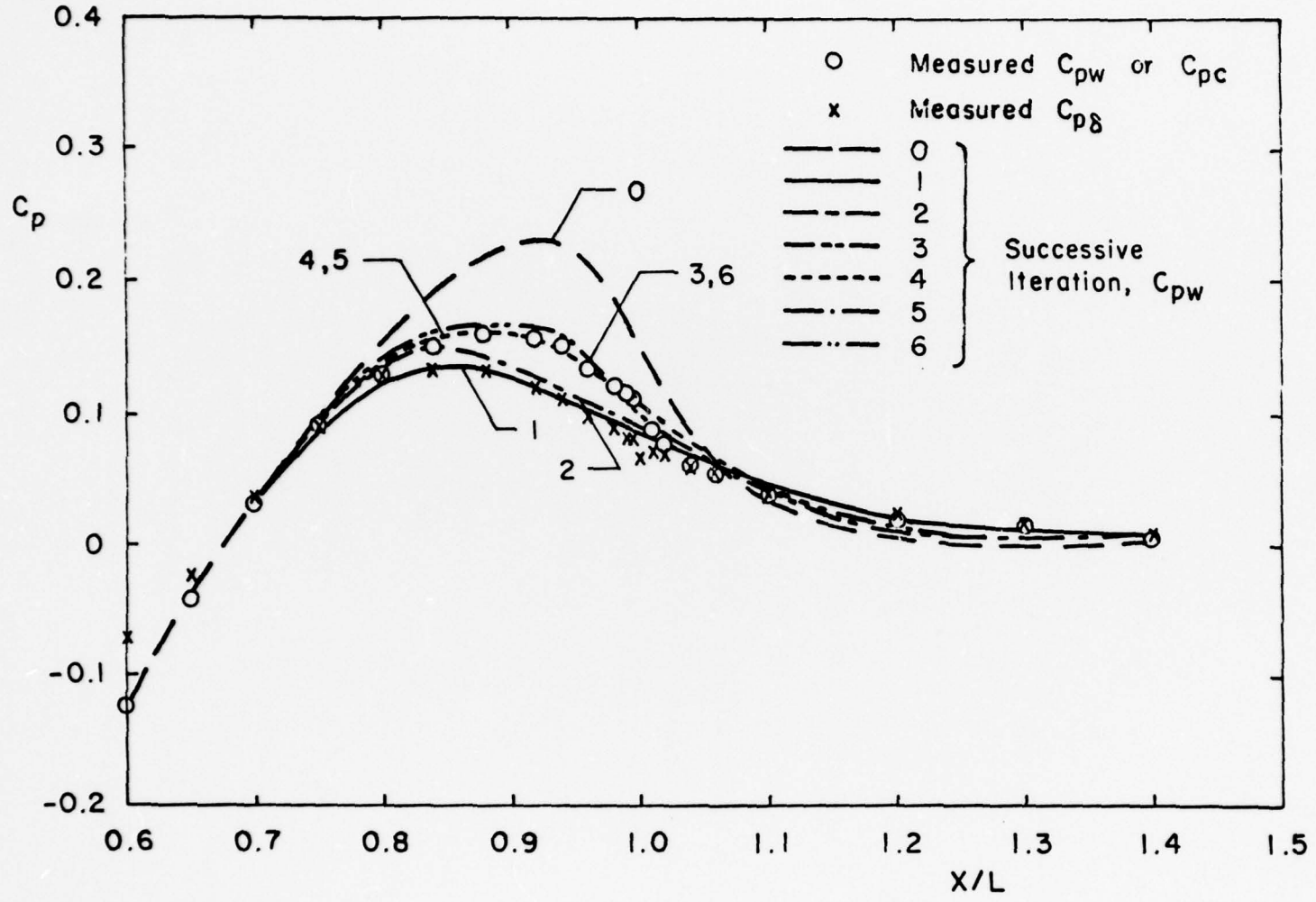

FIGURE 28. (cont'd.)
(b) PRESSURE DISTRIBUTION ON THE BODY SURFACE AND WAKE CENTERLINE, C_{pw}

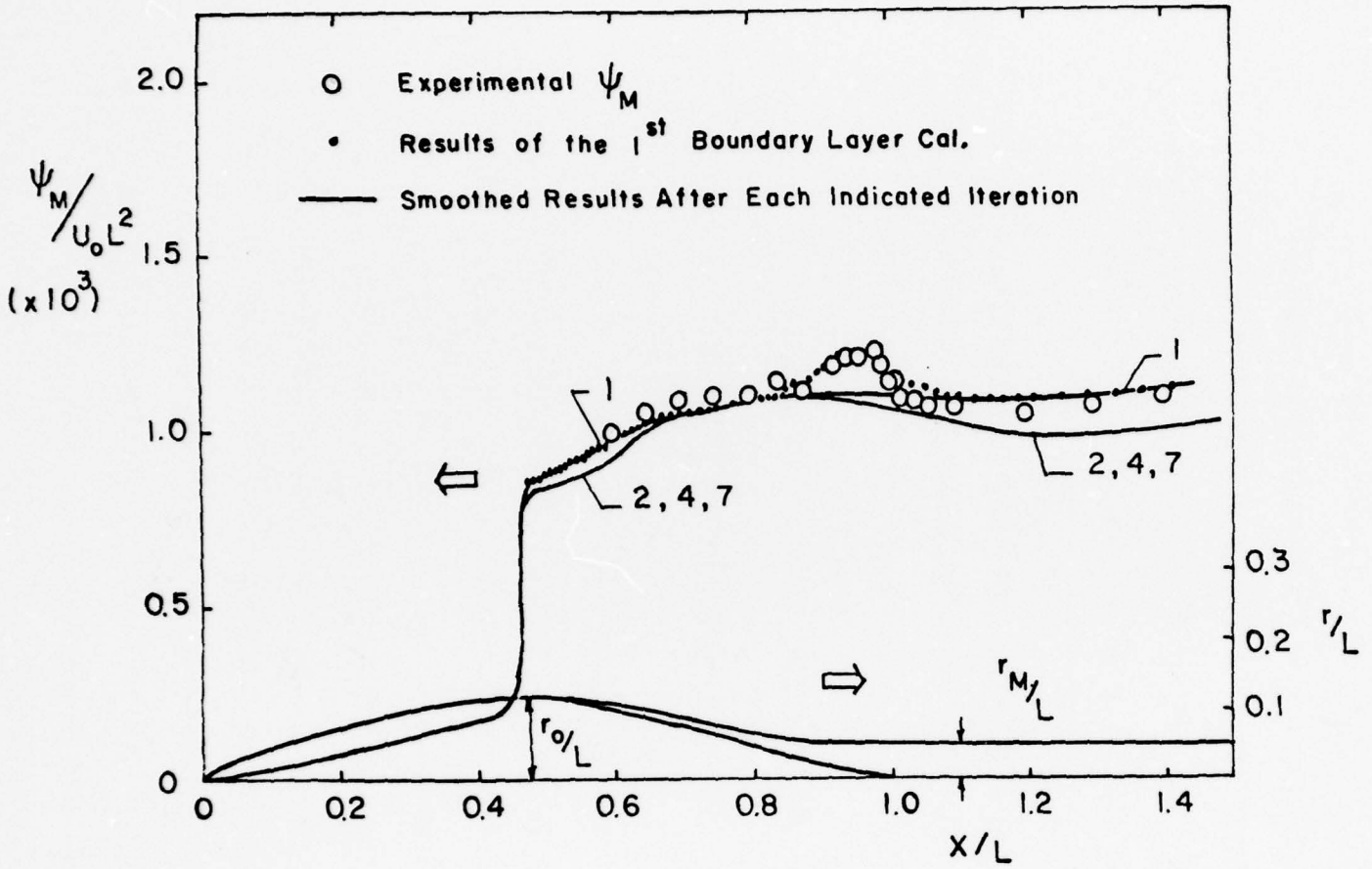

FIGURE 28. (cont'd.)
(c) BOUNDARY CONDITIONS OF THE POTENTIAL-FLOW CALCULATION

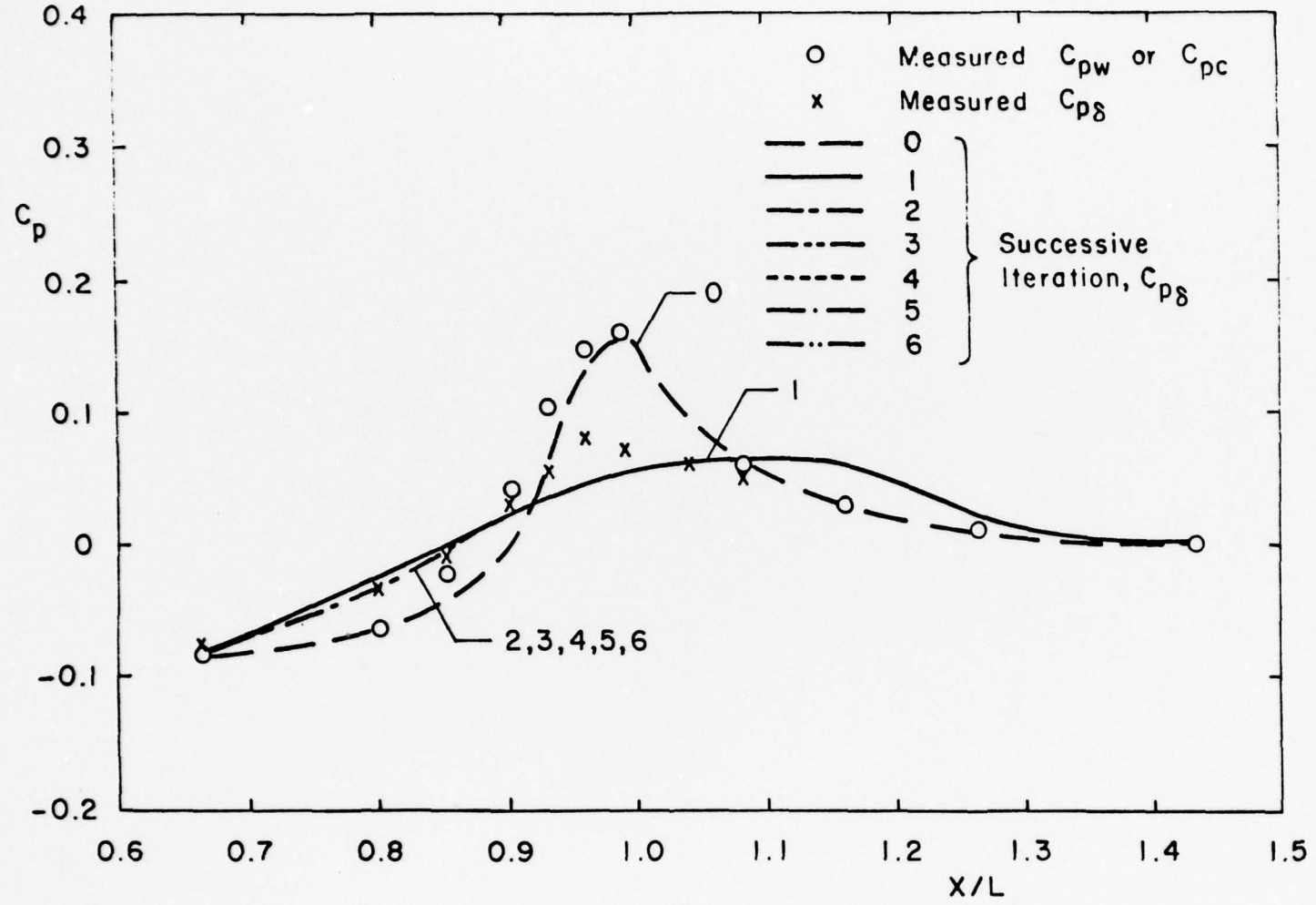

FIGURE 29. ITERATION RESULTS FOR THE MODIFIED SPHEROID
(a) PRESSURE DISTRIBUTION ALONG $y = \delta$, $C_{p\delta}$

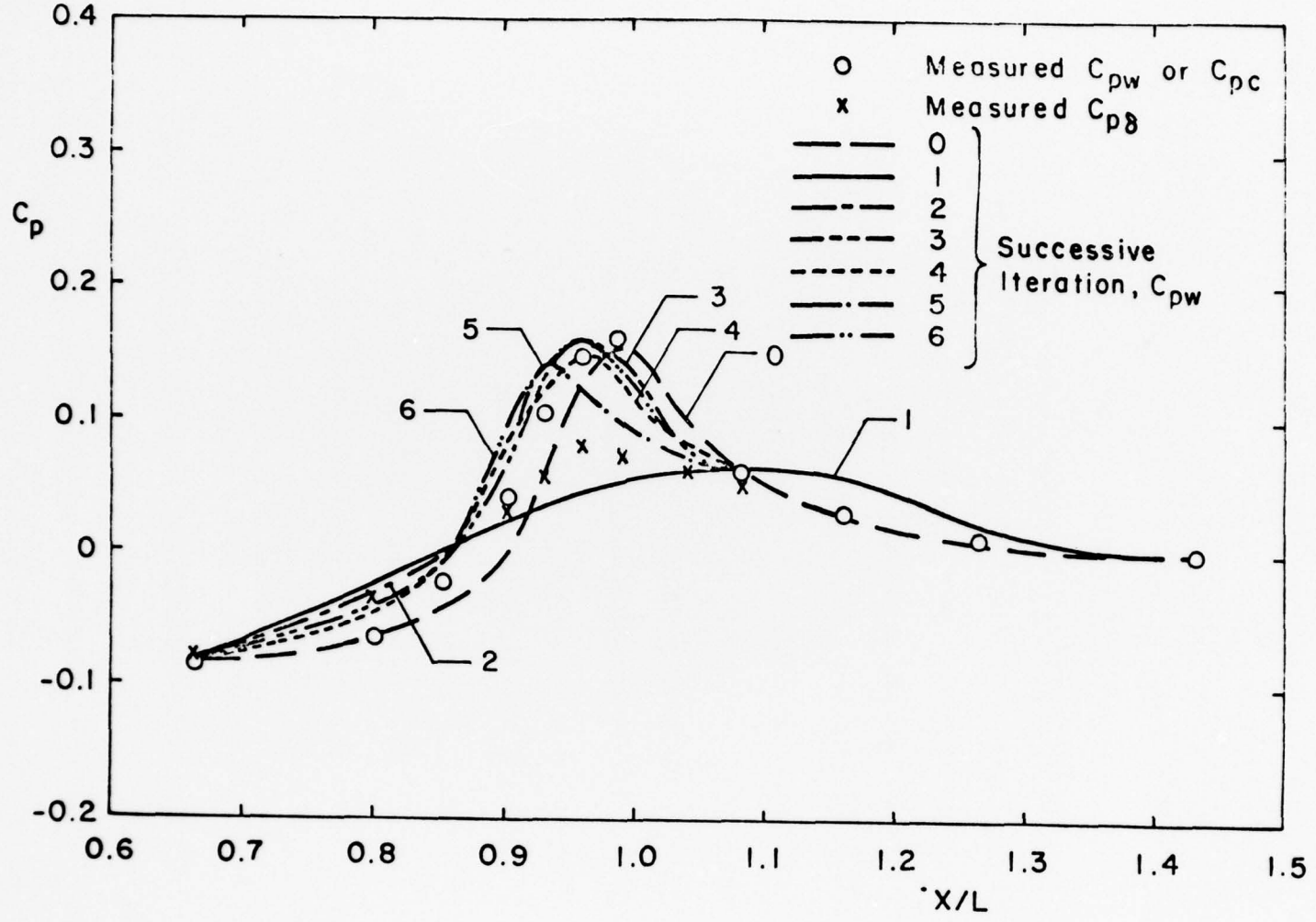

FIGURE 29. (cont'd.)
(b) PRESSURE DISTRIBUTION ON THE BODY SURFACE AND WAKE CENTERLINE, C_{pw}

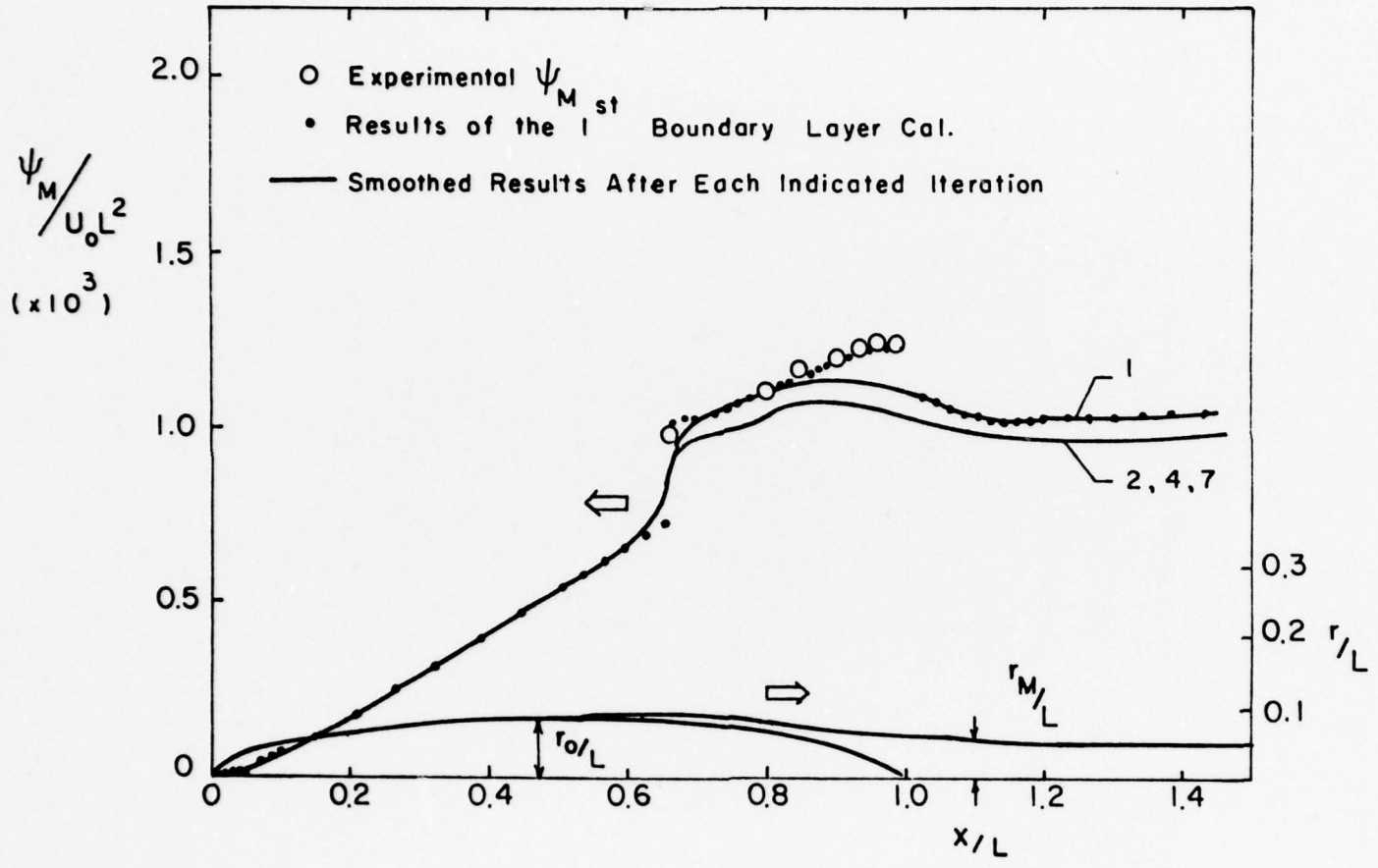

FIGURE 29. (cont'd.)
(c) BOUNDARY CONDITIONS OF THE POTENTIAL-FLOW CALCULATION

REFERENCES

Bradshaw, P. (1969). The Analogy Between Streamline Curvature and Buoyancy in Turbulent Shear Flow, J. Fluid Mech. 36, 177.

Bradshaw, P. (1973). Effects of Streamline Curvature on Turbulent Flow, AGARDograph No. 169.

Bradshaw, P. (1978). Higher-Order Viscous-Inviscid Matching, Imperial College Aeronautics Tech Note 78-103.

Bradshaw, P., and K. Unsworth (1976). Computation of Complex Turbulent Flows, in Reviews of Viscous Flows, Proceedings of the Lockheed-Georgia Company Symposium, 448.

Bradshaw, P., D.H. Ferriss, and N.P. Atwell (1967). Calculation of Boundary Layer Development Using the Turbulent Energy Equation, J. Fluid Mech. 28, 593.

Chambers, T.L., and D.C. Wilcox (1977). Critical Examination of Two-Equation Turbulence Closure Models for Boundary Layers, AIAA Journal 15, No. 6, 821.

Chevray, R. (1968). The Turbulent Wake of a Body of Revolution, ASME, J. Basic Engineering 90, 275.

Chieng, C.C., A.K. Jakubowski, and J.A. Schetz (1974). Investigation of the Turbulence Properties of the Wake behind Self-Propelled, Axisymmetric Bodies, Virginia Poly. Inst. and State Univ., VPI-Aero-25.

Glover, J.R. (1972). Old Gold Model, Type 4-2H Hot-Wire Anemometer and Type 2 Mean-Product Computer, Iowa Institute of Hydraulic Research, Rept. No. 136.

Granville, P.S. (1975). Similarity-Law Entrainment Method for Thick Axisymmetric Turbulent Boundary Layers in Pressure Gradients, David W. Taylor Naval Ship Research and Development Center, Rept. 4525.

Head, M.R. (1958). Entrainment in the Turbulent Boundary Layer, British ARC, R&M No. 3152.

Huang, T.T., H.T. Wang, N. Santelli, and N.C. Groves (1976). Propeller/Stern/Boundary-Layer Interaction on Axisymmetric Bodies: Theory and Experiment, David W. Taylor Naval Ship Research and Development Center, Rept. 0113.

Landweber, L. (1951). The Axially Symmetric Potential Flow About Elongated Bodies of Revolution, David W. Taylor Naval Ship Research and Development Center, Rept. 761.

Landweber, L. (1978). Viscid and Inviscid Flows and Their Interactions, Fifth David Taylor Lectures.

Laufer, J. (1954). The Structure of Turbulence in Fully Developed Pipe Flow, NACA Tech Rept. No. 1174.

Launder, B.E., G.H. Priddin, and B.I. Sharma (1977). The Calculation of Turbulent Boundary Layers on Spinning and Curved Surfaces, ASME, J. Fluids Engineering 99, No. 1, 231. See also discussions by P. Bradshaw and G. Mellor, (1977). ASME, J. Fluids Engineering 99, No. 2, 435.

Lighthill, M.J. (1958). On Displacement Thickness, J. Fluid Mech. 4, 383.

Mahgoub, H.E.H., and P. Bradshaw (1977). Calculation of Turbulent-Inviscid Flow Interactions with Large Normal Pressure Gradients, A.R.C. 37 572.

Meroney, R.N., and P. Bradshaw (1975). Turbulent Boundary Layer Growth Over Longitudinally Curved Surfaces, AIAA Journal 13, 1448.

Nakayama, A., V.C. Patel, and L. Landweber (1976a). Flow Interaction Near the Tail of a Body of Revolution, Part I: Flow Exterior to Boundary Layer and Wake, ASME, J. Fluids Engineering 98, 531.

Nakayama, A., V.C. Patel, and L. Landweber (1976b). Flow Interaction Near the Tail of a Body of Revolution, Part II: Iterative Soltuion for Flow Within and Exterior to Boundary Layer and Wake, ASME, J. Fluids Engineering 98, 538.

Nash, J.F. (1965). Turbulent-Boundary-Layer Behaviour and the Auxiliary Equation, AGARDograph 97, Pt. 1, 245.

Nash, J.F. (1969). The Calculation of Three-Dimensional Turbulent Boundary Layers in Incompressible Flow, J. Fluid Mech. 37, 625.

Parsons, J.S., and R.E. Goodson (1972). The Optimum Shaping of Axisymmetric Bodies for Minimum Drag in Incompressible Flow, Automatic Control Center, School of Mech. Engineering, Purdue Univ., Rept. ACC-72-5.

Patel, V.C. (1965). Calibration of the Preston Tube and Limitations on Its Use in Pressure Gradients, J. Fluid Mech. 23, 185.

Patel, V.C. (1973). A Unified View of the Law of the Wall Using Mixing-Length Theory, The Aero. Quar. 24, 55.

Patel, V.C. (1974). A Simple Integral Method for the Calculation of Thick Axisymmetric Turbulent Boundary Layers, The Aero. Quar. 25, 47.

Patel, V.C., and O. Guven (1976). Importance of the Near Wake in Drag Prediction of Bodies of Revolution, AIAA Journal 14, 1132.

Patel, V.C., and Y.T. Lee (1977). Thick Axisymmetric Turbulent Boundary Layer and Near Wake of a Low-Drag Body of Revolution, Iowa Institute of Hydraulic Research, Rept. No. 210.

Patel, V.C., A. Nakayama, and R. Damian (1974). Measurements in the Thick Axisymmetric Turbulent Boundary Layer Near the Tail of a Body of Revolution, J. Fluid Mech. 63, 345.

Preston, J.H. (1945). The Effect of the Boundary Layer and Wake on the Flow Past a Symmetrical Airfoil at Zero Incidence, Part I: The Velocity Distribution at the Edge of, and Outside the Boundary Layer and Wake, British ARC, R&M No. 2107.

Ramaprian, B.R., and B.G. Shivaprasad (1977). Mean Flow Measurements in Turbulent Boundary Layers Along Mildly-Curved Surfaces, AIAA Journal 15, 189.

Ramaprian, B.R., and B.G. Shivaprasad (1978). The Structure of Turbulent Boundary Layers Along Mildly Curved Surfaces, J. Fluid Mech. 85, 273.

Rodi, W. (1975). A Review of Experimental Data of Uniform Density Free Turbulent Boundary Layers, Studies in Convection I, ed. B.E. Launder, Academic Press, 79.

Schlichting, H. (1968). Boundary-Layer Theory, 6th edition, McGraw-Hill Book Co., 691.

Shivaprasad, B.G., and B.R. Ramaprian (1977). Some Effects of Longitudinal Wall-Curvature on Turbulent Boundary Layers, Proceedings of Symposium on Turbulent Shear Flows, Penn State Univ., 9.21.

Shivaprasad, B.G., and B.R. Ramaprian (1978). Turbulence Measurements in Boundary Layers Along Mildly Curved Surfaces, ASME, J. Fluids Engineering 100, 37.

So, R.M.C., and G.L. Mellor (1972). An Experimental Investigation of Turbulent Boundary Layers Along Curved Surfaces, NASA-CR-1940.

So, R.M.C., and G.L. Mellor (1974). Experiment on Convex Curvature Effects in Turbulent Boundary Layers, J. Fluid Mech. 60, 43.

So, R.M.C., and G.L. Mellor (1975). Experiment on Turbulent Boundary Layers on Concave Wall, The Aero. Quar. 26, 35.

Swanson, R.C., J.A. Schetz, Jr., and A.K. Jakubowski (1974). Turbulent Wake Behind Slender Bodies Including Self-Propelled Configurations, Virginia Poly. Inst. and State Univ., VPI-Aero-24.

SECURITY CLASSIFICATION OF THIS PAGE (When Data Entered)

REPORT DOCUMENTATION PAGE

READ INSTRUCTIONS BEFORE COMPLETING FORM

1. REPORT NUMBER: THESIS	2. GOVT ACCESSION NO.
3. RECIPIENT'S CATALOG NUMBER	
4. TITLE (and Subtitle): THICK AXISYMMETRIC TURBULENT BOUNDARY LAYER AND WAKE OF A LOW-DRAG BODY	5. TYPE OF REPORT & PERIOD COVERED: FINAL/THESIS
6. PERFORMING ORG. REPORT NUMBER: None	
7. AUTHOR(s): Yu-Tai Lee	8. CONTRACT OR GRANT NUMBER(s): N00014-75-C-0273
9. PERFORMING ORGANIZATION NAME AND ADDRESS: Institute of Hydraulic Research, University of Iowa, Iowa City, Iowa 52242	10. PROGRAM ELEMENT, PROJECT, TASK AREA & WORK UNIT NUMBERS
11. CONTROLLING OFFICE NAME AND ADDRESS: David W. Taylor Naval Ship R&D Center, Bethesda, Md. 20084 (Code 1505)	12. REPORT DATE: December 1978
	13. NUMBER OF PAGES: 120
14. MONITORING AGENCY NAME & ADDRESS (if different from Controlling Office): Office of Naval Research, 800 N. Quincy St, Arlington, Va 22217	15. SECURITY CLASS. (of this report): Unclassified
	15a. DECLASSIFICATION/DOWNGRADING SCHEDULE

16. DISTRIBUTION STATEMENT (of this Report)

APPROVED FOR PUBLIC RELEASE: DISTRIBUTION UNLIMITED

17. DISTRIBUTION STATEMENT (of the abstract entered in Block 20, if different from Report)

18. SUPPLEMENTARY NOTES

Sponsored by the Naval Sea Systems Command, General Hydromechanics Research (GHR) Program, administered by the David W. Taylor Naval Ship R&D Center, Bethesda, Md 20084 (Code 1505)

19. KEY WORDS (Continue on reverse side if necessary and identify by block number)

GHR Program
Thick axisymmetric Boundary Layer
Low drag body

20. ABSTRACT (Continue on reverse side if necessary and identify by block number)

Detailed measurements of pressure distributions, mean velocity profiles and Reynolds stresses were made in the thick, axisymmetric boundary layer and the near wake of a low-drag body of revolution. These measurements shed some light on the joint influence of transverse and longitudinal surface curvatures and pressure gradients on the boundary-layer development and on the manner in which an axisymmetric boundary layer becomes a fully-developed wake. The present data have been used to provide an independent check on the accuracy of the simple integral method proposed by Patel, and its ex-

DD FORM 1 JAN 73 1473 EDITION OF 1 NOV 65 IS OBSOLETE
S/N 0102-LF-014-6601

SECURITY CLASSIFICATION OF THIS PAGE (When Data Entered)

tension to the calculation of the near wake made by Nakayama, Patel and Landweber. Calculations have also been performed using the differential equations of the thick axisymmetric turbulent boundary layer and a rate equation for the Reynolds stress derived from the turbulent kinetic-energy equation along the lines suggested by Bradshaw and others. It is shown that the boundary layer in the tail region of a body of revolution is dominated by the extra strain rates arising from longitudinal and transverse surface curvatures. A new differential method is incorporated into the iterative procedure developed by Nakayama, Patel and Landweber for the solution of the interaction between the boundary layer, the wake and the external inviscid flow. The restuls of the iterative method have been compared with the experimental data obtained from the present low-drag body and those obtained earlier on a modified spheroid to demonstrate the agreement.